NASA/CR—2017-219410

N+2 Advanced Low NOx Combustor Technology Final Report

John Herbon, John Aicholtz, Shih-Yang Hsieh, Philip Viars, Shai Birmaher, Dan Brown, Nayan Patel, Doug Carper, Clay Cooper, Russell Fitzgerald, Raghavan Pandalai, and Zekai Hong
GE Aviation, Cincinnati, Ohio

March 2017

NASA STI Program . . . in Profile

Since its founding, NASA has been dedicated to the advancement of aeronautics and space science. The NASA Scientific and Technical Information (STI) Program plays a key part in helping NASA maintain this important role.

The NASA STI Program operates under the auspices of the Agency Chief Information Officer. It collects, organizes, provides for archiving, and disseminates NASA's STI. The NASA STI Program provides access to the NASA Technical Report Server—Registered (NTRS Reg) and NASA Technical Report Server—Public (NTRS) thus providing one of the largest collections of aeronautical and space science STI in the world. Results are published in both non-NASA channels and by NASA in the NASA STI Report Series, which includes the following report types:

- TECHNICAL PUBLICATION. Reports of completed research or a major significant phase of research that present the results of NASA programs and include extensive data or theoretical analysis. Includes compilations of significant scientific and technical data and information deemed to be of continuing reference value. NASA counter-part of peer-reviewed formal professional papers, but has less stringent limitations on manuscript length and extent of graphic presentations.

- TECHNICAL MEMORANDUM. Scientific and technical findings that are preliminary or of specialized interest, e.g., "quick-release" reports, working papers, and bibliographies that contain minimal annotation. Does not contain extensive analysis.

- CONTRACTOR REPORT. Scientific and technical findings by NASA-sponsored contractors and grantees.

- CONFERENCE PUBLICATION. Collected papers from scientific and technical conferences, symposia, seminars, or other meetings sponsored or co-sponsored by NASA.

- SPECIAL PUBLICATION. Scientific, technical, or historical information from NASA programs, projects, and missions, often concerned with subjects having substantial public interest.

- TECHNICAL TRANSLATION. English-language translations of foreign scientific and technical material pertinent to NASA's mission.

For more information about the NASA STI program, see the following:

- Access the NASA STI program home page at http://www.sti.nasa.gov

- E-mail your question to help@sti.nasa.gov

- Fax your question to the NASA STI Information Desk at 757-864-6500

- Telephone the NASA STI Information Desk at 757-864-9658

- Write to:
  NASA STI Program
  Mail Stop 148
  NASA Langley Research Center
  Hampton, VA 23681-2199

NASA/CR—2017-219410

N+2 Advanced Low NOx Combustor Technology Final Report

John Herbon, John Aicholtz, Shih-Yang Hsieh, Philip Viars, Shai Birmaher, Dan Brown, Nayan Patel, Doug Carper, Clay Cooper, Russell Fitzgerald, Raghavan Pandalai, and Zekai Hong
GE Aviation, Cincinnati, Ohio

Prepared under Contract NNC10CA10C

National Aeronautics and
Space Administration

Glenn Research Center
Cleveland, Ohio 44135

March 2017

Acknowledgments

Kathleen Tacina, NASA Program COTR, deserves to be recognized for leading and guiding a challenging program, which in the end delivered a major combustor demonstration of N+2 emission goals.

Chi-Ming Lee, Kathleen Tacina, Ken Suder, and Melissa Merrill provided programmatic solutions to enable the completion of a sector assembly and test.

Chi-Ming Lee, Kathleen Tacina, and Susan Adkins directed the sector testing with expertise to a successful finish, with assistance from Clarence Chang and several key ASCR staff.

Regarding the system studies in Task 1, the authors recognize Craig Nickol and Fay Collier from NASA LaRC for guidance and advice on concept aircraft capability and providing FLOPS input files that were used to model the aircraft used in the GE NASA N+2 mission studies. The authors also wish to recognize all the other NASA, Boeing, and industry personnel whose information in papers and other public documents was leveraged for the analyses in this report.

The authors are grateful to Sybil Cloud who edited and collated this Final Report.

This work was sponsored by the Environmentally Responsible Aviation Project at the NASA Glenn Research Center.

Level of Review: This material has been technically reviewed by NASA expert reviewer(s).

Available from

NASA STI Program
Mail Stop 148
NASA Langley Research Center
Hampton, VA 23681-2199

National Technical Information Service
5285 Port Royal Road
Springfield, VA 22161
703-605-6000

This report is available in electronic form at http://www.sti.nasa.gov/ and http://ntrs.nasa.gov/

Table of Contents

List of Figures

List of Tables

List of Acronyms and Abbreviations

ϕ	Equivalence ratio, fuel / air divided by stoichiometric fuel / air
ACC	Active combustion control
Ae	Effective area
ARRA	American Recovery and Reinvestment Act of 2009
ASCR	Advanced Subsonic Combustion Rig
AST	Advanced Supersonic Transport
BC	Boundary condition
BPR	Bypass ratio (fan bypass flow over core flow)
Bst	Boost – booster pressure ratio
CAEP	Committee on Aviation Environmental Protection
CCP	Ceramic Composites Products – GE
CFD	Computational fluid dynamics
CMC	Ceramic matrix composite
dB	Decibels
DOE	Design of experiments
DAC	Dual Annular Combustor
EICO	Emissions Index for CO (grams of CO per kilogram of fuel (g/kg))
EIHC	Emissions Index for HC (grams of HC per kilogram of fuel (g/kg))
EINOx	Emissions Index for NOx (grams of NOx per kilogram of fuel (g/kg))
EIS	Entry into service
EPNDB	Effective perceived noise Decibel
ERA	Environmentally Responsible Aviation (NASA project)
ETAPS	Enhanced Twin Annular Premixing Swirler
FAR	Fuel air ratio
FAR	Full annular rig
FAR25	Federal Acquisition Regulation Number 25
FAR4	Fuel-to-air ratio at station 4 (combustor exit)
FLOPS	Flight Optimization System (NASA software)
FN	Flow number, pph / psi**0.5
FPR	Fan pressure ratio
FT	Flame tube
HC	Hydrocarbon (emissions)
HTP	High temperature and pressure (flame tube rig)
HWB	Hybrid wing body
HZ	Hertz, cycles per second
ICAO	International Civil Aviation Organization
ISA	International standard atmosphere
IR	Infrared electromagnetic waves
J	Fuel jet momentum ratio
LaRC	Langley Research Center
LES	Large Eddy Simulation
LTO	Landing and Take-off
NOx	Oxides of nitrogen
OPR	Overall pressure ratio

P16	Pressure at station 16 – bypass duct discharge
P3	Pressure at station 3 – HPC discharge
P56	Pressure at station 56 – core duct discharge
PIV	Particle image velocimetry
PLIF	Planar laser induced fluorescence
PMT	Photomultiplier Tube
PP	Pilot primary
PPH	Pounds per hour
PQEX	Extraction Ratio (P16/P56)
PS	Pilot secondary
RANS	Reynolds-averaged Navier–Stokes based CFD design process
ROI	Regions of interest
RQL	Rich-Quench-Lean (combustor)
SAC	Single Annular Combustor
SFC	Specific fuel consumption lbs/hr – fuel flow / thrust
SN	Swirl number
SOA	State of art
SOW	Statement of work
SSBJ	Supersonic business jet
T3	Temperature at station 3 – HPC discharge
T4	Temperature at station 4 – combustor discharge
T41	Temperature at station 41 – turbine rotor inlet
TAPS	Twin Annular Premixing Swirler
TRL	Technology readiness level
Tsat	Fuel boiling point
T/W	Thrust-to-weight
UEET	Ultra Efficient Engine Technology (NASA program)
UG	Unigraphics (drawing software)
UV	Ultraviolet electromagnetic waves
V	Velocity
Vjet	Jet velocity
VOCs	Volatile Organic Compounds
W	Weight
W36	Gas flow station 36 – burner exit
WA36	Air flow station 36 – burner exit
We	Aerodynamic Weber number
WF36	Fuel flow station 36 – burner exit

N+2 Advanced Low NOx Combustor Technology

Final Report

John Herbon, John Aicholtz, Shih-Yang Hsieh, Philip Viars, Shai Birmaher,
Dan Brown, Nayan Patel, Doug Carper, Clay Cooper, Russell Fitzgerald,
Raghavan Pandalai, and Zekai Hong
GE Aviation
Cincinnati, Ohio 45215

1 Summary

In accordance with NASA's technology goals for future subsonic vehicles, this contract identified and developed combustor concepts toward meeting N+2 generation (2020) Landing and Take-Off (LTO) NOx emissions reduction goal of 75% from the standard adopted at Committee on Aviation Environmental Protection 6 (CAEP/6). An advanced engine cycle was identified to meet the N+2 goals for noise, emissions and fuel burn reduction as part of an overall aircraft system. The development of N+2 combustor technology proceeded from CFD-based conceptual design through single cup evaluation rigs and finally the design and fabrication of a 5-cup sector rig containing ceramic matrix composite (CMC) liners. Based on flame tube emissions, dynamics, and auto-ignition testing, one concept was down-selected for sector testing at NASA. The N+2 combustor sector successfully demonstrated >75% reduction for LTO NOx (vs. CAEP/6) and cruise NOx (vs. 2005 B777-200 reference) while maintaining >99.9% cruise efficiency, no increase in CO and HC emissions (vs. CAEP/6), and acceptable dynamic pressures for this stage of development.

The program also developed enabling technologies for the combustion system. Ceramic Matrix Composites (CMC) material properties test data were generated. A conceptual active combustion control scheme was developed, demonstrating reduction in low-frequency combustion dynamics amplitudes in a single-cup test rig. Finally, a laser ignition concept was evolved and tested in a 5-cup sector.

The cost share contract was made possible by the American Recovery and Reinvestment Act of 2009 (ARRA) and by GE cost share. The ARRA cost was required to be separately accounted. To capture cost separately, selected tasks were fully funded by NASA (ARRA), and the remaining tasks were fully funded by GE cost share. The contract was initiated March 12, 2012.

2 Introduction

GE Aviation has extensive experience with low emissions rich burn combustion systems and more recently lean burn systems. Lean burn technology provides a breakthrough in NOx emission levels compared to Rich-Quench-Lean (RQL) designs.

GE has demonstrated the ability to take low NOx technology from concept, through demonstration, to a fielded product. TAPS I (Twin Annular Premixing Swirler) development initiated more than 10 years ago with NASA AST mixer studies, and included a technology demonstration on a CFM56 engine. TAPS I has shown the capability to achieve even greater NOx reductions at cruise than those demonstrated for the Landing and Takeoff (LTO) cycle. This is important because roughly 90% of total NOx from aircraft is emitted at high altitude, and scientific studies indicate that this high altitude NOx significantly affects both climate and surface air quality over much of the globe.

The GEnx TAPS I combustor is shown in *Figure 1*. The design consists of two independently controlled, swirl stabilized, annular flames for low power (pilot) and high power (cyclone) operation. The central pilot flame provides good low power operability and low CO and HC emissions. The cyclone or main flame is concentric with the pilot flame and was designed to produce low NOx emissions during high power operation.

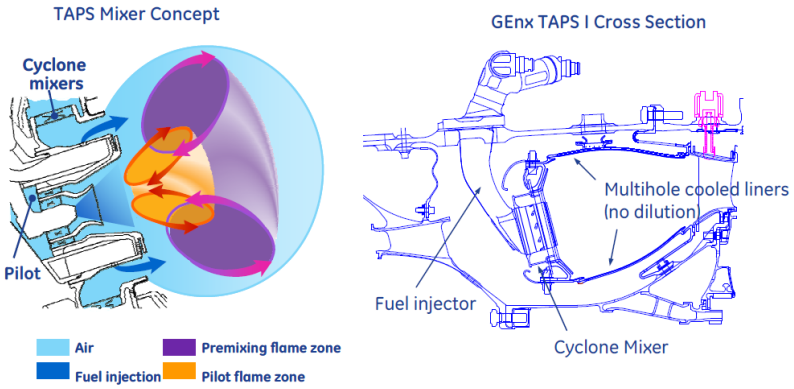

Figure 1 – TAPS I combustor.

During the N+2 Advanced Low NOx Combustor Technology Program, GE has developed a combustor and enabling technologies to target the NASA N+2 NOx goal of 75% reduction below CAEP/6 requirements. As an evolution of the successfully fielded TAPS combustor, the N+2 work is relevant to GE products and can be implemented into advanced combustor designs within the N+2 technology timeframe (2020-2025). The program has pursued this objective through the following series of tasks:

- Extensive design space trade studies were performed around a high bypass advanced engine cycle to find the best balance between fuel burn and acoustics,

while ensuring the advanced low NOx combustor concept could meet the N+2 NOx emissions goal. Preliminary analysis indicated that the concept engine with the advanced Low NOx combustor should be able to meet the N+2 NOx emissions goal of 25% of CAEP/6.

- An extensive RANS-based concept design study was conducted to identify fuel / air mixers and fuel injection concepts for further evaluation in a mixer trade study, mixer diagnostic tests, and flame tube testing. Four major mixer concept groups were evaluated for Single Annular Combustor (SAC) and Dual Annular Combustor (DAC) architectures. Based on the analyses, the team determined total mixer and pilot air flow split targets and down selected three main mixer concepts, based on the SAC geometry, to be further optimized. The concepts were paired with multiple fuel injection schemes and further analyzed to screen and optimize the configurations. A total of 15 mixer/fuel nozzle configurations were down selected for flame tube testing.
- To assist in the assessment of fuel-air mixing performance of the key fuel nozzle/mixer concepts, a laser diagnostic method was developed to evaluate mixedness downstream of the fuel injector. The Planar Laser Induced Fluorescence (PLIF) method enables direct, accurate measurements of fuel / air concentration. Equivalence ratio variations of .02 can be discriminated with better than 3% accuracy. The diagnostic properly accounts for spatial variations in fluorescence signal due to temperature gradients from evaporative cooling and changes in local laser fluence from absorption. Five mixers were tested, including a baseline, over a range of jet momentum ratios to delineate general features of the mixing field, to quantify radial variations in fuel concentration, and to assess relative mixing performance. All of the N+2 nozzles have demonstrably better mixing than the baseline.
- Flametube emissions tests were conducted to screen the down selected configurations and identify designs that could meet the NASA N+2 LTO NOx reduction goal. A flame tube combustor was designed, constructed, and instrumented. Seven concept fuel nozzles and seven mixers were designed and manufactured. The designs were mixed and matched, based on expected performance from earlier CFD results. Flame tube emissions testing was completed for 14 fuel nozzle / mixer configurations. Multiple concepts showed promise to meet or exceed the N+2 LTO NOx Technology Goal of 75% emissions reduction from the ICAO CAEP/6 standard. Three concepts were further down selected for additional flametube tests based on NOx emissions, relative combustion efficiency, and initial combustion dynamics data.
- Three N+2 fuel nozzle / mixer configurations were next tested in the Tunable Combustor Acoustics (TCA) rig to evaluate combustion dynamics sensitivities. The resulting combustion dynamics maps contributed to the ranking of concepts going into the high temperature and pressure flametube tests, and were part of the overall down selection for the final sector configuration.
- The High Temperature and Pressure (HTP) single cup flame tube rig was utilized to evaluate auto-ignition boundaries and emissions performance at near-engine cycle conditions. Three fuel nozzle designs were tested, with all three showing promise to meet the N+2 LTO NOx Technology Goal of 75% emissions reduction

from the ICAO CAEP/6 standard. Emissions data and auto-ignition operability margins were compared, and a single design was down-selected for the sector rig as the best overall performer of the tested configurations.

- The ultimate performance of the advanced technology combustor was demonstrated in a 5-cup combustor sector test at NASA's Advanced Subsonic Combustion Rig facility. An all-new combustor sector rig was designed, fabricated, and instrumented for testing up to the full takeoff conditions of the new N+2 cycle. The combustor incorporates ceramic matrix composite (CMC) liners to enable low liner cooling flows, high mixer air flow splits, and increased levels of fuel-air mixing to achieve the aggressive NOx reduction goals. A set of the final down-selected fuel nozzles and mixers was manufactured and mounted on the combustor prior to delivery to NASA. The combustor testing was completed successfully, including measurements on emissions, combustion dynamics, and thermal data at conditions up to the 85% ICAO cycle point combustor inlet temperature and pressure. While facility limitations prevented testing up to the 100% ICAO takeoff condition, the data was useful for evaluating the combustor performance and indicates that the combustor will achieve >75% reduction of LTO NOx below CAEP/6 standards.

In parallel to the advanced combustor development work described above, enabling technology development was pursued in the following areas:

- Combustion dynamics mapping was conducted on three different test vehicles, including a full annular combustor rig, a core engine, and a turbofan engine. The data generated provide important insight to GE regarding operation of these lean burn combustors.
- Active combustion control concepts were evaluated using a modern aviation gas turbine fuel nozzle in an atmospheric pressure combustor that could be set up to exhibit a low-frequency dynamics mode under fuel-rich conditions. An advanced, fast algorithm was developed to enable closed-loop control, whereby a significant reduction in the amplitude of the low-frequency dynamics mode was achieved.
- GE conducted ignition tests for a laser optical igniter and a standard electrode igniter in a 5-cup sector, demonstrating progress toward the implementation of the laser optical igniter. The laser igniter performance was mapped at various circumferential and axial igniter mounting locations, with two different lens focal lengths and a translating optical stage providing a range of radial positions for the laser spark. The ability for a laser to optimize the spark location within the combustor holds promise for improving aircraft engine ignition and altitude relight capability, especially for highly premixed TAPS combustor configurations.
- CMC material maturation work was performed, evaluating basic material behavior of the GE-developed Ceramic Matrix Composite (CMC) material system. The principal focus was to understand durability of the material system and lay the groundwork for development of life prediction methodologies.

3 Detailed Summary of Combustor Concept Development

3.1 GE N+2 Advanced Low-NOx Combustor Technology

Starting with the legacy Twin Annular Premixing Swirler (TAPS) design developed via multiple technology and commercial programs, including GEnx and LEAP (*Figure 2*), GE has advanced the capabilities of this technology to meet the aggressive N+2 NOx and performance goals. The engine architecture, scale, and cycle were set by an engine-aircraft system analysis, pointing to a concept Hybrid Wing Body (HWB) aircraft and engine that could meet the key N+2 objectives for NOx, fuel burn, and noise reduction. The basic concept behind GE's N+2 combustor design is to increase the fraction of air used for premixing in the front end of the combustor beyond the 70% used in previous TAPS designs [1], while simultaneously adding features that further enhance the fuel-air mixedness. Increased premixing air can present a significant challenge to both operability (efficiency and combustion dynamics) as well as durability (less cooling air for the combustor dome and liner). To meet these challenges, the new combustor design concepts were benchmarked against data from previous successful development programs. A series of combustion tests ultimately provided the opportunity to down-select and further optimize the designs, leading up to the testing of one final configuration in a new 5-cup sector at NASA.

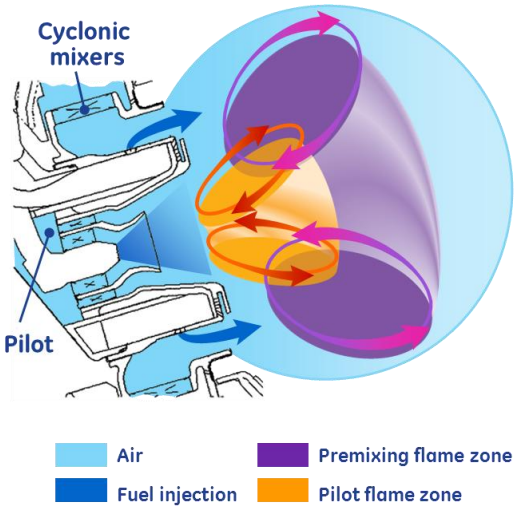

Figure 2 – TAPS Mixer Concept [1]

The combustor development program began with an extensive CFD effort to identify and optimize a suite of main mixer / swirler and main fuel injector concepts that could increase fuel-air mixedness while maintaining the required operability across the range of engine cycle conditions. Main stage swirler concepts included multiple designs intended to increase turbulence for fuel-air mixing, while simultaneously avoiding generation of such excessive turbulence that the swirl number was detrimentally decreased (impacting flame stability) or transporting coherent turbulence downstream into the flame front (impacting combustion dynamics). Concepts included both co-

rotating and counter-rotating vanes. Seven different swirler concepts were down-selected and manufactured for the initial flame tube testing, denoted here as M1-M7.

The CFD effort also explored options for the number and sizing of the main stage fuel injection orifices. Main stage fuel injection concepts included varying both the radial and axial location of fuel injection (relative to the mixer exit), as well as varying the number of fuel injection points. Other concepts explored means for increasing jet penetration into the main stage air flow either mechanically or aerodynamically. Seven different main injection concepts were down-selected and manufactured for the initial flame tube testing, denoted F0-F6. In all of the concept fuel nozzles, a GEnx-style pilot was scaled and utilized for the N+2 combustor due to its proven operational capability.

3.1.1 Flame Tube Testing

In the first combustion screening tests, 13 fuel / air mixer concepts were evaluated in a single-cup flame tube (FT) rig at GE Aviation. The test facility was able to achieve pressure and temperature conditions up to 250psia and 1000F. While this is significantly lower than the take-off and climb cycle points important to the LTO NOx evaluation, the conditions were high enough to enable fully-staged operation (fuel splits similar to the takeoff design point) and perform a relative assessment of the NOx performance of the different designs. NOx emissions were measured over a range of temperature and pressure conditions, fuel / air ratios, and pilot / main fuel splits. Data was collected using a single point probe, taking samples at multiple discrete radial locations at steady-state conditions. Dynamic pressures in the combustor were measured through the flame tube liner using Kulite sensors. Comparative data at the 100% ICAO fuel/air ratio (FAR) is shown in *Figure 3*.

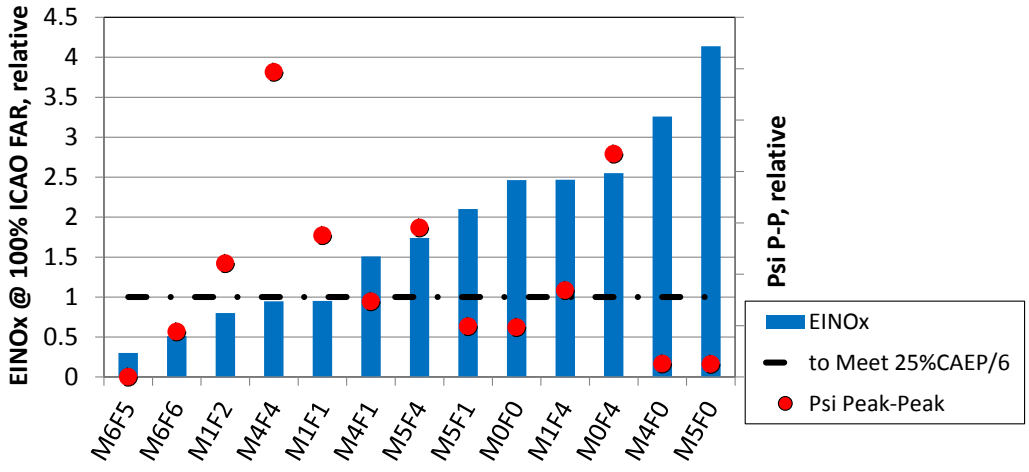

Figure 3 – Flametube EINOx Emissions and Combustion Dynamics Data at Max Rig Conditions

Flametube EINOx emissions and combustion dynamics data (100% ICAO fuel / air ratio) at maximum rig conditions (1000F/250psia). The dynamic pressure data represent the maximum peak-to-peak amplitude recorded during steady-state operation at these specific conditions, and serves as a relative indicator of potential dynamics concerns for each concept. A normalized EINOx = 1 indicates the target EINOx value required at these conditions and fuel / air ratio to meet 25% CAEP/6 LTO NOx in the full combustor.

The expected performance of each concept relative to the LTO NOx goal is a critical assessment, and provides a quantitative target for acceptability of any given design. Rig data at this stage of the program was limited to low T3/P3 conditions (1000F/250psia) in the flame tube geometry. LTO NOx was therefore estimated from the flame tube data – corrected for T3, P3, and flame tube-to-engine combustor correlation factors based on legacy programs. Those calculations provide a target EINOx level for the 100% ICAO fuel / air ratio, as measured at maximum flame tube conditions, which would be required to meet the 25% CAEP/6 objective in the eventual sector test.

The flame tube testing provided a fairly clear comparison of the performance of the various concepts. The configurations were ranked based on NOx emissions, the most important factor in the down-select. Efficiency calculations, based on CO and unburned hydrocarbon measurements, were also evaluated and used to compare concepts. Quantitative efficiency measurements are considered less reliable in the flame tube versus an actual combustor due to the differences in flame geometry and recirculation zones; however, these measurements highlight a potential challenge that must be met as combustor designs continue to get leaner and more premixed. At the lower cruise fuel / air ratios, the lowest-NOx designs also tend to have efficiencies that fall off faster as fuel / air ratio decreases. Finally, dynamic pressure data identified two concepts with elevated concerns for combustion dynamic sensitivities, specifically the M0 / M1 mixer family and F4 fuel nozzle design.

Based on flame tube data, three concepts were chosen for further design and testing. The M6F6 concept was chosen due to its ultra-low NOx performance and a slightly better efficiency than the M6F5. The M1F2 concept provided the next-best NOx performance, with better relative efficiency than M6F6 but somewhat higher dynamic pressure signatures. Finally, the M4F1 concept was chosen for its fairly good NOx performance, but especially its improved dynamics and slightly better efficiency than the M1F2 concept. These three designs provided a range of mixer and fuel injection strategies going into the next round of screening tests.

3.1.1.1 Tunable Combustor Acoustics Testing

The three concepts down-selected from flame tube testing were further evaluated in a similar flame tube rig with tunable acoustic boundary conditions. This rig allows a more detailed mapping of the relative acoustic sensitivities of the designs. The dynamics data provide relative comparisons of the operability limits of the three tested configurations, and delineates the differences and features of these designs. At 1000F, the M4F1 and M6F6 configurations show acceptable acoustics throughout the desired FAR36 and main / pilot split range of the nozzles. The M1F2 design, with its more aggressive mixer, encounters the dynamic pressure boundary limit at lower FAR36 and Main fuel flow split, making it the less attractive design from an acoustics point of view.

3.1.1.2 High Temperature / Pressure Flame Tube Testing

In the next round of testing, new engine-style fuel nozzles were manufactured to advance the concepts into the form that would eventually be tested in the 5-cup sector. These final single-cup flame tube tests were designed to validate the concepts at high T3, P3 conditions near the 100% ICAO cycle point, including high power emissions measurements and evaluation of durability risk due to auto-ignition. Three concept nozzles were manufactured: F1, F2, and F6. The F1 and F2 nozzle concepts were slightly modified to improve durability as well as achieve an expected further reduction in NOx emissions. Both nozzles were tested with the M4 mixer due to its lower acoustics sensitivity compared to M1.

Emissions data on JetA fuel was collected using a single point, traversing probe. The probe tip location yields an effective combustor volume similar to a single cup in the sector rig. Most data was collected using a 5-point traverse in order to get data at more conditions in the available test time. Initial data points each day were conducted using a 9-point traverse (every 10% of diameter), and emissions data was calculated using all 9 points as well as only 5 points to ensure low sensitivity to the reduced number of points.

Area-averaged NOx data for all three tested configurations at 85% and near-100% ICAO generated the final ranking of the concepts with respect to LTO NOx. The less aggressive mixing of the M4F2 resulted in predictably worse NOx than the M4F1. Similar to the initial flame tube measurements, the M6F6 configuration exhibits the best NOx performance but worse CO (and therefore efficiency) compared to the M4 designs.

3.1.1.3 Auto-Ignition Margin Data

The high temperature / pressure flame tube rig also was utilized to collect auto-ignition data for all three configurations. Auto-ignition boundaries were mapped at various combustor inlet conditions up to the maximum facility capabilities. Due to facility and schedule constraints, only one data point for M6F6 could be collected.

Auto-ignition data were reduced using GE design tools, and a relative risk is calculated for the different designs at 100% ICAO N+2 conditions on JetA fuel. Of the three N+2 designs, only the M4F1 meets the criteria for acceptable operational margins. The risk level can be re-assessed for the specific alternative fuels of interest to NASA for use in future ASCR tests.

3.1.1.4 Conclusions for Flame Tube Testing

Data from the three flame tube test campaigns is summarized in *Table 1*, and leads to the down-select of a design for the 5-cup sector. An LTO NOx re-assessment, based on the high temperature and pressure flame tube data, indicated that all three designs could likely meet the 25% CAEP/6 NOx target. This assessment uses a correction for flame tube versus sector emissions data. Among the three designs tested in all three rigs, the M4F1 design resulted in the best balance between NOx emissions

performance, combustion efficiency, auto-ignition margin, and combustion dynamics; and was selected for the sector test.

Table 1 – Summary of Flame Tube Results

TCA/HTP Configs	FT Normalized EINOx	FT P4' p-p Ranking 1 = Best	FT Cruise Eff. Ranking 1 = Best	TCA P4' p-p Relative to max limit	HTP Normalized EINOx	HTP A/I margin Relative to limit
M6F6	0.512	1	3	-	0.343	-
M1F2	0.800	3	2	>		
M4F2					1.07	-
M4F1	1.509	2	1	<	0.720	+

At 100% ICAO FAR for the top concepts

3.1.2 Sector Testing

A major part of the combustor development program was the design and manufacturing of a new 5-cup sector rig for operation at the NASA ASCR facility (*Figure 4*). The combustor design utilizes high temperature liner materials in order to reduce cooling air requirements and enable the high mixer air flow split. Mechanical and thermal analyses were performed, and the cooling design and mechanical construction were optimized to ensure viability of the hardware up to the takeoff conditions of the engine cycle.

Figure 4 – GE N+2 5-Cup Combustor Sector Rig

The combustor rig has four emissions rakes, each with four sample elements. Rakes are located within Cups 2, 3, and 4, and are spaced in different locations relative to the cup centerline in order to capture a comprehensive averaged sample when all 16 sample points are ganged together (*Figure 5*). Generally, data is taken at a fixed rig T3, P3, and dP/P3 while the overall fuel / air ratio is swept over the range of interest.

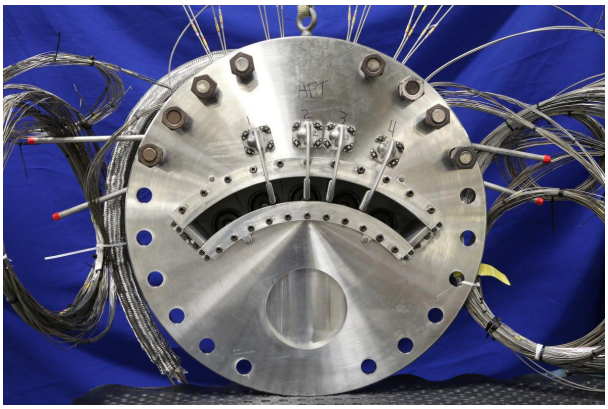

Figure 5 – GE N+2 Sector Rig – Emissions Rake Layout

Combustor emissions data is presented in *Figure 6 through Figure 8*. Data for 7% ICAO is shown in *Figure 7*. Additional single points taken on two other test days are shown to confirm fairly good repeatability of the data. Data for 30% ICAO is shown in *Figure 8*. Data for the 85 and 100% ICAO points are shown in *Figure 8*.

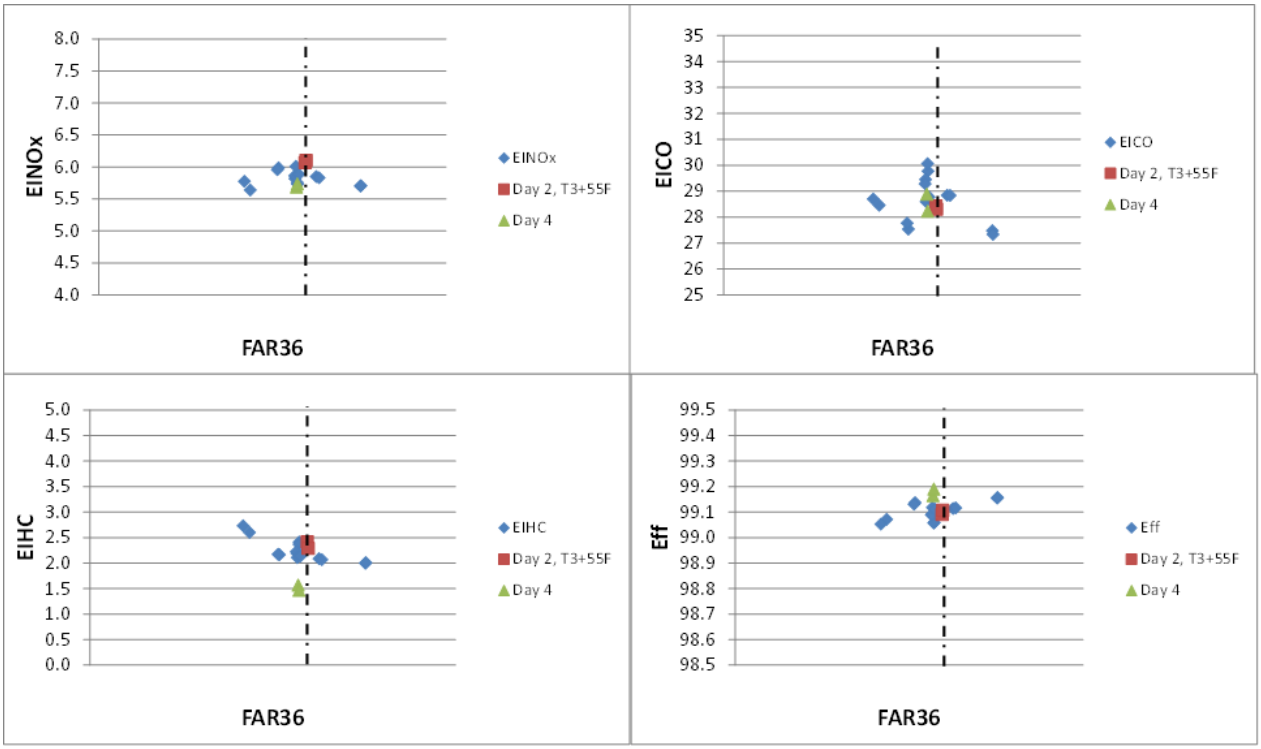

Figure 6 – Sector Rig Emissions Data for 7% ICAO

Sector rig emissions data (EINOx, EICO, EIHC, and combustion efficiency) at the 7% ICAO point, plotted versus the fuel / air ratio based on sampled emissions. Repeated points taken on 2 additional test days are shown for repeatability. The vertical line indicates the target 7% ICAO cycle fuel / air ratio.

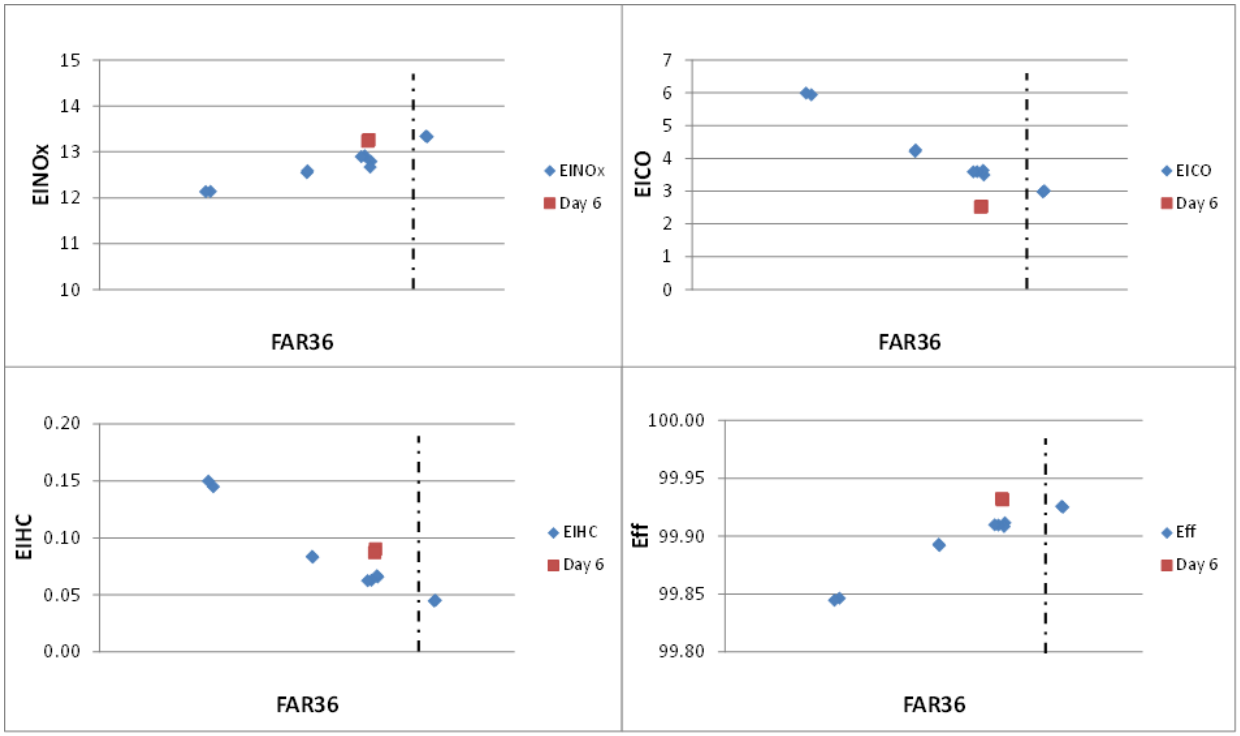

Figure 7 – Sector Rig Emissions Data for 30% ICAO

Sector rig emissions data (EINOx, EICO, EIHC, and combustion efficiency) at the 30% ICAO point. The vertical line represents the target fuel / air ratio.

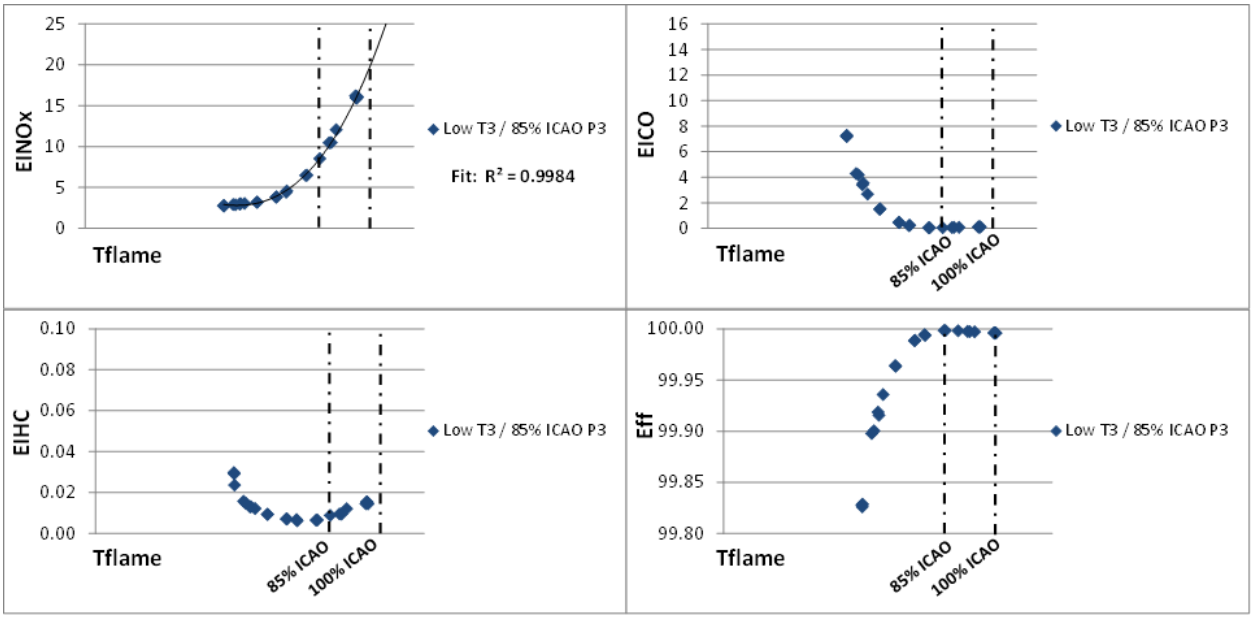

Figure 8 – Sector Rig Emissions Data for 85 and 100% ICAO

High pressure, fully staged emissions data at the 85% ICAO P3 and maximum facility T3 for this air flow rate, for determination of the 85 and 100% ICAO NOx values. Vertical dashed lines represent the target cycle flame temperature for 85% and 100% ICAO.

In general, NOx emissions results in the sector tests were in line with expectations based on correlations (low power, pilot-only points) and the high temperature / pressure flame tube data (high power, fully staged operation). *Table 2* summarizes the LTO emissions data for the ICAO points. The facility was unable to deliver T3 temperatures high enough to run the 85% and 100% ICAO points at the exact T3 / P3 / flow / FAR conditions. The 85% ICAO point is taken directly from the data in *Figure 8* at the appropriate mixer flame temperature. For the 100% ICAO point, the data in *Figure 8* was curve fit and extrapolated to the appropriate flame temperature. The standard humidity correction, based on the measured dew point in the combustor inlet air, was applied to *Figure 6 through Figure 8* to arrive at the final EINOx values in *Table 2*.

Table 2 – LTO Emissions Results for the GE N+2 5-Cup Sector

% ICAO	EINOx	EICO	EIHC
100	17.62	0.20	0.01
85	7.89	0.05	0.01
30	11.75	3.13	0.05
7	5.18	28.44	2.13
% CAEP/6:	**18.9%**	**20.4%**	**8.8%**

Cruise NOx emissions and efficiency were also measured. The combustor demonstrated 76% reduction in EINOx over the 2005 best-in-class, with better than 99.9% efficiency.

3.1.3 Conclusions

Based on the emissions data from the 5-cup sector, the GE combustor has delivered 19% CAEP/6 NOx, surpassing the N+2 goal of 25% CAEP/6, with good combustion efficiencies and acceptable dynamic pressures for this stage of development. Further advancement of this technology will focus on thermal and mechanical durability, manufacturability, and optimization of the design to balance combustion efficiency and dynamics versus LTO NOx capability.

4 Methods, Assumptions, and Procedures

4.1 Task 1.1 – Systems Analysis and Advanced Engine Cycle Selection (NASA Funded)

4.1.1 Summary

Extensive design space trade studies were performed around a high bypass advanced engine cycle to find the best balance between fuel burn and acoustics, while ensuring the advanced low NOx combustor concept could meet the N+2 NOx emissions goal. The initial studies identified a fan diameter and pressure ratio that would provide the best balance in making 60,000 lb reference take-off thrust while maximizing fuel burn and minimizing noise. Based on the T3/T41 parametric study investigating the trade between fuel burn and emissions at various core temperatures, a core configuration was selected that had the best balance between fuel burn and emissions. Preliminary analysis indicated that this engine with the advanced Low NOx combustor would be able to meet the N+2 NOx emissions goal of 25% of CAEP/6. When flown with NASA advanced Hybrid Wing Body (HWB) aircraft, the resulting average engine performance fuel burn improvement exceeded -40% relative to the 777-200ER. Based on GE's preliminary design acoustic prediction methodology and achieving 20 dB acoustic shielding from the HWB, it is estimated that this configuration has the potential to achieve NASA N+2 noise goals.

4.1.2 Introduction

The focus of this effort was to design an advanced engine cycle with an advanced combustor that would meet the NASA N+2 goal for LTO (landing and takeoff) NOx emissions of 25% of CAEP/6, with technologies aimed at TRL 6 by 2020. The purpose of Task 1.1 was to identify the engine design trade space and select an advanced engine cycle consistent with the NASA N+2 timeframe with improved fuel burn and noise characteristics. The intent was to show the capability to meet the N+2 goals for noise, emissions, and fuel burn as part of an overall aircraft system.

4.1.3 Methods, Assumptions, and Procedures

4.1.3.1 Kick-off

The program kick-off meeting was held at NASA's Glenn Research Center on April 20, 2010, satisfying the first required program deliverable. Fay Collier (NASA LaRC) spoke to the group about NASA's recent adjustments to their N+2 goals moving TRL 6 further out to 2020 (*Table 3*), including a stretch goal of 50% fuel burn reduction. While GE was not contractually required to make this adjustment, Fay indicated that he would like GE to consider introducing additional technologies that might be potentially available in this extended time period.

Table 3 – NASA ERA Goals, Including a Stretch Goal of -50% Aircraft Fuel Burn

	N+1 (2015 TRL6)	N+2 (2020 TRL6)	N+2 (2030 TRL6) ?
CORNERS OF THE TRADE SPACE	**N+1 (2015 EIS) Generation Conventional Tube and Wing (relative to B737/CFM56)**	**N+2 (2020 IOC) Generation Unconventional Hybrid Wing Body (relative to B777/GE90)**	**N+3 (2030-2035 EIS) Advanced Aircraft Concepts (relative to user defined reference)**
Noise (cum. below Stage 4)	**-32 dB**	**-42 dB**	**55 LDN at average airport boundary**
LTO NOx Emissions (below CAEP 6)	**-60%**	**-75%**	**better than -75%**
Performance: Aircraft Fuel Burn	**-33%**	**-40%** -50%	**better than -70%**

Task 1.1 began in late March. Goals, assumptions, and preliminary cycle data from these studies were presented at the program kick-off meeting with NASA. The GE team chose to target a Hybrid Wing Body (HWB) aircraft configuration to help meet the program fuel burn and aircraft noise goals, *Figure 9*. [2]

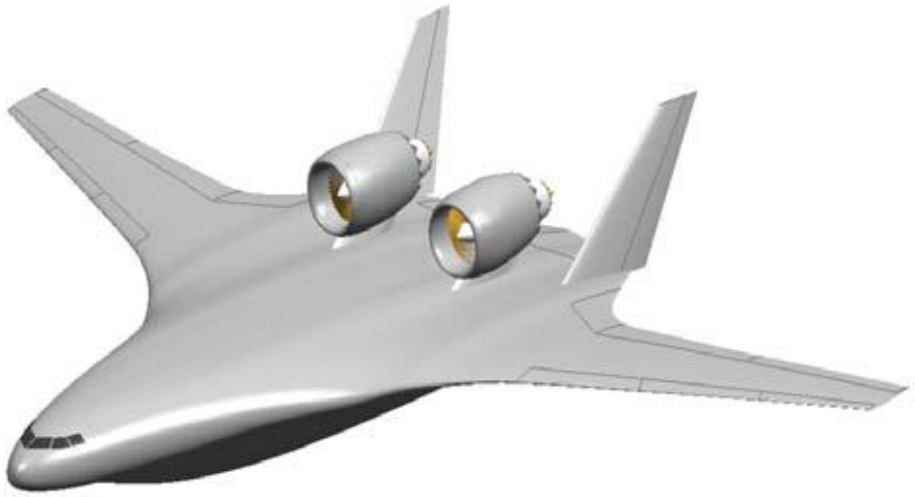

Figure 9 – NASA Hybrid Wind Body Configuration HWB [2]

Based on a number of NASA and industry studies [3,4,5], the HWB configuration appeared to be capable of delivering an additional 20 dB (see *Figure 10*) reduction in cumulative noise due to shielding from the large wing while matching the fuel burn reduction capability of advanced tube and wing configurations [2,5,6,7].

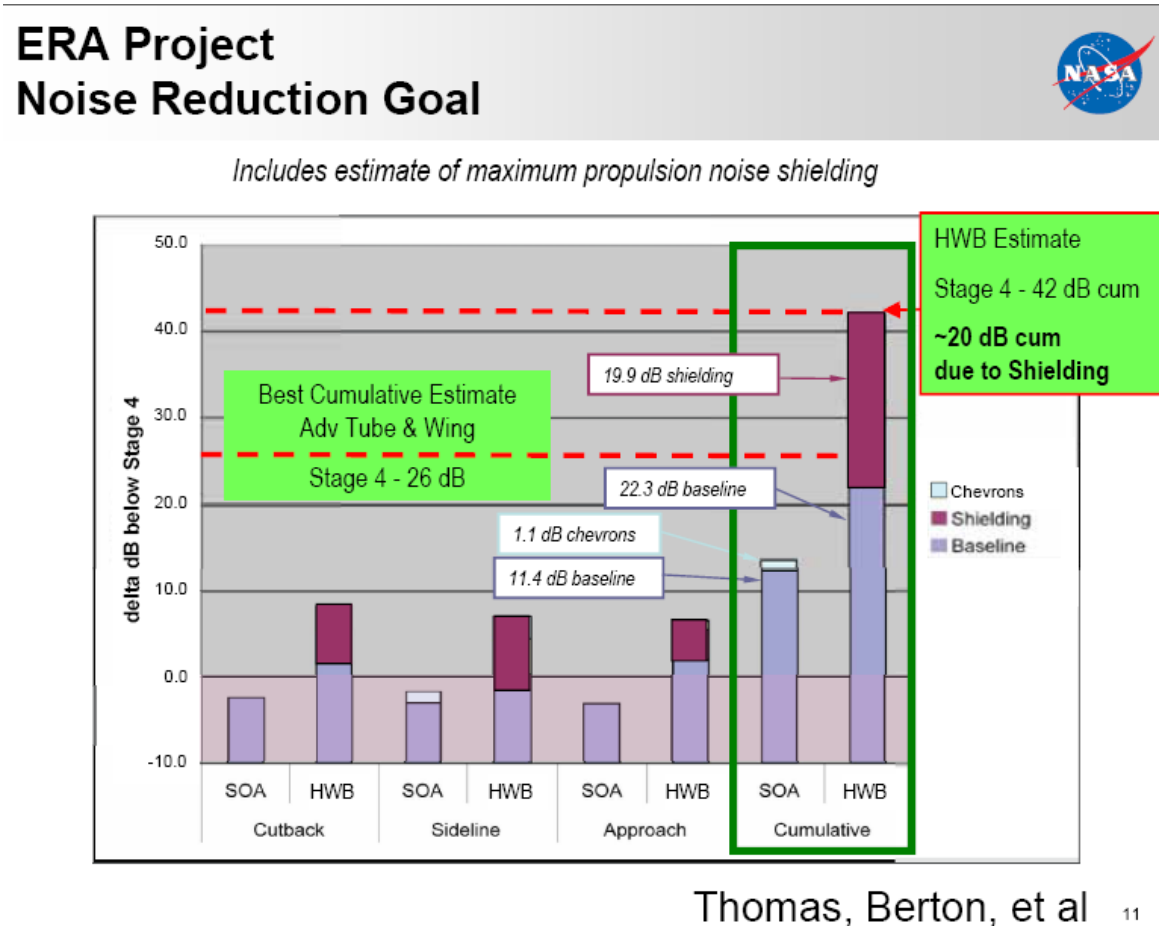

Figure 10 – NASA Estimates for Acoustic Noise Reduction for HWB [5]

Based on NASA and other industry studies [2,5,6,7], the HWB with its advanced composite structure and advanced aerodynamics has been shown to be able to meet 30% to 35% out of the desired 50% N+2 fuel burn goal (*Figure 11*). NASA has been performing studies around an advanced podded HWB to replace the 777-200ER and 777-200LR. The aim of this investigation was to leverage those studies and use the GE N+2 Low NOx Combustor engine in place of the advanced engine that has been used in the NASA studies. An attempt was made to carry the same payload at the same design range with the GE N+2 engine at a size no larger than the contractually required thrust limit of 60,000 lb. The engine had to meet minimum Thrust to Weight (T/W) requirements for take-off and low speed acoustic climb-out performance. If the 60,000 lb thrust engine did not meet the 777-200ER, then reductions in payload or range were investigated to develop a configuration that best balanced all of the goals and requirements.

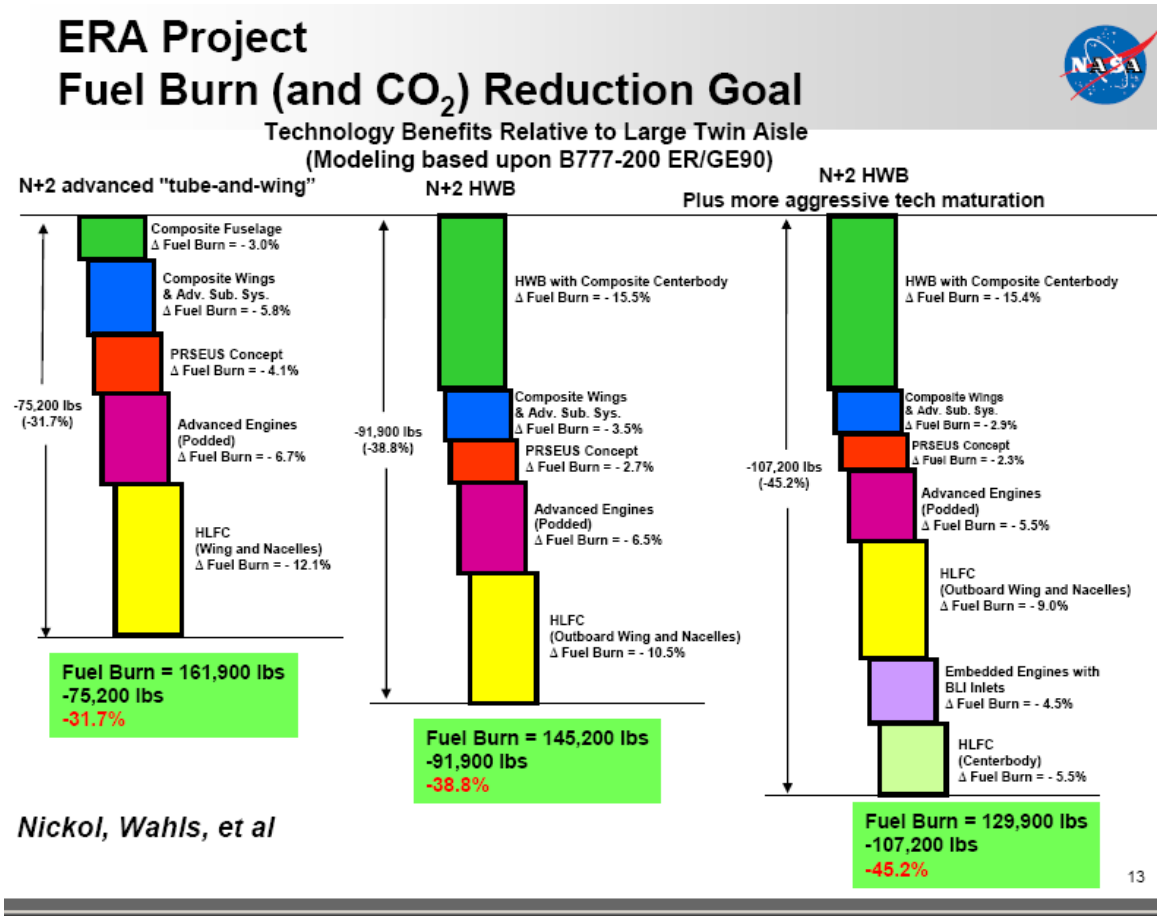

Figure 11 – NASA Estimates for Fuel Burn Reduction from HWB [2]

4.1.3.2 Initial System / Cycle Studies

The initial cycle studies were focused on designing an engine with 50,000 to 60,000 lb of take-off reference thrust. For the purpose of this study, take-off reference thrust is defined as 1.25 times Mach 0.25 sea level ISA +27F thrust.

4.1.3.3 Cycle / Acoustics Design Space Trade Analysis

For these cycle studies, GE initially generated a 25 engine DOE and fit a response surface to it, in order to isolate desired FPR and some other cycle characteristics, including BPR, OPR, and Extraction Ratio (PQEX). Design maximum T41 typically sets BPR or core size and T3 sets OPR. Extraction ratio (PQEX) is bypass duct exit pressure over core exit pressure (P16/P56).

Results from the response surface analysis did not indicate a clear optimum extraction ratio (PQEX, P16/P56), so an additional parametric study focusing on PQEX was performed. An extraction ratio typical for high bypass turbofans was chosen for the next set of engine studies.

A final parametric study was performed to determine the best FPR to balance acoustics and fuel burn in the engine selection for the system study.

4.1.3.4 T3 / T41 / Emissions Design Space Trade Analysis

The next phase of the cycle selection study involved generating a matrix of engines designed over a range of T3's (OPR) and T41's (BPR) to assess the overall impact of emissions on fuel burn. The range of core temperature variations were set to cover early GE90 temperatures up to levels considered possible for a 2020 TRL 6.

This cycle data was passed on to the Combustor Group to calculate emissions over the range of T3 and T41 for the engines. The emissions data was then used to set the design T3 and T41 for the final cycle selection.

4.1.3.5 Combustor Technology / Emissions Design Space Trade Analysis

One of the primary goals of NASA N+2 is to develop combustor technology capable of demonstrating NOx emissions levels of 25% of the CAEP/6 requirements. As NOx increases significantly with increasing combustor operating temperatures (T3 and T4), this goal is in conflict with the N+2 goal associated with fuel burn savings. Typical turbofan engine cycles running at higher levels of T3 and T4 show reduction in engine Specific Fuel Consumption (SFC), and thereby lower fuel burn.

In conjunction with the engine cycle performance study, a study of the predicted levels of NOx emissions over the ICAO LTO (Landing Takeoff) cycle for various types of TAPS lean burn mixers was conducted. The ICAO LTO cycle was based on four engine operating points: 100%, 85%, 30%, and 7% of rated engine thrust at sea level standard day conditions. This LTO cycle was meant to look at emissions in and around airports as aircraft depart and arrive. *Table 4* shows the operating times assigned for each of these operating points.

Table 4 – ICAO LTO Cycle Points and Time Scales

Landing-Takeoff Cycle (Represents operation below 3000 Ft)		
Mode	% Power	Time (min)
Taxi-Idle	7	26.0
Takeoff	100	0.7
Climb	85	2.2
Approach	30	4.0

LTO NOx emissions numbers were generated on a single engine basis using available NOx emissions correlations based on GEnx TAPS engine certification data and limited available data from advanced TAPS mixers tested under the GEnx and PROP21 programs. The LTO NOx level was normalized by the engine operating pressure ratio and then compared to the ICAO CAEP/6 requirement for the N+2 engine thrust class to present the NOx emissions as a percent of the CAEP/6 requirement. At this stage in

the program, this study included looking at two classes of TAPS main stage mixers: the GEnx mixer and an advanced TAPS mixer. For each of these two main stage mixers, three different levels of main stage mixer air flow split were analyzed. The NOx predictions were made for each engine configuration (T3 and T41 combination) of the engine cycle performance model study. The NOx prediction results were plotted along with the engine SFC reductions versus engine operating T41.

The information from these plots provides insight into what level of TAPS main mixer technology and mixer air flow level will likely be required to support the N+2 fuel burn and NOx emissions goals. As the engine T3 and T41 increase in support of meeting fuel burn goals, the need to use advanced mixers with increasing mixer flow is evident. The results of this study indicate that we will need technology beyond the legacy mixer design, and we will most likely need higher mixer air flow split.

4.1.3.6 Final Engine Cycle Selection

After review of the data from the T3/T41 matrix (*Section 4.1.3.4*) and the emissions trade studies (*Section 4.1.3.5*), the core temperatures for the cycle for the NASA N+2 Combustor study were selected A preliminary design of the combustor sector rig for the Phase I tests was conducted based on the final engine cycle chosen. For the Low NOx combustor design, LTO cycle data was generated and delivered to the Combustor Group for the preliminary design of the rig.

4.1.3.7 HWB Mission, Sizing, and Fuel Burn Analysis

In a meeting with NASA personnel, Craig Nickol (NASA LaRC) discussed more aggressive aircraft technologies expected to be developed to Technology Readiness Level 6 by 2020 for the advanced hybrid wing body configuration as shown in *Figure 12*.

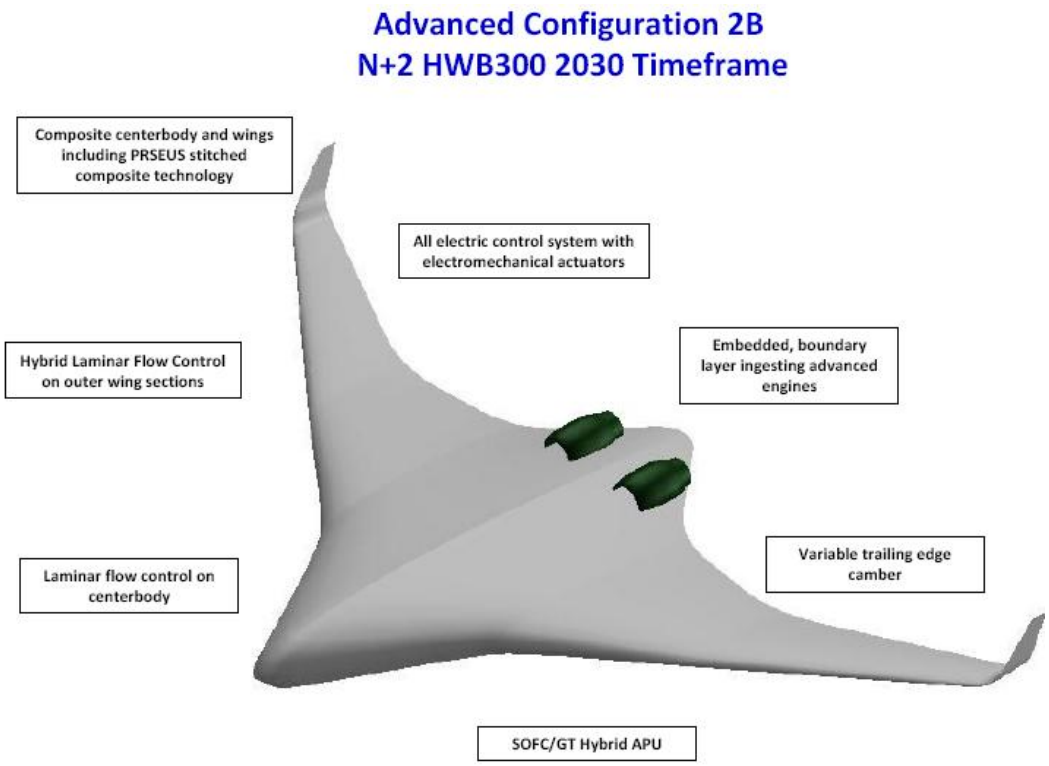

Figure 12 – Advanced N+2 HWB Using Aggressive Technologies [7]

4.1.3.8 HWB Low Speed Performance Analysis

The N+2 acoustic goal is that the predicted noise be at or below FAR Stage IV –42 dB analyzed cumulatively at three points in the sky relative to the airport. These three points specified in FAR 25 are illustrated in *Figure 13*. To perform the acoustic analysis, it is necessary to estimate the thrust required at each acoustic measuring point, along with the aircraft velocity, altitude, and distance.

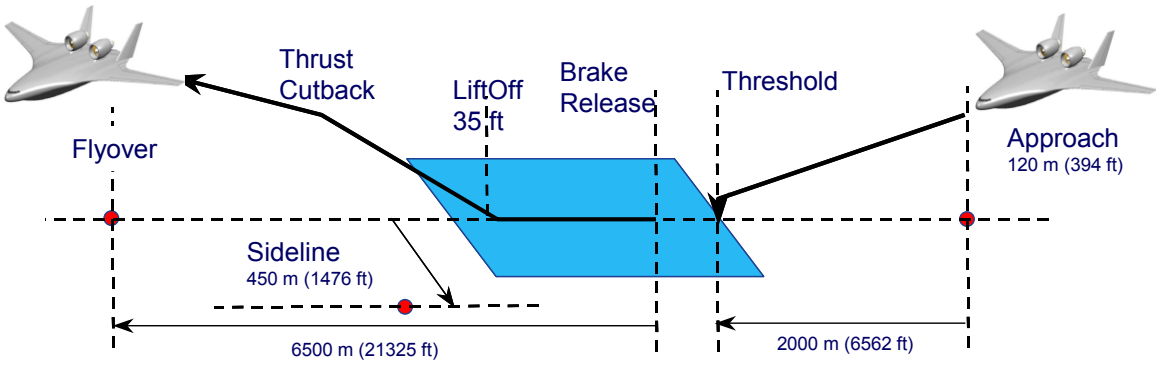

Figure 13 – Acoustic / Low Speed Performance

4.1.3.9 HWB Acoustic Analysis

To determine the feasibility of reaching the N+2 acoustic goals shown in *Table 3*, a community noise assessment was performed using GE's preliminary design noise

estimate tool. Results of the acoustic analysis for the advanced aircraft and engine system defined for the advanced low NOx combustor design showed that meeting the acoustic goal of 42 EPNdB cumulative margin (from the three FAR25 specified measurement points – see *Figure 13*) below Stage 4 limits (52 EPNdB cumulative margin below Stage 3) without the introduction of unconventional advanced acoustic technology is achievable.

4.1.4 Conclusions

The purpose of Task 1.1 was to identify the engine design trade space and select an advanced engine cycle consistent with the NASA N+2 timeframe that could meet the NASA N+2 goal for LTO NOx emissions of 25% of CAEP/6 with technologies aimed at TRL 6 by 2020. The intent was also to identify an engine cycle with improved fuel burn and noise characteristics that support the intent to meet the N+2 goals for noise, and fuel burn as part of an overall aircraft system.

Extensive design space trade studies were performed around a high bypass advanced engine cycle to find the best balance between fuel burn and acoustics, while ensuring the advanced combustor concept could meet the N+2 NOx emissions goal. An engine capable of 60,000 lb reference take-off thrust was designed. Based on T3/T41 parametric study, the final engine cycle was selected. The emissions trade study showed that this engine with the advanced Low NOx combustor should be able to meet the N+2 NOx emissions goal of 25% of CAEP/6.

When flown with the NASA advanced Hybrid Wing Body (HWB) aircraft, the resulting average engine performance fuel burn improvement exceeded the N+2 goal of -40% relative to the 777-200ER.

Based on GE's preliminary design acoustic prediction methodology and achieving 20 dB acoustic shielding from the HWB, GE's acoustic PD prediction tools indicated this configuration has the potential to achieve Stage IV –45 dB.

All results from the GE Systems Analysis and Advanced Engine Cycle Selections for the NASA N+2 Low NOx Combustor contract should be considered as nominal (50% confidence) preliminary design data with no implied guarantee or commitment on the part of GE Aviation.

4.2 Task 2.1A – Design Identification of Combustor, Fuel Injector, and Mixers (GE Funded)

4.2.1 Summary

The objective of this Task was to identify fuel / air mixers and fuel injection concepts for further evaluation in mixer trade study, mixer diagnostic, and flame tube testing. In this Task, GE carried out an extensive RANS-based design study for the proposed mixer concepts, based on the Single Annular Combustor (SAC) and the Dual Annular Combustor (DAC) combustor architectures. Over forty mixer configurations in total were designed and analyzed using RANS CFD. Non-reacting and reacting flow fields and NOx emission indices for all the configurations were post-processed from the simulation results to rank the mixer performances. Based on the analyses of flow fields and NOx emissions, the team concluded that in order to achieve the low NOx emission goal of this program the total mixer air should be increased above legacy experience. In addition, mixers that can generate high turbulence levels have potential of producing good premixing fuel / air mixture and low NOx emissions. Therefore, the team down-selected 3 specific mixer concepts based on the SAC combustor architecture to be further studied and optimized in the mixer trade study task.

4.2.2 Introduction

One of the primary goals of the N+2 program was to develop combustor technology capable of demonstrating NOx emissions levels of 25% of the CAEP/6 requirements. With the trend for NOx to increase significantly with increasing combustor operating pressure and temperatures, it was a daunting task for meeting this goal without innovative combustion technology development. Based on experience gained from Twin Annular Premixing Swirl (TAPS) technology development under Advanced Supersonic Transport (AST), Ultra Efficient Engine Technology (UEET), Propulsion 21, and Supersonic Business Jet (SSBJ) programs; and TAPS technology transition to the GEnx product, GE has developed the technical expertise required to successfully operate low-emissions combustors throughout the engine operating regimes without adversely impacting other critical design requirements. *Figure 14* shows the schematic of the TAPS combustion concept. The key to success is how to transition the complex gas turbine combustor flame structure from pilot diffusion flame anchored around the fuel nozzle to multiple flame stabilization regions with a varying degree of mixing that produces ultra-low NOx emissions, as illustrated in *Figure 14*.

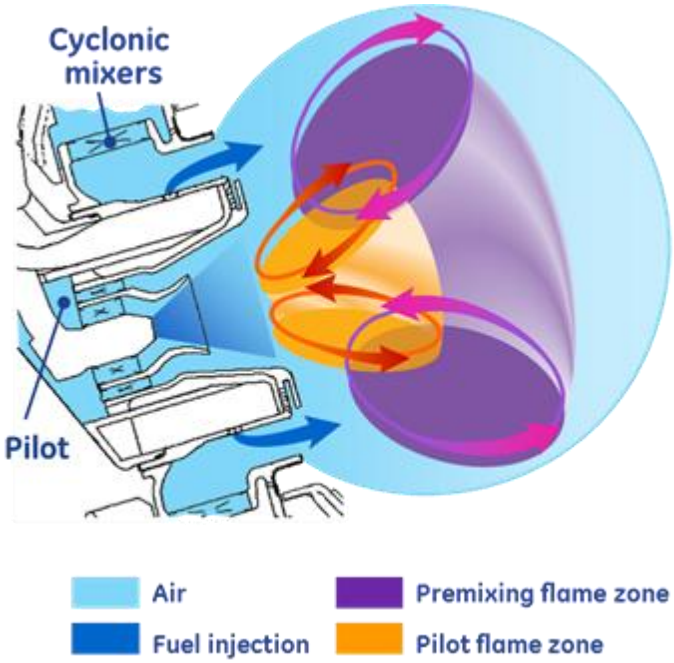

Figure 14 – Schematic of TAPS Combustion Concept

From emissions assessments conducted using the preliminary N+2 cycle conditions, the team believed that further development of TAPS combustion concept has a great potential of achieving the program requirement. Therefore, the main focus of this task was placed on identification of combustor, fuel nozzle, and mixer concepts, based on TAPS combustion technology, that show potential of meeting program requirement for further design optimization study in Task 2.1. The remainder of this portion of the report is organized as follows: *Section 4.2.3* describes the method of approach and Reynolds-Averaged Navier-Stokes (RANS) CFD-based design process used in this Task. *Section 4.2.4* discusses the results from this study. Finally, the conclusion of this study is presented in *Section 4.2.5*.

4.2.3 Methods, Assumptions, and Procedures

The method employed in this task for identifying combustion concepts, mainly mixer and fuel nozzle configurations, was a combination of Reynolds-Averaged Navier–Stokes (RANS)-based CFD design process and correlations developed at GE Aviation.

4.2.4 Results and Discussion

Task 2.1A began with a brainstorming and concept identification meeting. At this meeting, a number of GE engineers from Aviation and the Global Research Center (with extensive experience on a variety of combustor development programs) discussed combustor architecture, fuel / air mixing, and combustor cooling technologies that could be considered for the NASA N+2 program. Following this meeting, a list was developed of main mixer concepts to be studied in this task via RANS-based CFD analysis. Main stage mixer concepts included multiple designs intended to increase turbulence for fuel-

air mixing, while simultaneously avoiding generation of such excessive turbulence that the swirl number was detrimentally decreased (impacting flame stability) or transporting coherent turbulence downstream into the flame front (impacting combustion dynamics). Concepts included both co-rotating and counter-rotating vanes. Four different swirler primary concepts were laid out for evaluation in this task, eventually becoming the mixer designs denoted as M0/M1 (two versions of the same design), M4, M5, and M6/M7 (two versions of the same design) in later Tasks.

Emissions estimations using CHEMKIN calculations were carried out and then compared to data correlations from existing combustors. Compared to legacy designs, more of the combustor air should be directed through the pilot and main mixers to provide the target NOx reduction relative to current TAPS technology. In addition, TAPS technology with the Dual Annular Combustor (DAC) architecture shows significant NOx reduction compared to the Single Annular Combustor (SAC) architecture. Therefore, the team decided to pursue both SAC and DAC combustor architectures in this task. Preliminary airflow splits were then defined for each main mixer / fuel nozzle and combustor architecture concept so that the main mixers and fuel nozzles could be sized appropriately.

4.2.4.1 Auto-Ignition and Fuel Penetration Study

Before the team fully engaged in design studies of the above-mentioned mixer concepts, the team first conducted an auto-ignition risk investigation and fuel penetration study to determine the fuel injection location for the main mixer. Since the combustor will operate at very high pressure and temperature, auto-ignition is a potential concern. Balancing this factor along with fuel / air mixing determines the target location for fuel injection.

The team post-processed all the reacting flow results, analyzing the fuel/air mixing characteristics. The NOx emissions index was estimated using a GE Proprietary post-processing tool for each of the configurations analyzed, and the configurations were ranked and down selected for further optimization in Task 2.1.

4.2.5 Conclusions

In this Task, an extensive RANS-based design study has been carried out for the proposed mixer concepts, including a variety of designs intended to manipulate turbulence intensity and fuel-air mixing, based on the Single Annular Combustor (SAC) and the Dual Annular Combustor (DAC) combustor architectures. Non-reacting and reacting flow fields and NOx emission indices for all the configurations were post-processed from the simulation results to rank the mixer performances. Based on the NOx emissions analysis, the team concluded that the mixer configuration should have a mixer air flow split somewhat higher than in legacy designs, in order to achieve lean premixed combustion for low NOx emissions. Also, mixers that can generate high turbulence level have potential of producing good premixing fuel / air mixture and low NOx emissions. However, due to the complexity of the DAC combustor architecture and the cost of fuel nozzle, the team decided to stay with the SAC combustor

architecture. Therefore, the team down-selected the 3 mixer concepts based on the SAC combustor architecture to be further studied and optimized in the mixer trade study task.

4.3 Task 2.1 – Design and Trade Studies of Combustor, Fuel Injector, and Mixers (NASA Funded)

4.3.1 Summary

The objective of this Task was to carry out an extensive RANS-based design and optimization study for the three down-selected mixer / fuel nozzle concepts from Task 2.1A and identify multiple configurations for further evaluations in flame tube testing. Over thirty mixer configurations in total were designed and analyzed using RANS CFD. Non-reacting and reacting flow fields and NOx emission indices for all the configurations were analyzed and post-processed from the simulation results to screen the mixer configurations. Based on the design criteria and Figure Of Merit (FOM) established in this study, the team concluded that the M1 and M6 mixer configurations have a great potential of meeting the NOx emission goal of this program because of the enhanced fuel / air mixing produced by the strong turbulence generated by the mixers. A total number of fifteen mixer / fuel nozzle configurations were down-selected by the team, including seven M1 configurations, three M4 configurations, two M6 configurations, and three M5 (baseline) configurations, for flame tube testing to further validate the design.

4.3.2 Introduction

In Task2.1A of this program, GE carried out an extensive RANS-based preliminary design study for the proposed mixer concepts, based on the SAC and the Dual Annular Combustor (DAC) combustor architectures. Based on the analyses of flow fields and NOx emissions, the team down-selected mixer concepts based on the SAC combustor architecture to be further studied and optimized.

The main objective of this task, Task 2.1, was to carry out an extensive RANS-based design and optimization study for the three down-selected mixer / fuel nozzle concepts and identify multiple configurations for further evaluations in flame tube testing. Many important features of the mixer / fuel nozzle concepts were carefully examined, including counter versus co-rotating vanes, fuel injection location, number of fuel injection orifices, and fuel injection aerodynamic/hydraulic features. Main stage fuel injection concepts included varying both the radial and axial location of fuel injection (relative to the mixer exit), as well as varying the number of fuel injection points. Other concepts explored means for increasing jet penetration into the main stage air flow either mechanically or aerodynamically. Four different main injection concepts were evaluated in this Task, eventually becoming the fuel nozzle designs denoted as F0 (baseline), F1/F2, F4/F3, and F5/F6 (each of these have 2 versions of the same concept design) for use in later Tasks.

4.3.3 Method

The method employed in this task for design and trade studies of mixer and fuel nozzle concepts was mainly based on the Reynolds-averaged Navier–Stokes (RANS)-based CFD design process used in Task 2.1A.

4.3.4 Results and Discussion

4.3.4.1 Baseline Case

Before the team fully engaged on design optimization of the down-selected three mixer concepts, the team first conducted the analysis of a reference mixer / fuel nozzle configuration. The objective of this study was to establish baseline comparison criteria and Figure Of Merits (FOM) for screening mixer / fuel nozzle configurations and serve as a design reference. Reacting flow RANS calculation was carried out for the reference mixer / fuel nozzle in a flame tube environment at the N+2 100%ICAO condition. The target pilot / main fuel split were used for reacting flow calculations.

Based on the conclusion of Task 2.1A, the team decided to focus the figure of merits for mixer / fuel nozzle screening on the flow and fuel / air mixing characteristics at the main mixer exit. From the Task 2.1A study, we concluded that higher turbulence will enhance fuel / air mixing inside the mixer for low NOx emissions.

Figure 15 presents the fuel / air mixing characteristics generated by the reference mixer at the mixer exit. As can be seen in the mean mixture fraction contours, the fuel / air mixture is not well spread out circumferentially and radially. It implies that the fuel and air are still not quite well mixed at the mixer exit.

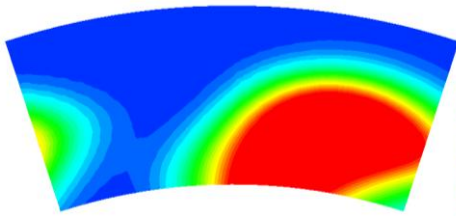

Figure 15 – Mean Mixture Fraction at Mixer Exit for Reference Nozzle/Mixer Design

This serves as a reference point for screening all the other mixer / fuel nozzle configurations based on the down-selected mixer concepts. The following three sub-sections describe the summary of the design optimization of the mixer concepts.

4.3.4.2 M1 Mixer Configuration

After the team completed the above-mentioned reference case, the majority of the effort of this Task was focused on design optimization of the three down-selected mixer concepts. According to the Task 2.1A study, the team concluded that in order to achieve the low NOx emission goal of this program the total mixer air should be higher than in the reference design. Also, the team focused the effort mainly on design and optimization of the main mixer and fuel nozzle. The pilot mixer was taken directly from a pilot mixer developed under a different program. Based on these assumptions and the design criteria established in the previous sub-section, the design targets are summarized in the following:

- Maintain target increased split of total mixer air (main + pilot mixer air)
- Design scope is limited to main mixer design and main fuel injection scheme optimization
- Fuel injection location is limited to a range of distances upstream of mixer exit
- Main mixer Ae
- Maximum mixedness
- EINOx < 30

During the course of this Task, the team investigated more than 30 configurations, and all the CFD analyses were carried out N+2 100% ICAO condition. Only limited sets of configurations are included in this report. The first set of M1 configurations is the M1 with F1 and F2 fuel nozzles. The fuel penetrates a lot more radially by the time it reaches the mixer exit with the F1/F2 fuel nozzles compared to the baseline fuel nozzle. The spreading of the fuel / air mixture is also better than the baseline mixer due to the strong turbulent mixing generated by the M1 mixer. The M1 mixer with F1 fuel nozzle and increased injection orifice count provides enhanced mixing, better fuel / air distribution, and better fuel penetration. Thus, we can conclude that this configuration has a potential to meet the program NOx emission goal.

The second set of M1 configurations was the M1 mixers with F4 fuel nozzle. The F4 achieved the design intent, enhancing the fuel penetration. We can conclude that the configuration has a potential of meeting the NOx goal.

4.3.4.3 M4 Mixer Configurations

The same design approach mentioned in the previous sub-section was taken to study the M4 mixer concept. Again, the team investigated many configurations using RANS CFD design methodology; only limited sets of configurations were included in this report. The first set of M4 configurations is the M4 mixers with F1 and F2 fuel nozzle. The fuel penetration height is similar to the M1 mixer with F1 nozzle. However, the spreading of the fuel / air mixture is worse than the reference mixer. The two M4 configurations may not be able to meet the NOx emission goal of this program because of poor mixedness and spreading of the fuel/air mixture.

The second set of M4 configurations is the M4 mixer with F3 and F4 fuel nozzles. The second M4 shows limited improvement in terms of circumferential spreading of the fuel / air mixture over the first M4 mixer. The two M4 configurations only show slight improvements in terms of fuel / air mixing over the previous M4 mixers with F1 or F2 fuel nozzles. Again, these two configurations may not be able to meet the NOx emission goal of this program based on our estimation of NOx emissions.

In summary, no clear stand-out of enhanced fuel / air mixing were observed from the M4 mixer / fuel nozzle concept. Nonetheless, historical experience of early versions of the M4 mixer concept supports lower combustion acoustics signature relative to the M1 mixer concept and better fuel / air mixing than the reference mixer concept.

4.3.4.4 M6 Mixer Configurations

The M6 mixer/fuel nozzle is a different mixer/fuel nozzle concept than the above-mentioned M1 or M4 mixer/fuel nozzle concepts. This concept is leveraged from an existing GE patent. There are many design parameters that can be changed to optimize the main mixer, including vane length, vane height, number of vanes, vane thickness, fuel injection location, mixing length, vane inner wall radius, etc. A significant amount of effort was spent by the team to optimize this mixer configuration.

Table 5 presents the fuel / air mixing characteristics for the best M6 mixer configuration with F6 fuel nozzle. It is clearly observed from the mean mixture fraction contours that the mixer can produce very high mixedness level and wide spreading of fuel / air mixture. It implies that we will be able to achieve very low NOx emission with the configuration to meet the program goal. In summary, the M6F6 mixer / fuel nozzle concept shows a great potential of producing ultralow NOx emissions.

Table 5 – Fuel / Air Mixing Characteristics for best M6F6 Mixer Configuration

mixture fraction contour	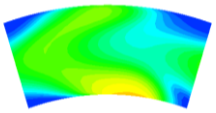

4.3.5 Conclusions

In this Task, an extensive RANS-based design study was carried out for the down-selected mixer concepts from the Task 2.1A study. Non-reacting and reacting flow simulations and NOx emission indices for all the configurations were carried out and post-processed from the results to screen the mixer configurations. Based on the design criteria and FOM established in this study, the team concluded that the M1 mixer configuration with F1 and F4 fuel nozzles have potential of meeting the NOx emission goal of this program because the strong turbulence, generated by the M1 mixer, enhances the overall fuel / air mixing inside the mixer. In addition, the M6F6 mixer / fuel nozzle concept demonstrated much better fuel / air mixing characteristics than the M1 and M4 mixer concepts, and has a great potential of producing ultralow NOx emissions. From the results of this study, the team then down-selected fifteen mixer / fuel nozzle configurations, including seven M1/M0 configurations, three M4 configurations, 2 M6/M7 configurations, and 3 M5 (baseline) configurations, for flame tube testing to further validate the design.

4.4 Task 3.1A – Fuel Air Mixing Studies (GE Funded)

4.4.1 Summary

Measuring and assessing fuel air mixing performance for GE Aviation fuel injectors is the subject of this study. Our work has demonstrated that similar jet breakup and evaporation as that in a real combustor can be achieved with acetone as a fuel surrogate for Jet A. Use of the surrogate enables direct, accurate measurements of fuel / air concentration using Planar Laser Induced Fluorescence (PLIF). Equivalence ratio variations of .02 can be discriminated with better than 3% accuracy. The diagnostic properly accounts for spatial variations in fluorescence signal due to temperature gradients from evaporative cooling and changes in local laser fluence from absorption by acetone.

Five mixers have been tested (i.e., baseline, F1, F2, F4, and F6 nozzles) for a range of jet momentum ratios to delineate general features of the mixing field, to quantify radial variations in fuel concentration, and to assess relative mixing performance. The baseline fuel/nozzle mixer is a 0^{th} Generation nozzle/mixer; a non-production experimental design specifically used for diagnostics development purposes. Results show consistent trends for each mixer across the range of fuel flow rates tested and for multiple measurement planes. Additional measurements of velocity and pilot flame shape for the baseline in this work make up an unlimited rights data set useful for validation of computational mixing models.

4.4.2 Introduction

The experiments in this work are motivated by several key objectives: 1) Give a basis of comparison for computational mixing predictions, 2) Develop a diagnostic for quantifying fuel / air mixing, 3) Discriminate performance between the baseline TAPS mixer and several other next-generation GE Aviation fuel mixers, and 4) Assess mixing at conditions relevant (i.e., similar) to a real engine operating condition. Measurements of fuel distribution immediately downstream of the mixer using a Planar-Laser-Induced-Fluorescence (PLIF) technique are the primary objective. Additionally, for the baseline TAPS nozzle (one of five nozzles tested), non-reacting air velocity fields are quantified using Particle Image Velocimetry (PIV), and pilot flame shapes are determined from images of chemiluminescence. Taken together, these measurements comprise an experimental data set useful for validating computational models of mixing and combustion. To ensure that these data are relevant, operating conditions needed to achieve similar fuel jet break-up and evaporation to that in an engine are first determined.

4.4.3 Methods, Assumptions, and Procedures

4.4.3.1 Similarity and Operating Conditions

4.4.3.1.1 Jet Break-Up and Air Flowrates

Main fuel mixing is the primary focus in these studies. To ensure that conclusions about mixing performance are relevant, the similarity of physical mechanisms associated with main jet break-up and evaporation for engine and test rig conditions are considered. At such conditions, the break-up mechanism of a jet in cross-flow is dominated by the shearing of liquid columns into ligaments [8] as illustrated in *Figure 16* and *Figure 17* (taken from Wu et al.). In a test rig having the same dP/P, air momentum scales with pressure:

$$\frac{\rho U_{air,rig}^2}{\rho U_{air,engine}^2} = \frac{\Delta P_{rig}}{\Delta P_{rig}} = \frac{\left(\frac{dP}{P}\right)_{rig}}{\left(\frac{dP}{P}\right)_{engine}} \frac{P_{rig}}{P_{engine}} \quad (1)$$

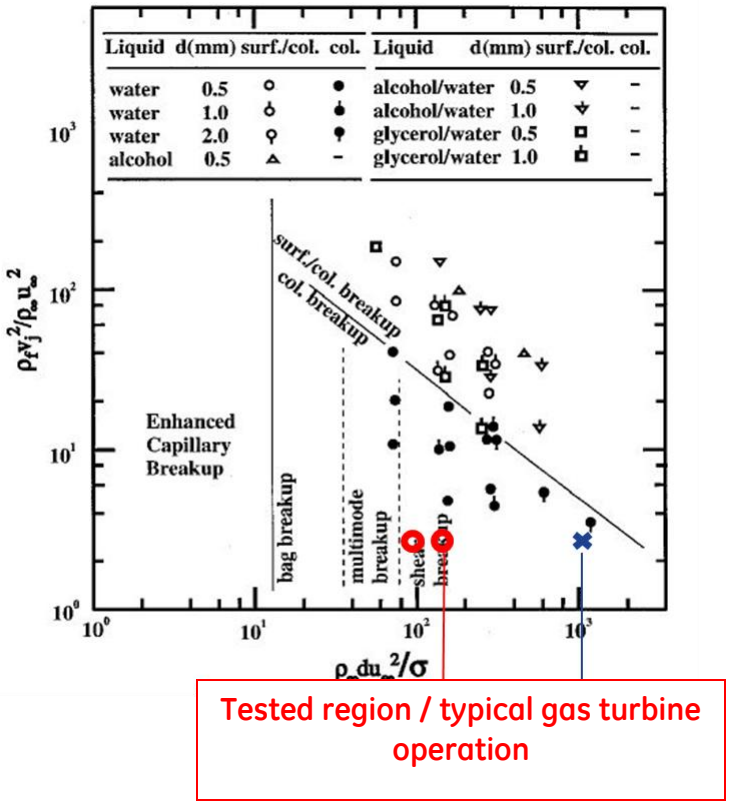

Figure 16 – Plot of Engine and Rig Operating Points

Plot of engine (blue x) and rig (red circle) operating points in terms of jet momentum ratio (y-axis) and aerodynamic Weber number (x-axis). Plot of jet breakup regimes is reproduced from Wu et al [8].

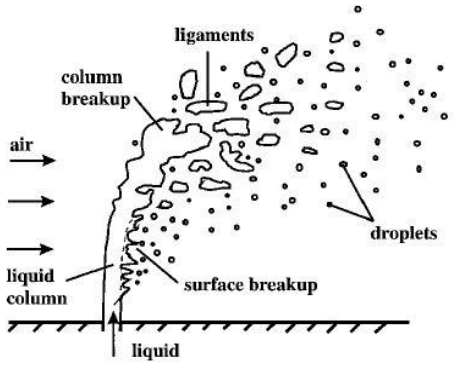

Fig. 7 Sketch of a typical liquid breakup process in an air cross-flow.

Figure 17 – Illustration of Jet Break-Up in Crossflow (from Wu et al. [8])

Consequently, at atmospheric pressures, the air momentum and fuel jet Weber number are lower and much closer to the multi-mode regime in which bag-breakup becomes important. To avoid departure from similarity, the target dP/P (and airflow) for these mixing studies has been increased, ensuring that shear break-up is still the dominant break-up mechanism.

4.4.3.1.2 Jet Evaporation and Fuel Choice

Properly assessing mixing performance with rig tests also requires similar evaporation. Governed by the Spalding number, B, rates of evaporation logarithmically scale with the fuel's propensity to evaporate divided by its resistance to evaporation [9]:

$$B = \frac{Y_{o,\infty} Q_c + c_{p,g}(T_\infty - T_{sat})}{h_{fg} + c_{p,g}(T_{sat} - T_o)} \tag{2}$$

Since we are interested in mixing from the point of main fuel injection to the mixer dump plane, droplet combustion is neglected (the first term in the numerator). The evaporation rate is therefore governed by the available enthalpy of the mixer air (at T_∞) relative to the fuel boiling point (T_{sat}) divided by the latent and sensible heats needed to evaporate the liquid. To match the evaporation rate of JetA (T_{sat}~ 485°F) at engine conditions in an atmospheric rig for which the maximum T_∞ is only 600°F, a surrogate fuel with low boiling point is necessary.

With a boiling point near 130°F, acetone is an excellent surrogate, especially since it is also a commonly used fluorescent fuel tracer. Its vapor concentration in air is therefore readily measured using laser-induced fluorescent techniques. Because the computed Spalding numbers and relative evaporation rates for engine conditions are sufficiently matched by acetone in an atmospheric rig the effect of evaporation on mixing performance should be similar.

4.4.3.2 Experimental Rig and Hardware

The experimental rig used for testing mixers in this study is relatively simple (see *Figure 18*). Air enters the back of a cylindrical plenum via a single manifold and flows in parallel through a radial cyclone and pilot air swirler, through the dome and dump plane into a quartz combustor (137mm ID, 4mm thickness). A 4" long quartz section was used for PIV measurements; all other studies employed an 8" long quartz section to increase the field of view. Flow exits the quartz combustor via a converging section (3:1 nozzle area ratio) intended to mimic the area contraction prior to the turbine in a jet engine. Air flowrate is metered by an upstream venturi and controlled by an air-actuated control valve. An electric heater enables a maximum preheat temperature, T3 of ~ 600°F as measured by a free-stream thermocouple in the plenum.

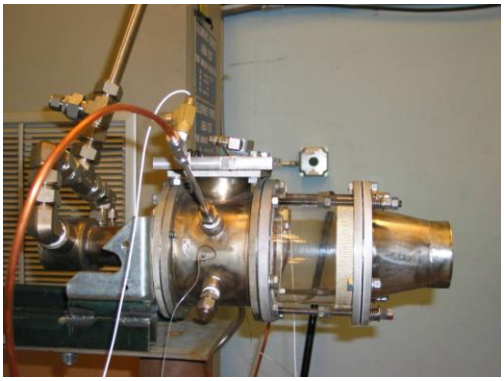

Figure 18 – Photograph of Optical Atmospheric Rig Used for Mixing Experiments

Fuel enters the rig via several possible paths. The stem-type TAPS nozzle (see *Figure 19*), mounted in the rig through a port in the top of the plenum, allows fuel flow through pilot and main flow circuits. A piston-driven laboratory chemical pump (FMI) delivers and meters the surrogate fuel (acetone) to each circuit. Unused pilot circuits were capped.

Figure 19 – Solid model of baseline (non-production experimental) TAPS nozzle

The set of five nozzles and mixers tested in this work span a variety of designs and require slightly different hardware for integration. The TAPS nozzle (*Figure 19*) served as a benchmark. Mixing measurements of this nozzle were made using an existing "flared" dome plate and test-rig hardware that ultimately limited measurements to planes

no closer than 1” from the nozzle tip. A flat dome was machined to accommodate the N+2 mixers for subsequent tests. This enabled measurements to be made in close proximity (3/32”) to the nozzle tips, an improvement needed to amplify differences in mixing performance. Mixing was also quantified for the N+2 nozzles at a distance of 1” so as to characterize their performance relative to that measured for the TAPS nozzle.

A modest array of instrumentation is required for these tests. A venturi measures rig air flow-rate. Pressure taps and transducers measure the static pressure on each side of the dome and the corresponding pressure drop. Plenum temperature (T3) is measured with a thermocouple mounted in the free stream. Fuel flow-rates are determined from measured pump speed / flow correlations. These are determined prior to each test by weighing the fuel displaced by the pump for a set interval at each pump speed.

4.4.3.3 Diagnostic Approach and Image Processing

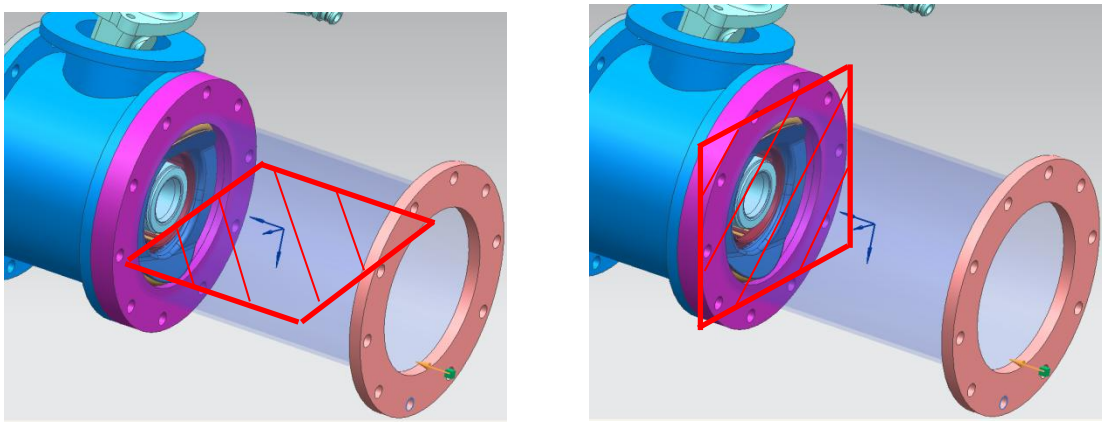

Figure 20 – Modeled Images Illustrating Two Measurement Planes

Modeled images illustrating two measurement planes used in this study. The horizontal orientation (left) was used for PIV and flame shape measurements. The vertical orientation (right) was used for fuel / air mixing (PLIF) measurements.

4.4.3.3.1 Planar Laser Induced Fluorescence (PLIF)

When a ketone tracer such as acetone is excited by a coherent, ultraviolet light source, the resulting fluorescent intensity, S_f, is predictable:

$$S_f = \frac{E}{hc/\lambda}\eta_{opt} dV_c \left[\frac{\chi_{fuel} P}{kT}\right] \sigma(\lambda, T)\phi\left(\lambda, T, P, \sum_i \chi_i\right) \quad (3)$$

in which $\frac{E}{hc/\lambda}$ is the number of exciting photons (proportional to the laser intensity), η_{opt} is the efficiency of the collection optics, dV_c is the probe volume, the bracketed term is the tracer number density, σ is the absorption cross-section, and ϕ is the fluorescence quantum yield [10]. For isothermal, isobaric conditions with an optically thin path, the fluorescence is directly proportional to the tracer concentration:

$$S_f \sim S_f^+ \chi_{fuel} \tag{4}$$

for which S_f^+ is the temperature dependent fluorescence per mole. This linear dependence enables measurement of unknown concentrations by scaling a known concentration, χ_{cal} by a ratio of measured fluorescence and known photo-physical properties, S_f^+:

$$\chi_{fuel} = \frac{S_f}{S_{f,cal}} \frac{S_{f,cal}^+}{S_f^+} \chi_{cal} \tag{5}$$

Thus, to measure spatially varying fuel concentration, several things must be known or acquired – namely, a fluorescent image of the field of interest (S_f) - like that shown in *Figure 21*, a calibration image ($S_{f,cal}$) of a field of known concentration (χ_{cal}), and temperature distribution for calculation of spatially varying photo-physical properties. Determination of this temperature field complicates data reduction since an iterative approach is required. Nevertheless, the problem is still tractable.

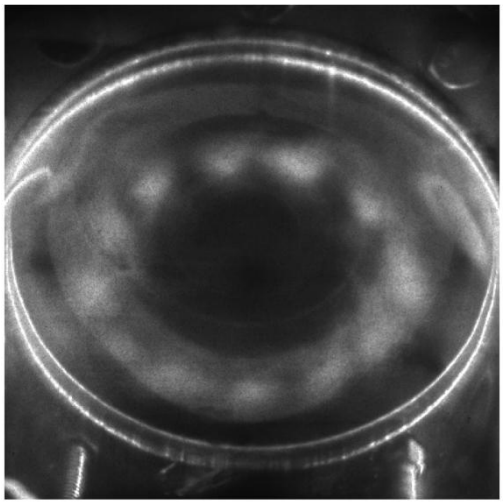

Figure 21 – Raw Fluorescence Image

Raw fluorescence image captured near the mixer dump plane for injection of acetone through the main fuel circuit.

To determine the temperature field, the local fuel concentration is estimated from Eq. (5), assuming a uniform temperature (i.e. T_3, measured by a thermocouple). Next, by assuming an adiabatic mixing process between the points of measurement and injection, the local fuel / air mixture temperature can be determined from a first law model of evaporative cooling:

$$\left(1 - X_{fuel}\right) c_{p,g} \left(T_{air,in} - T_{mix}\right) = X_{fuel} \left[c_{p,l} (T_{mix} - T_0) + H_{vap}\right] \tag{6}$$

From this relation, it is clear that the acetone cools the hot air as internal energy is required for evaporation. *Figure 22* shows a typical temperature field that results from injecting acetone through the main fuel jets into air at a temperature of 600°F. Dimensions in this and other plots are relative to the outer radius, R_o, of the sensor viewing area. The plot illustrates that evaporative cooling can reduce mixture temperatures by more than 150°F. From this temperature field, photo-physical properties (S_f^+) can be determined from the literature [11] for each spatial location and used to recompute the fuel concentration field from equation (5). This process is iterated for each measurement until a reasonable convergence criterion is met.

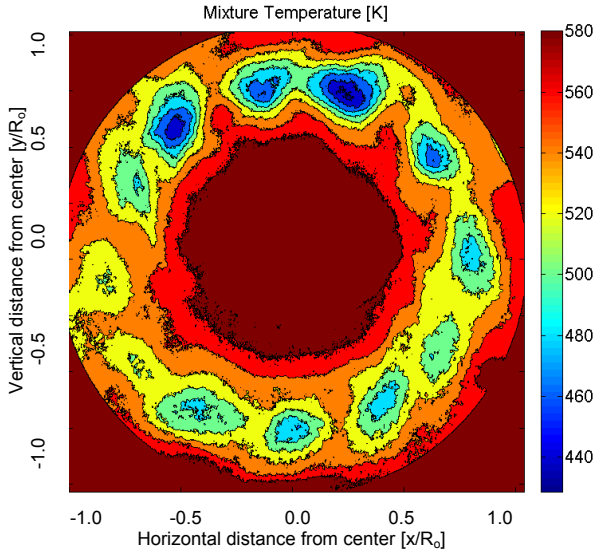

Figure 22 – Example Temperature Contours

Example temperature contours inferred from fluorescence measurements using a 1st law adiabatic mixing model.

This iterative approach includes an additional step to account for the effect of laser absorption (by acetone) along the sheet path. From equation (3) it is clear that the local fluorescence signal depends on the spatially varying laser fluence (i.e., the number of incident photon flux). Changes in local laser fluence are readily corrected by computing absorption along the laser sheet path from the estimated fuel concentration field and the Beer-Lambert law:

$$dI = -IN\sigma dx \tag{7}$$

This relation is integrated along the path to compute the local intensity relative to that incident on the flame-tube wall. By including this correction with fluorescent temperature sensitivity in the iterative loop, we were able to reach a convergent solution for the temperature and fuel concentration fields. A clear evaluation of the effectiveness of these non-uniformity corrections is presented in *Section 4.4.5.1.1*.

A couple additional operations are necessary to convert the measured fluorescence image to a spatially resolved temperature field. A reference image of the interrogation

region must be acquired for pure airflow to correct for spurious background signal, reflections, and fluorescence of the quartz flametube. This reference image is subtracted from both the measured fluorescence image and the calibration image prior to any further processing. Because the camera is at an oblique angle to the laser sheet and measurement plane, a correction for optical distortion is necessary to properly map the measured field to precise spatial coordinates. This is accomplished by imaging a reference grid (as shown in *Figure 23*) in the flame-tube prior to each measurement campaign to empirically determine the correct mapping.

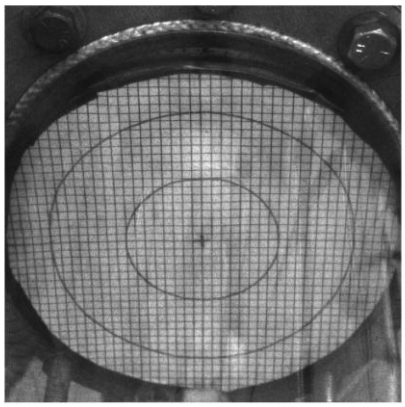

Figure 23 – Image of Grid

Image of grid used for correcting image distortion (i.e., optical coordinate stretching and compressing) for fuel/air mixing measurements.

Though the general measurement approach developed for this work is a bit involved, it has become relatively straightforward in its implementation. Nevertheless, it is important to assuage concerns about diagnostic accuracy, precision, and the overall reliability of these measurements. These are addressed in *Section 4.4.5* after the presentation of results.

4.4.4 Results

In this section, observed mixer performance is quantified for five nozzle/cyclone sets. With a focus on planar fuel / air distributions, mixing fields for four next generation aviation mixers are shown and compared with distributions for a reference mixer, i.e. the baseline TAPS. Velocity and pilot flame shape measurements are also presented for the TAPS nozzle.

4.4.4.1 Fuel Air Mixing Studies

Fuel / air mixing data acquired using Planar Laser Induced Fluorescence (PLIF) are presented in this section as image comparisons, radial fuel concentration profiles, and variations in scalar unmixedness for a wide range of conditions. Images enable direct comparisons between measured mixing fields and computational simulations; whereas, average normalized radial profiles indicate how fuel is spatially distributed (radially), thereby elucidating the effects of different mixer design features. Comparisons of scalar

unmixedness serve as the simplest means of comparing quantifying hardware performance over a broad range of operating conditions.

4.4.4.1.1 Image Details and Comparisons

Planar images of measured local equivalence ratio are generated. Local equivalence ratio is determined at each spatial location using measured fuel mole fraction, Y_{fuel} and well-known relations for a binary mixture:

$$\varphi = \frac{FAR}{FAR_s} = \frac{Y_{fuel}}{Y_{air} FAR_s} = \frac{Y_{fuel}}{\left(1 - Y_{fuel}\right) FAR_s} \tag{8}$$

Note: Using Eq. (8), it is a simple matter to convert from measured mole fraction to fuel to air ratio, *FAR*, and local equivalence ratio, φ, given that the stoichiometric fuel air ratio for acetone is .0552.

At an axial distance of 1" from the fuel tip, where comparisons can be made with the baseline (non-production, experimental) TAPS nozzle, differences in the performance of the next generation N+2 mixers relative to the prior TAPS technology are visually striking. *Figure 24* shows that distinct fuel jets are still present for the baseline nozzle; whereas large gradients are clearly mixed out for the F2 and F6 mixers.

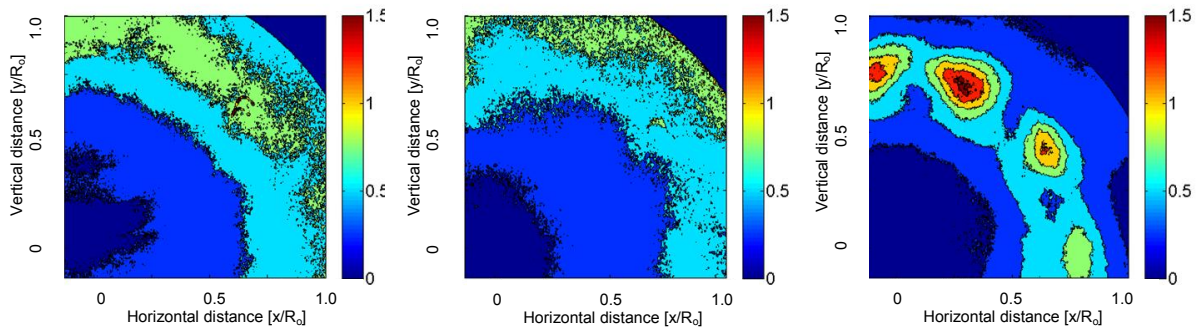

Figure 24 – Contour Images – 1"

Contour images of local equivalence ratio acquired at an axial distance of 1" from the F2 (left), F6 (center), and baseline (right) mixers. For each image the jet equivalence ratio is near 0.45.

While these spatial contour images are useful for visualizing basic trends and offer a direct means of validating mixing models, a more rigorous quantitative approach is needed to clarify differences in mixing performance.

4.4.4.1.2 Defining Unmixedness

To succinctly describe the level of mixing achieved for a specific mixer, operating condition, and axial location, the global unmixedness parameter, U_g is defined as:

$$U_g = \frac{\sigma_Y^2}{\mu_Y(1 - \mu_Y)} \tag{9}$$

in which μ_Y and σ_Y are the mean and standard deviation of the fuel mole fraction (i.e., a conserved scalar) measured for a particular interrogation region. Defined in this way, unmixedness is expressed as the spatial variance of fuel mole fraction appropriately normalized by its mean to confine possible values between zero and unity [12]. A high value of U_g indicates a poorly-mixed region; whereas, a low value indicates a well-mixed region. The "global" subscript designates that the parameter is computed for an extensive interrogation region rather than just a single point. In this work, global unmixedness is assessed for an interrogation region confined to a narrow annular region (0.75" < r < 1.5") encompassing the fuel jet as illustrated in *Figure 25*. By excluding other regions, unmixedness is quantified in a location where we expect to see the greatest variations in performance for each mixer and operating condition.

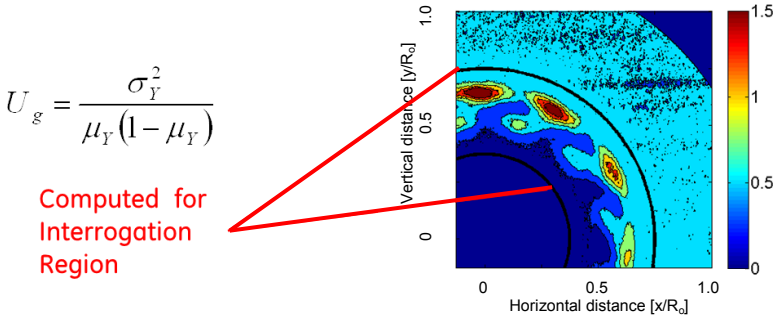

Figure 25 – Interrogation Region Used for Computing Global Unmixedness Parameter

Illustration of the interrogation region used for computing U_g, the global unmixedness parameter for a particular operating condition.

4.4.4.1.3 Mixing Progress with Axial Distance

Computing the mean of U_g for a range of jet equivalence ratios at each axial distance quantifies mixing progress as fuel is carried downstream of the dump plane. *Figure 26* illustrates these trends for all four tested N+2 mixers. In general, mixing progresses exponentially with axial distance, e.g. the F2 mixer exhibits a decline in U_g by a factor of 10 over a distance of less than 1". Consequently, mixers are best differentiated by measurements near the dump plane, although, the 5/32" location appears to be optimum given slightly ambiguous trends at 3/32". Ambiguities suggest that the jets are not yet fully developed. At all downstream measurement locations, mixer ranking persists, with the F6 nozzle still showing the best performance. To directly compare the performance of the baseline (non-production, experimental) TAPS nozzle to that of the next generation nozzles, global unmixedness for the TAPS nozzle is plotted at z = 1". It clearly exhibits the highest unmixedness of the mixers with nearly an order of magnitude higher U_g than those for the best next generation mixers. This result is also consistent with apparent trends shown *Figure 24*.

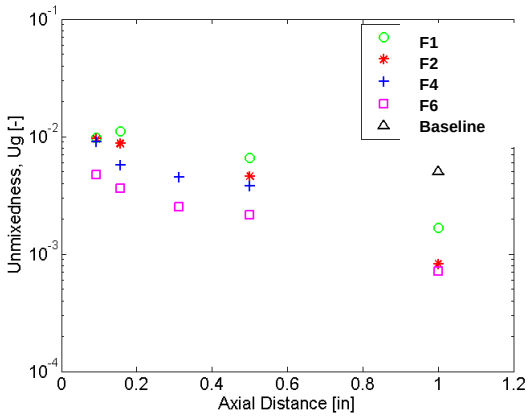

Figure 26 – Average Trends in Global Unmixedness

Average trends in global unmixedness with axial distance from the dump plane.

These results are generally reinforced by the radial profiles shown in *Figure 27* for several mixers at an axial location of 1.0" from the nozzle tip. As measurements are made further from the dump plane, deviations of the local concentration from a global mean become less pronounced, particular for the mixers exhibiting best performance. In *Figure 27*, it is clear that the baseline TAPS nozzle has the highest relative peak concentration and a relatively non-uniform concentration profile, even at a distance of 1" downstream of the dump plane. These trends in the fuel spread directly manifest themselves in the unmixedness parameter.

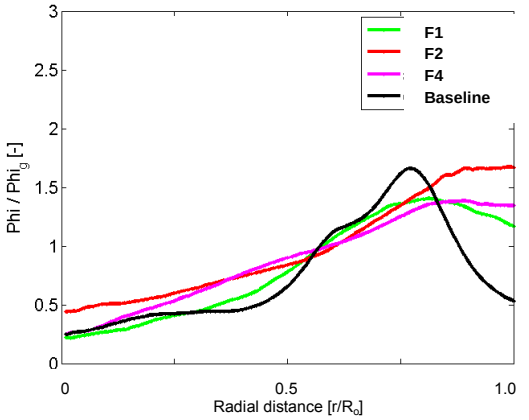

Figure 27 – Normalized Radial Equivalence Ratio Profiles – 1"

Normalized radial equivalence ratio profiles for four mixer designs at an axial distance of 1" from the nozzle tips.

4.4.4.2 Baseline Validation Measurements

In addition to fuel / air mixing distributions, velocity fields and flame shapes have been measured for the baseline nozzle as a reference data set for future model validation. These data serve to supplement mixing studies and to delineate distinct features of the non-reacting and reacting flow-fields. Velocity data obtained using Particle Image Velocimetry (PIV) show flow-field jets and recirculation zones in the non-reacting

flowfield for a couple of different air flow-rates (dP/P) and exhaust nozzle area ratios (i.e., boundary conditions). OH* chemiluminescence images indicate pilot flame shapes for a range of fuel flowrates and equivalence ratios.

4.4.4.2.1 Velocity Measurements

General baseline flowfield features in the vicinity of the mixer dump plane are visible in *Figure* 28, which shows measured velocities at three different horizontal planes. The top image delineates the velocity field in the horizontal plane that is just above the mid-plane (y/R_o = .06); whereas, the measurement location for the middle and lower plots are at the mid-plane and just below (y/R_o = -.06) the combustor mid-plane. Bulk flow is from left to right and scaled cross-sections of the baseline TAPS mixer shown in the figure provide a visual reference. Axial velocity contours are overlaid in color on the plots to illustrate jet flows and recirculation zones.

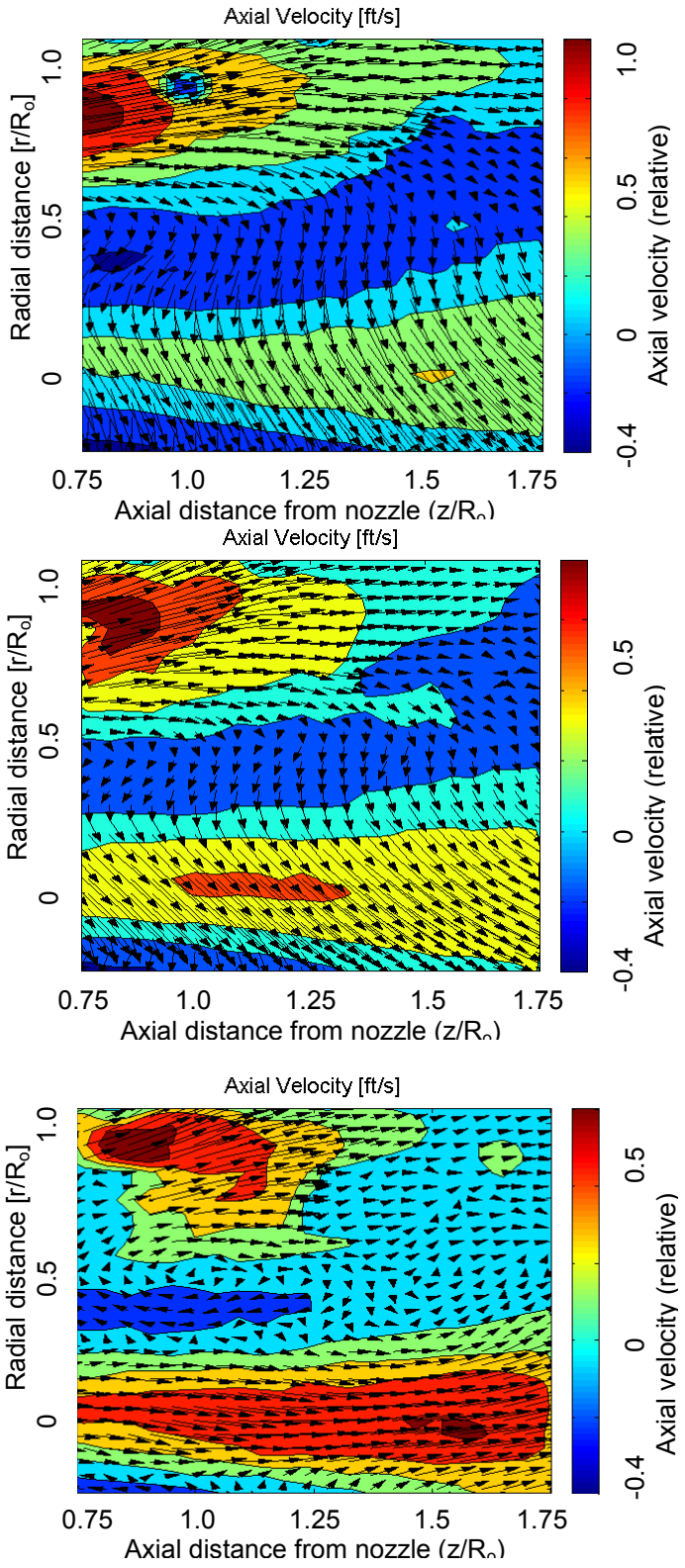

Figure 28 – Comparison of Velocity Fields for Dome Air

Comparison of velocity fields acquired for dome air dP/P near 4.0 for three different horizontal planes at distances of y/R_o=0.06 (top), 0" (middle), and y/R_o= -0.06 (bottom) from the combustor mid-plane. Axial

velocity color contours are plotted to illustrate jet locations and recirculation zones. The nozzle area ratio for these cases is 3.0.

Basic flowfield features include a high velocity annular air jet emanating from the radial swirler at distances between r/R_o = 0.5 and 1.0 from the centerline. Each measurement plane represents a different cut of the jet annulus so that the apparent location of maximum velocity is shifted. A recirculation zone indicated by negative axial velocities extends downstream of the nozzle heat shield. A center air-jet proceeds from the pilot mixer and expands with axial distance from the nozzle as indicated by a spreading region of higher axial velocity. In fact, most of the flow features are observed to expand with axial distance as a result of air moving from the small area restrictions of the nozzle to the dump plane and larger area of the flametube.

Careful examination of the velocity trends with measurement plane height reveal that the aerodynamic center of the hardware is not at the combustor mid-plane; instead, it is near r/R_o = 0.06 below the mid-plane. (This is most likely due to hardware installation in the test rig; i.e. the nozzle/mixer is allowed to "float" somewhat within the dome opening, and may not be centered exactly in the dome and quartz liner at the time of measurement.) This is evident in progressing from the top to bottom images of *Figure* 28 as the pilot swirler air jet straightens out (with a radial velocity component near zero). Naturally, the same horizontal combustor plane has the highest pilot air axial velocity. It is clear from these results that the velocity field in the pilot region varies significantly as we move away from the centerline.

These general flowfield features persist for different total air flowrates (and dP/P). *Figure 29* compares velocity vector fields at a horizontal sheet height of r/R_o = 0.06 above the centerline for dP/P = 3.9 (left image) and dP/P = 1.9 (right image). As one would expect, the maximum velocities in each plot scale with the square root of dP/P so that the ratio of maximum velocities for the two conditions is ~ (1.9/3.9)^0.5 = 0.7 or 70/100 as shown in *Figure 29*. By similarly scaling the color contours of axial velocity for each flow condition, we clearly observe that the two flow-fields are nearly identical (similar). These results are consistent with previous investigations by others [13, 14] who have demonstrated that general flow-field characteristics are relatively insensitive to changes in dP/P.

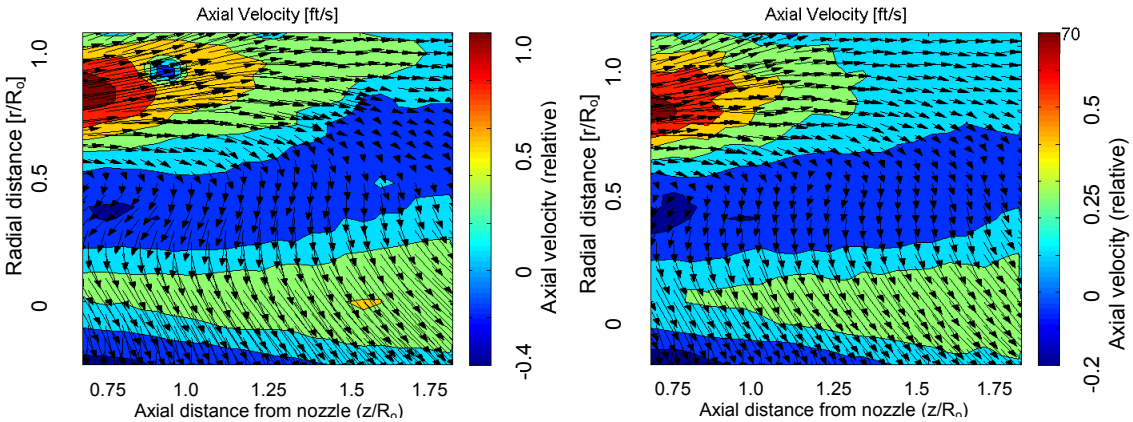

Figure 29 – Comparison of Velocity Fields for Two Different Air Flowrates

Velocity fields for two different air flowrates with dome dP/P = 3.9 (left) and 1.9 (right). Contours have been scaled according to the bulk flowrate to illustrate similarity. The nozzle area ratio for these cases is 3.0. Data correspond to the horizontal plane that is r/Ro = 0.06 above the combustor mid-plane.

4.4.4.2.2 Flame Shape Study

To study features of the reacting flow field for the baseline (non-production, experimental) TAPS nozzle, UV images (310nm) of OH* chemiluminescence were acquired. These images delineate heat release from the pilot flame for a range of fuel (Jet-A) flowrates. Experiments were constrained to pilot-only operation due to problems with wall impingement and poor combustion efficiency when main fuel circuits were employed at atmospheric pressures. Nevertheless, these results show the spatial distribution of heat release and delineate stoichiometric contours for diffusion-limited (pilot) operation.

Figure 30 illustrates changes in the apparent flame shape as fuel flowrate is increased from 7 to 20pph. From the images, it appears as though some heat release occurs in regions of the fuel jet near the centerline; however, this is simply an artifact of path-averaged emission from an axi-symmetric flame. Using an Abel inversion [15] to operate on the raw images allows determination of the intensity in a single mid-plane slice assuming symmetry about the combustor centerline. Corresponding transformed images shown in *Figure 31* reveal that the heat release is indeed limited to a stoichiometric contour between the rich pilot jet and the outer airflow. As the pilot fuel flow (and equivalence ratio) increases, the heat release extends further downstream as a longer distance is required to mix fuel and air. Although these results are not particularly surprising or groundbreaking, the heat release location and axial distribution are particularly useful in that they may be compared directly with computational results to discern if a model is properly capturing fuel / air mixing processes.

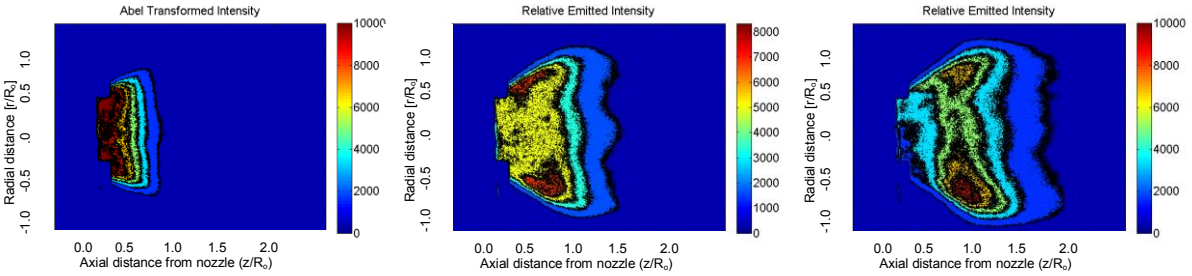

Figure 30 – Uncorrected Images of OH* Chemiluminescence

Uncorrected images of OH chemiluminescence for three pilot flames with total flowrates of 7pph (left), 13pph (center), and 20pph (right). For these studies, T3 = 515°F and dP/P = 3.9.*

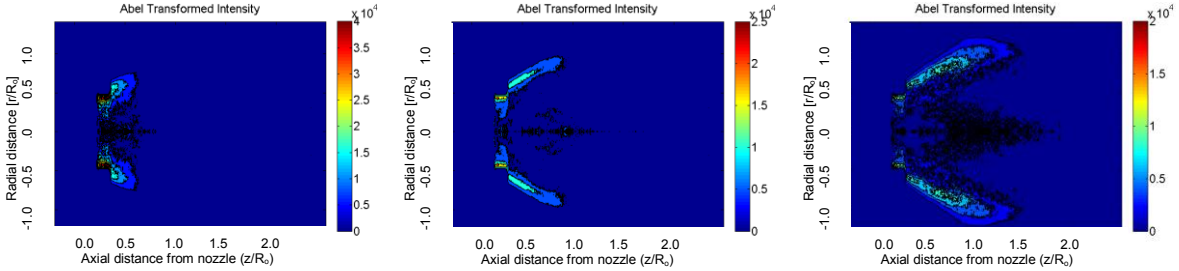

Figure 31 – Abel Transformed Images of OH* Chemiluminescence

Abel transformed images of OH chemiluminescence indicating heat release in a slice through the combustor mid-plane for three different pilot fuel flows : 7pph (left), 13pph (center), and 20pph (right). Images were transformed from raw data shown in Figure 30.*

4.4.5 Discussion

In this section several key issues are discussed, including: accuracy and precision of fuel / air mixing measurements, potential confounding effects, general trends in performance, relevance of general findings, and broader implications of these results.

4.4.5.1 Accuracy and Precision of Fuel Air Mixing Measurements

The usefulness of the fuel / air mixing measurements in this work hinges on the accuracy and precision of the diagnostics employed. If we have failed to properly account for signal inhomogeneities due to factors other than concentration, or, if some other bias remains, results in previous sections could be misleading. To address these concerns, studies of accuracy and precision have been performed for premixed and non-premixed operation. These studies bolster confidence in the measurements and apparent trends while justifying their use in assessing mixer performance.

4.4.5.1.1 Premixed Validations

Several validations of diagnostic accuracy have been performed by examining trends in measured signal for a homogeneous mixture of fuel and air of known mole fractions. For such a mixture, variations in measured fluorescent intensity with mean temperature can be compared with known photo-physical data found in the literature [11]. Plotting measured fluorescence per mole (S_f^+) of acetone in *Figure 32* reveals acceptable

agreement with literature values, confirming that we are observing proper temperature dependence of the fluorescence signal. Capturing this dependence is critical for accurate measurements of mole fraction, particularly when evaporative cooling creates a non-isothermal mixing field as shown in *Figure 23*.

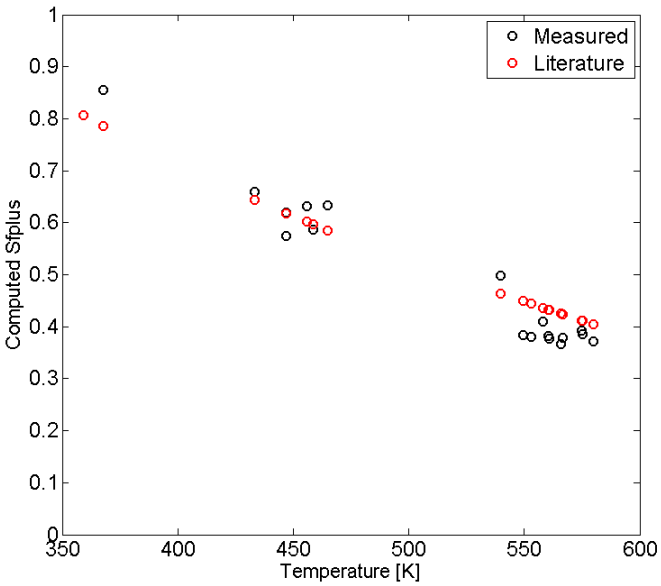

Figure 32 – Comparison of Measured Fluorescence with Literature Data

Comparison of measured fluorescence per mole (S_f^+) *with literature data over a range of mean mixture temperatures. Results confirm that temperature dependence of signal is properly captured.*

Another validation approach is to compare mean and spatial variations in fuel concentration indicated by the diagnostic with the known uniform value. The data is processed and apparent mole fraction is computed with and without correction factors for: 1) fluorescence dependence on temperature, and 2) fluorescence dependence on local laser fluence. (Recall that the latter factor arises from laser light absorption by acetone along the sheet path). Results, plotted in *Figure 33* show the effectiveness of each correction factor and the accuracy of the diagnostic.

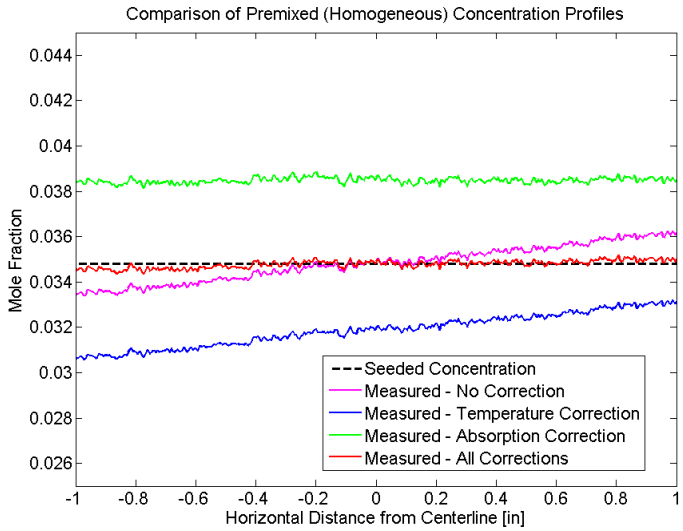

Figure 33 – Comparison of Spatially Varying Fuel Concentration with Known Distribution

Comparison of spatially varying fuel concentration with the known distribution for a homogeneous fuel / air mixture. Curves of apparent concentration are shown when correction factors are included and excluded to demonstrate effectiveness of each correction and overall diagnostic accuracy.

The horizontal dotted dashed line in *Figure 33* indicates the actual uniform acetone mole fraction of .0347 for the mixture. If no corrections are applied, the mean concentration agrees reasonably well with the actual value; however, the local value decreases with horizontal distance from the centerline in the direction of laser sheet propagation (i.e., the negative x-axis). Neglecting this factor would clearly introduce a spatial bias in measured fuel distributions. When variations in local laser fluence are corrected by accounting for light absorption along the sheet path, the spatial bias is removed and the green curve results. Although the apparent mole fraction is now relatively uniform, the mean value for the green curve differs from the actual value by 10% because fluorescence dependence on temperature is not corrected. If both corrections are applied, the red curve results. Clearly, this approach achieves excellent agreement with the actual fuel distribution with accuracy of better than 1%. These results are encouraging and go a long way toward establishing required confidence in the fuel / air distributions measured in this work.

4.4.5.1.2 Fuel Closure Calculations

To reinforce our confidence in concentration measurements for non-premixed (main and pilot) fuel injection, fuel closure calculations have been performed. This involves measuring the fuel concentration field for a given flow-rate and determining the local flux through the measurement plane to compute total apparent fuel flowrate. This result is then compared with known fuel flowrate delivered by the pump to determine if reasonable closure is achieved.

For a binary mixture (fuel and air), the local fuel flux can be expressed as:

$$\dot{m}''_{fuel} = \dot{m}''_{air} FAR = \rho_{air} V_{air} \frac{X_{fuel}}{1 - X_{fuel}} \quad (10)$$

Integrating over the combustor area gives an expression for the total fuel flow-rate as a function of the air velocity field, fuel mass fraction field, and the air density:

$$\dot{m}_{fuel} = \int \rho_{air} V_{air} \frac{X_{fuel}}{1 - X_{fuel}} dA \quad (11)$$

Fuel closure calculations from Equation (11) were performed for the baseline (non-production, experimental) TAPS nozzle since velocity field data from PIV was already available (see *Section 4.4.4.2.1*). To compensate for differences in density between cold PIV measurements and hot fuel PLIF measurements, measured local velocities were scaled by mass flow ratios and temperatures. The scaled air velocity field was integrated over the entire area and the computed total air flow was compared with the actual measured value to verify proper scaling. *Figure 34* shows a typical radial distribution of the axial velocity component. Assuming an axisymmetric profile, the velocity field of interest (like that shown in *Figure 35*) is computed. From this result and the measured fuel mass fraction field at a corresponding axial location, the fuel flowrate for each differential area of the combustor can be determined from Equation (11). *Table 6* lists apparent fuel flowrates calculated in this manner for several regions of interest as denoted in *Figure 36*. The results delineate variations in flow-rate from jet to jet and confirm that a significant portion of the total fuel flux is outside of the regions of interest. Nevertheless, all regions may be summed, giving a total indicated fuel flowrate of 52.2pph. This differs by less than 1% from the actual fuel flowrate metered by the pump (52.1pph).

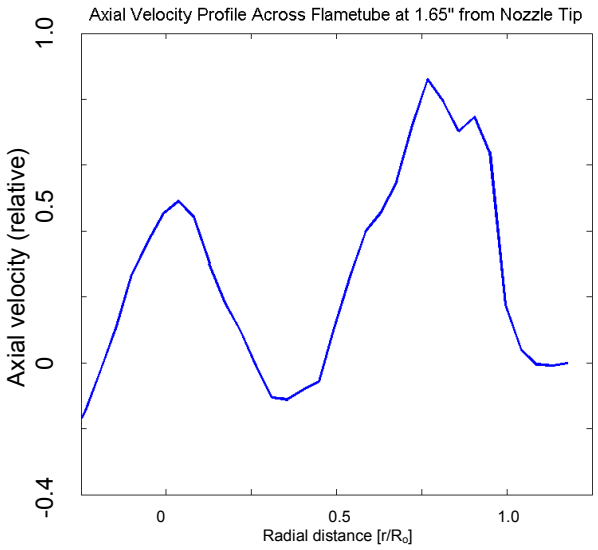

Figure 34 – Radial Distribution of Axial Air Velocity

Radial distribution of the axial air velocity at an axial distance of 1" from the baseline nozzle tip. Profile was computed from PIV data that is appropriately scaled by air mass flowrate and temperature to account for density differences.

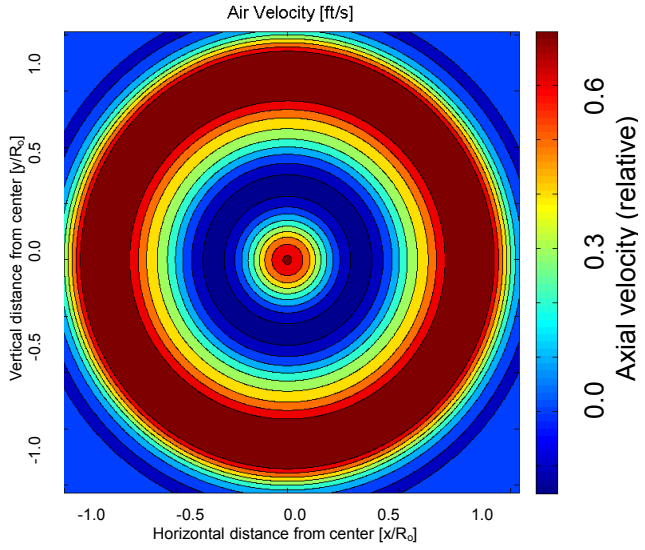

Figure 35 – Axial Air Velocity Field

Axial air velocity field inferred from measured PIV data. Assumption of symmetry about the centerline allows construction of the near dump plane velocity field used for performing fuel closure calculations.

Table 6 – Estimates of Fuel Delivery for Regions of Interest

ROI #	Fuel Flowrate [pph]
1	3.6
2	2.5
3	2.5
4	2.2
5	2.5
6	2.4
7	2.6
8	1.8
9	1.9
10	2.3
11	3.3
12	2.9
Indicated fuel in ROIs	30.8
Indicated fuel outside ROIs	21.4
Total Indicated fuel	52.2
Actual delivered fuel	52.1

Estimates of fuel delivery for each of twelve Regions Of Interest (ROIs), some of which are shown in Figure 36. Values are computed by integrating the product of fuel to air ratio and air flux estimated from measured velocity profile. Total integrated fuel delivery is compared with actual fuel delivery to confirm accuracy.

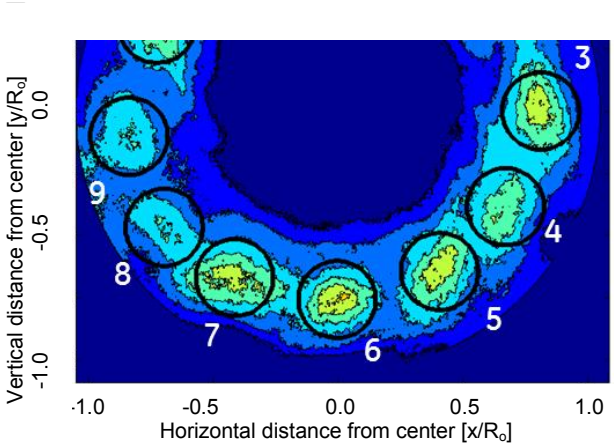

Figure 36 – Local Fuel Mole Fraction Field

Local fuel mole fraction field used for fuel closure calculation. Fuel flowrates through each region of interest are listed in Table 6.

Closure of the fuel delivery for non-premixed injection of fuel through the main circuits further bolsters confidence in the accuracy of measurements of local fuel concentration. Taken with results from *Section 4.4.5.1.1* that showed the ability of the diagnostic to account for non-uniform effects of evaporative cooling and absorption, we may safely rely on this measurement approach to collect data for model validation and to assess mixing performance.

4.4.5.1.3 Diagnostic Precision

The value of fuel air mixing measurements depends not only on the diagnostic accuracy but also on the ability to sufficiently resolve equivalence ratio variations. To adequately resolve actual spatial variations in equivalence ratio requires that the noise equivalent variations be relatively small. This is easily assessed from equivalence ratio profiles like that shown in *Figure 37*. The plot of local equivalence ratio variations with horizontal distance from the flametube centerline corresponds to a traverse across several jets. The physical variations in local equivalence ratio have peaks as high as ϕ/ϕ_{max} = 0.9 and valleys as low as ϕ/ϕ_{max} = 0.3. The fine variations in equivalence ratio superposed on the larger structures correspond to diagnostic noise. For these measurements, the apparent signal to noise ratio is about 50:1, providing an excellent gage for tracking real physical variations and drawing conclusions about mixedness. The noise equivalent variations in ϕ/ϕ_{max} are ~ 0.01, thus, the diagnostic achieves excellent precision and is sufficient for resolving the equivalence ratio variations needed for this study.

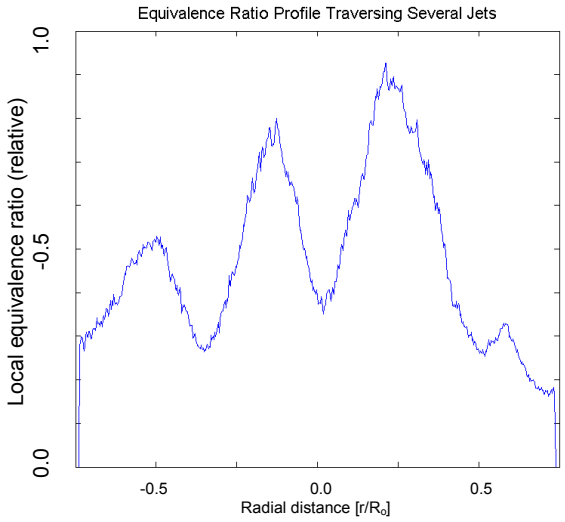

Figure 37 – Equivalence Ratio Profile for Horizontal Mixer Traverse

Equivalence ratio profile for horizontal mixer traverse across several jets. Variations in equivalence ratio are due to unmixed fuel and diagnostic noise. The apparent signal to noise ratio is ~ 50:1.

4.4.5.2 Multi-Phase Flow Issues and Other Caveats

As mentioned earlier, the use of a low boiling point fuel (acetone) introduced the possibility of jet / jet variations and varied liquid / vapor quality depending on the residence time and flow path through the relatively hot nozzle. This problem is further complicated by our need for a flow-field with few liquid droplets in order to simplify and optimize fuel PLIF measurements – i.e., cooling the acetone discourages spatial variations in the fuel liquid / vapor quality, but fosters unwanted liquid droplets. Furthermore, increasing the acetone inlet temperature too far can lead to complete evaporation in the nozzle and a loss of jet momentum similarity (though we have already demonstrated that the latter does not have a strong relative effect on mixing performance). To cope with this problem, a water cooling line and thermocouple were

installed with the fuel line a few inches upstream of the nozzle tip to provide a metric and some degree of control over the fuel boundary conditions. *Figure 38* illustrates conditions for which a lot of cooling is used, evidenced by persisting droplets in the dump-plane (left image), and a condition for which very little cooling is used (right image) and few, if any droplets persist.

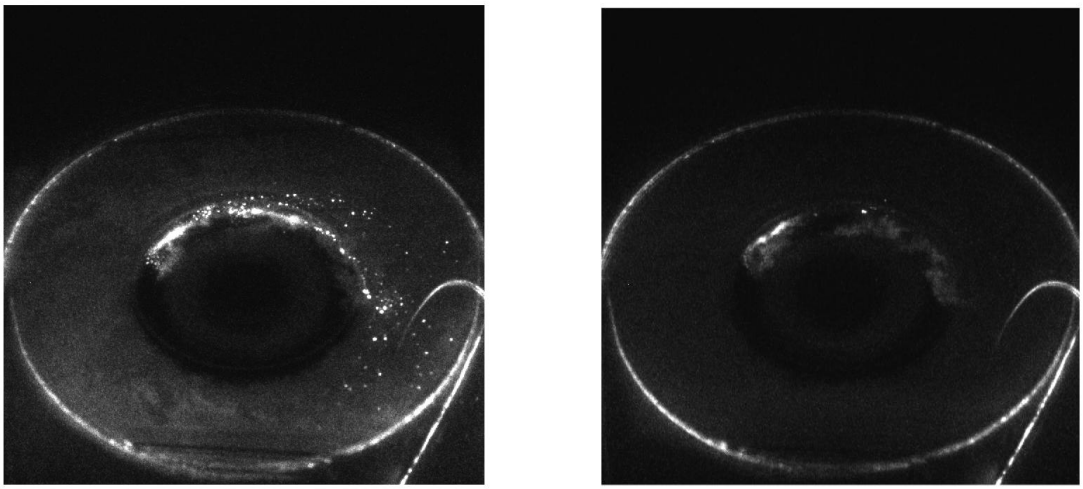

Figure 38 –Conditions for Which Cooling is Used

Raw images of acetone fluorescence for the F1 nozzle, illustrating effects of fuel inlet temperature. Droplets persist in the measurement plane (z = 3/32") for inlet temperatures below 120°F (left image). For fuel inlet temperatures above 125°F, few if any droplets are observed. In both cases, relatively more fuel flows through the single orifice (11 o'clock) since it is nearest the cool fuel inlet.

To quantify the effect of these varying boundary conditions on mixing performance, fuel concentration measurements were made for a range of fuel jet equivalence ratios (i.e., flow-rates). For these tests, global unmixedness is compared in *Figure 39* for three different ranges of acetone inlet temperatures to determine the net effect of multi-phase injection. An image corresponding to the low inlet temperature range (represented by blue markers in *Figure 39*) is shown on the left in *Figure 40*. Images corresponding to the mid (green markers) and high (red) temperature ranges are pictured in the center and right images, respectively. Images in *Figure 40* show some clear differences in the fuel distribution as inlet boundary conditions are changed, particularly with regard to symmetry. Note that the coldest inlet temperature case exhibits the most droplets and the greatest asymmetry; whereas the hottest inlet temperature has no droplets and relatively good symmetry, possibly as a result of the injection of gaseous rather than liquid acetone through the orifices. Nevertheless, the relative distribution of fuel in the jet region (i.e., an annular sector) remains relatively constant. This is evident in *Figure 39* as the unmixedness in the region of interest is compared for the three different fuel temperature regimes. The lack of statistical difference in the results suggests that multi-phase flow effects have little impact on the relative performance as quantified in these studies. Although a deeper investigation of the multi-phase flow induced asymmetry is probably warranted, these results give additional credence to the conclusions drawn from relative mixer performance studies in this work.

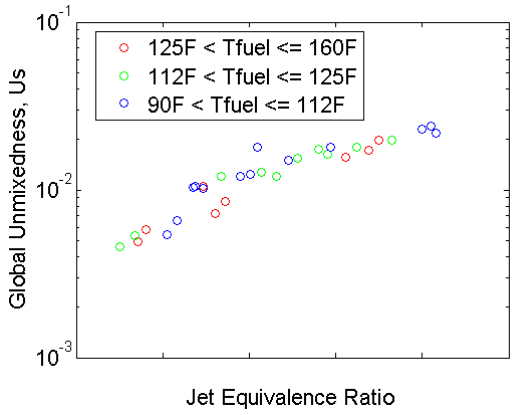

Figure 39 – Global Unmixedness Comparison

Comparison of unmixedness for a range of jet equivalence ratios and fuel inlet temperatures.

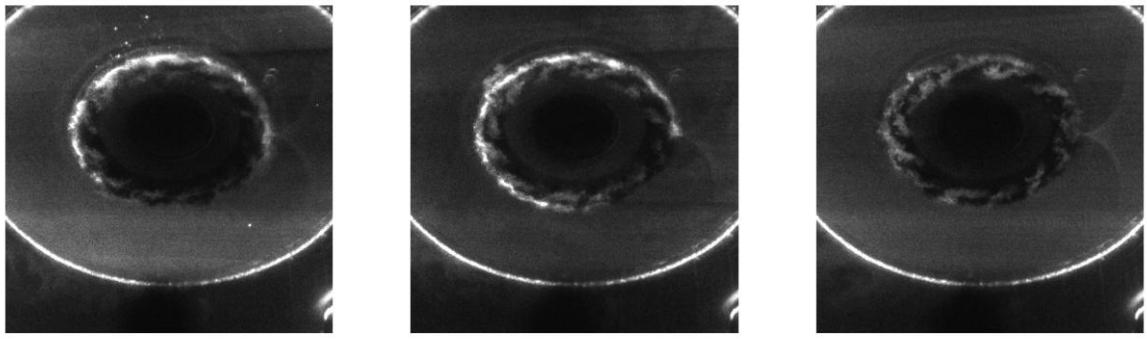

Figure 40 – Effect of Acetone Inlet Temperature for the F2 Mixer

Additional images illustrating effect of acetone inlet temperature for the F2 mixer: The left, center, and right images correspond to inlet fuel temperatures of 109°F, 125°F, and 145°F, respectively.

4.4.6 Conclusions

In this study, we set out to accurately quantify mixer performance for several hardware concepts at conditions that are relevant to actual engine operation. Similarity criteria were established and met in an effort to bolster confidence in results from atmospheric tests. This work has demonstrated that similar modes of jet break-up and evaporation can be achieved with non-reacting surrogate fuels injected in a low-pressure atmosphere. Use of acetone as a surrogate fuel was found to facilitate similarity and direct measurements of fuel concentration in the mixing field. The diagnostic achieved excellent accuracy and precision after correcting for non-homogeneities in the measurement plane due to evaporative cooling and variations in the local laser fluence, providing additional confidence in the results. Extension of this diagnostic approach to higher pressures is feasible, provided that other key complications are addressed, particularly, signal quenching by oxygen.

Several general observations were made in this work that shed light on the nature of fuel / air mixing for a broad range of operating conditions. Though absolute mixedness depends on fuel flowrate, relative mixing performance between designs (as indicated by measurements of global unmixedness and normalized radial fuel distributions) was found to be invariant for changes in jet momentum ratio. This conclusion was not particularly surprising given that the range of jet momentum ratios examined was not extensive enough to force a jet breakup regime change (see *Figure 16*). Mixer ranking was also found to be independent of the axial measurement location, though the optimal location for mixing measurements was observed near the dome where unmixedness is most pronounced. Studies of fuel inlet thermal boundary conditions also demonstrated that changes in evaporation have a minor impact on the overall mixedness relative to that of the jet breakup and flow-field characteristics.

The approach used in this work has been effective in discriminating mixer performance for modest and radical changes in hardware design. Nevertheless, this effort highlights the need for additional correlative comparisons and direct, detailed validation of LES modeling results. Though such an effort will likely clarify the shortcomings of each technique, it represents an exciting opportunity to gain the clearest picture of mixing and develop tools that will be indispensable for meeting future performance goals.

4.5 Task 3.2 – Flame Tube Emissions Testing of Fuel Injector / Mixer Concepts (NASA Funded)

4.5.1 Summary

The objective of this task was to identify designs that will meet the NASA N+2 NOx goal of 75% reduction below CAEP/6 standards, and to down-select designs for subsequent testing in the TCA and HTP rigs in Tasks 3.3 and 3.8. A flame tube combustor was designed, constructed, and instrumented. Seven concept fuel nozzles and seven mixers were designed and manufactured. The designs were matched into various configurations based on expected performance from earlier CFD results. Flame tube emissions testing was completed for 14 fuel nozzle / mixer configurations. Data analysis indicates that multiple concepts show promise to meet or exceed the N+2 LTO NOx Technology Goal of 75% emissions reduction from the ICAO CAEP/6 standard. Three concepts were down-selected for the Task 3.3 TCA tests based on NOx emissions, relative combustion efficiency, and initial combustion dynamics data.

4.5.2 Introduction

The flame tube test provides a cost-efficient method for rapidly screening a set of fuel nozzle / mixer designs. The flame tube geometry does not mimic a true combustor, specifically in the sense of cup-to-cup mixing and the size and shape of corner recirculation zones. Generally, a single module rig (i.e., a single cup sector) or a 3 to 5 cup sector combustor, is the ideal vehicle to fully screen designs across the operating space. These rigs are more difficult and expensive to manufacture, and in the case of a multiple-cup sector, more expensive to test for each configuration. However, comparison of designs within a flame tube geometry is a key screening method. Relative NOx emissions performance is expected to be well-captured in the flame tube environment; while CO, Unburned HydroCarbons (UHC), and, therefore, efficiency are anticipated to be less reliable due to the higher liner cooling flow split and liner area / combustor volume ratio.

The flametube tests conducted here were used to down-select from the multiple concepts and fuel nozzle / mixer design families developed via CFD methods, to a smaller number that were tested in the TCA and HTP rigs. It also provided the initial evidence as to the potential for any of the concepts to achieve the ultimate goal of the program – 75% LTO NOx reduction below CAEP/6 standards.

4.5.3 Methods, Assumptions, and Procedures

4.5.3.1 Fuel Nozzle / Mixer Design

The dual orifice pilot fuel circuits adopted for this program are hydraulically equivalent to those validated on another combustor program. Mechanically, the pilot fuel tip was designed as a simpler "tip-on-a-stick" assembly to facilitate our typical flame tube test rig installation. The aero design of the pilot swirler, a subassembly of the fuel nozzle, was leveraged from a prior program.

The mechanical design has been completed for a total of seven fuel nozzles and seven main mixers. The concepts are divided into two groups. The first group consisted of five fuel nozzles (F0-F4) and mixers (M1-M5) which can be tested in any combination. Approximately 15 configurations were identified for testing based on initial CFD analyses, and the most promising designs received highest priority during the flame tube tests. The second group consisted of the F5/F6 fuel nozzle concept, of which there were two fuel nozzles and two main mixer designs (M6/M7), for a total of 4 different configurations.

4.5.3.2 Flametube Rig Design

The flametube dome, mixers, and fuel nozzles were manufactured specifically for the N+2 program, but the liner was existing hardware from another GE Aviation program with higher cooling effective area than the intended N+2 design. Therefore, the flametube liner was overcooled relative to the combustor.

4.5.3.3 Flametube Instrumentation Design

Static pressure was measured upstream of the baffle, between the baffle and dome, at the liner cooling passage inlet and outlet, and at three axial locations along the liner hot side. Thermocouples were used to measure flametube inlet temperature and to monitor liner temperature. During the test, the airflow across each flametube component was calculated using the measured inlet temperature, the static pressure drop across each component, and measured component effective areas. The total airflow was calculated as the sum of the components and also calculated using the pressure drop across an upstream orifice plate.

Figure 41 depicts the flame tube single-point emissions probe. The probe was traversed vertically to measure emissions at the five indicated immersions. EINOx, EICO, EIHC, and efficiency measurements at each immersion were area-weighted as shown to provide average outlet emissions and efficiency values. The heavy weighting of the outer radius locations is aggravated by the tapered liner, which limits the proximity of the starting point near the wall. The resulting emissions index and efficiency values were weighted heavily toward the flametube liner.

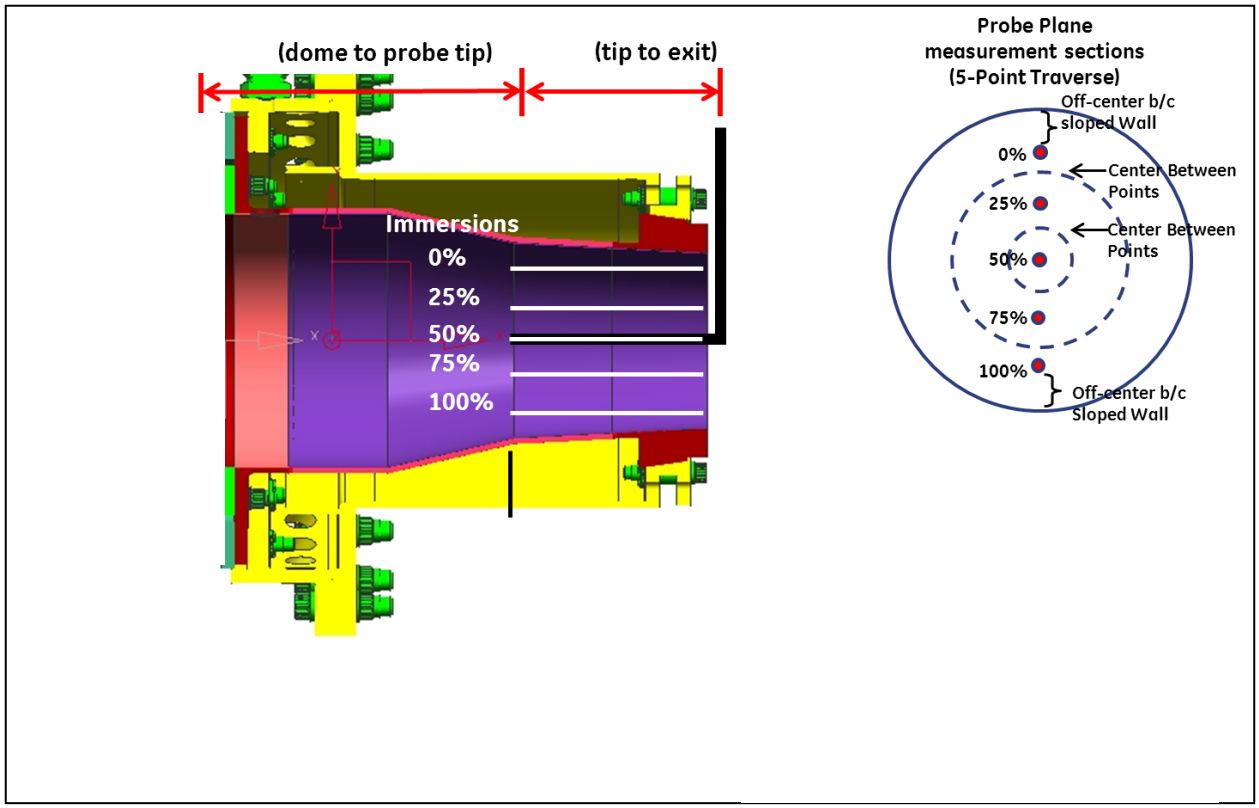

Figure 41 – Flametube Emissions Probe Installation and Radial Immersion Locations

The flametube was installed in the pressure vessel, with ports for the emissions probe, pressure, and temperature instrumentation, and a Hydrogen igniter torch. A bracket assembly held the fuel nozzle against the dome and supported the fuel lines to prevent vibration. Each nozzle was inspected for damage after testing.

4.5.3.4 Flametube Test Plan

This section summarizes the flametube test plan for the mixers. The first three test points were conducted at 800F inlet temperature, 250psia inlet pressure, target pressure drop, and three levels of mixer Fuel-Air Ratio (FAR). The remaining test points were conducted at 1000F inlet temperature. The flametube inlet pressure was first held at 250psia and tests were conducted at the target minimum pilot fuel split with varying levels of pressure drop and total mixer FAR. Next, inlet pressure was reduced to 200psia and 150psia, and the tests at the target pilot fuel split were repeated. Finally, tests were conducted with higher pilot fuel split at 250psia. The purpose of the higher pilot tests was to compare the emission penalty between configurations when pilot fuel split is increased. Emissions values and relative emissions trends between configurations had relatively weak dependence on inlet pressure in the tested range. Therefore, the 200psia and 150psia test points were eventually dropped to reduce test time. Emissions also had weak dependence on pressure drop, so typically only the target pressure drop was tested.

4.5.3.5 CFD Pre-Test Predictions

The team finished all of the flametube reacting flow CFD calculations. The run conditions for these flametube CFD cases were set at the maximum conditions that our test facility can reach, P3 = 250 psia and T3 = 1000 F. The overall mixer fuel / air ratio was set to match the flame temperature at take-off conditions, with the target pilot / main fuel split. *Figure 42* presents the CFD NOx predictions for 13 different configurations. As another comparison point, select configurations were run with the same fuel / air ratio for take-off cycle conditions (*Figure 43*). Inspection of these two data sets indicates that NOx performance ranking remains consistent for the four concepts analyzed at two different fuel / air ratios.

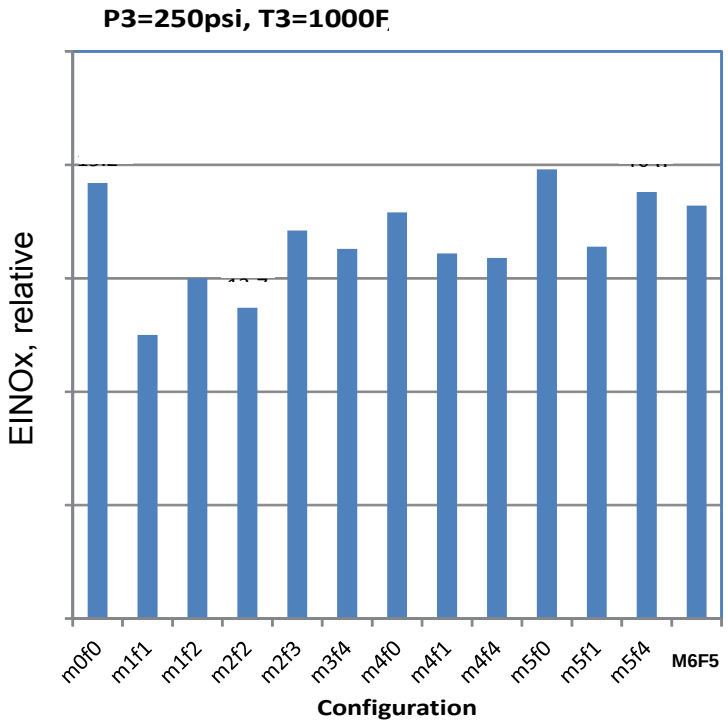

Figure 42 – Predicted EINOx for Different Mixer / Fuel Nozzle Configurations

At flame tube rig test conditions. The FAR_mixer results in a primary zone flame temperature matching that for take-off conditions.

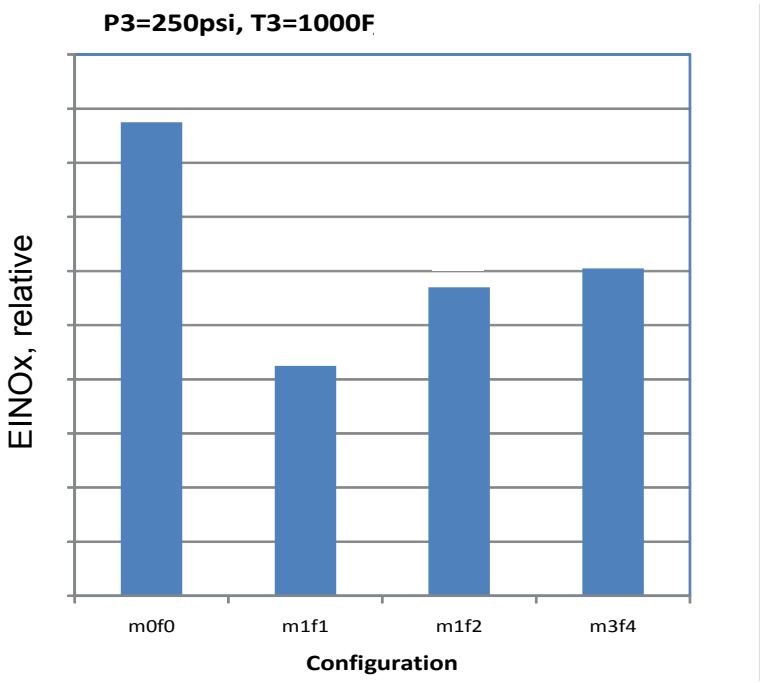

Figure 43 – Predicted EINOx for Different Mixer / Fuel Nozzle Configurations

At flame tube rig test conditions. The FAR_mixer matches the total mixer fuel / air ratio for take-off conditions.

The CFD pre-test predictions indicate that it may be difficult to differentiate mixer performance for some of the mixer / fuel nozzle configurations at the flame tube test conditions. In addition, the lower T and P rig conditions for these preliminary flame tube tests may confound conclusions about the relative behavior at engine cycle conditions of interest, making it difficult to accurately compare the mixer performance primarily due to differences in fuel jet injection properties at rig versus engine conditions. Test points included derivatives on dome dP/P, T3, and P3 in an attempt to correlate measured NOx to expectations at actual cycle conditions. Acoustics spot-check data is considered in the mixer / nozzle down-select, especially if measured NOx is very similar between tested configurations. The results of these tests are used along with Tunable Combustion Acoustics (TCA) rig data (Task 3.3) and High Temperature and Pressure (HTP) rig data (Task 3.8), as well as comparisons from CFD, in order to make the final fuel nozzle / mixer concept down-select for the sector rig.

4.5.4 Results and Discussion

4.5.4.1 Flametube Test Summary

The flametube test campaign was completed in July 2011. This section summarizes the flametube test configurations, final results, configuration ranking, and the down-selection for the Tunable Combustor Acoustics (TCA) tests as part of Task 3.3.

The tested configurations consisted of combinations of the optimized mixer and fuel nozzle designs from Tasks 2.1A and 2.1, mixers M0 thru M7 and fuel nozzles F0

through F6. Each configuration was tested up to 1000F / 250psia, at mixer fuel / air ratios spanning the cruise, 85% thrust, and 100% thrust engine cycle points. In the interest of time, M5F2 was not tested since the results were expected to be similar to M5F1 (M1F2 and M1F1 had shown similar performance to one another.) Finally, M7F6 was not tested because M7F5 produced unacceptable dynamics levels compared to the M6 main mixer in combination with either the F5 or F6 fuel nozzles.

4.5.4.2 Data Quality – Closures

Closure calculations are routinely performed as part of the test plan in order to verify that the combustor is operating as expected. Metered air flow rate is compared to a calculated air flow rate based on measured pressure drops and the effective areas from pre-test flow checks. Metered fuel flow rate is compared to a calculated fuel flow rate based on measured pressure drops and the flow number for the circuit, measured before the fuel nozzle is installed in the test rig. Finally, the calculated fuel / air ratio based on sampled emissions is compared to a calculated fuel / air ratio based on metered flows. In all three calculations, the calculated values agreed to within 10% of the metered values, which is considered acceptable closure.

4.5.4.3 NOx Emissions Results and Concept Ranking

A summary of the EINOx measurements for each configuration is shown in *Figure 44* for the target pilot fuel split, 1000F inlet air temperature, 250psia inlet pressure and 3 to 5% dome pressure drop (dP/P3). The dP/P3 dependence was very weak, allowing the entire dP/P3 range to be combined into each series. The single extra reference point drawn on each graph represents the EINOx value at 100% ICAO Fuel / Air Ratio (FAR) that was predicted to scale to 25% CAEP/6 LTO NOx (see the description of this correlation below).

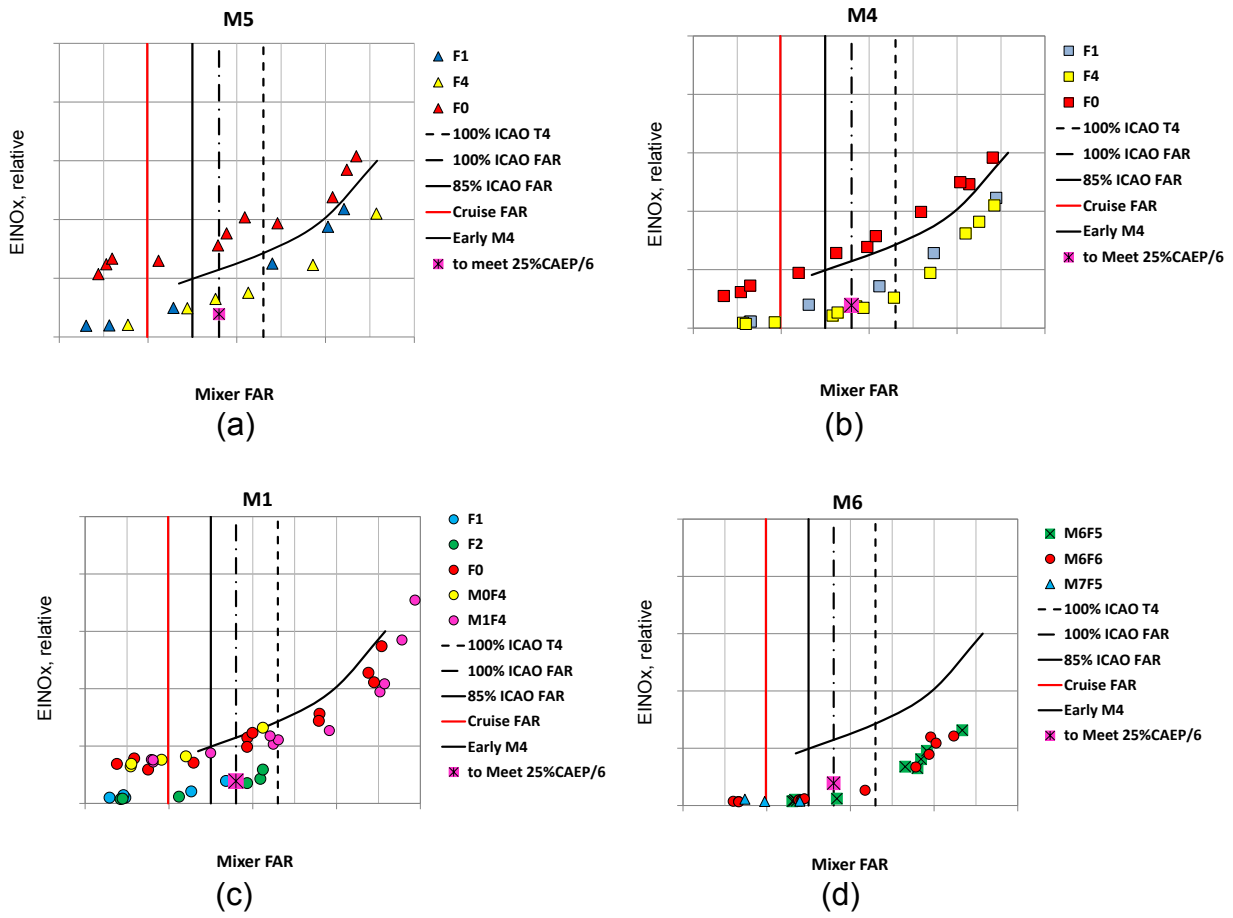

Figure 44 – Summary of EINOx versus Mixer FAR for Each Configuration

For all tested mixer / nozzle configurations at minimum target pilot fuel split, 250psia inlet pressure, 1000F inlet temperature, and 3-5% dome pressure drop: (a) M5 mixer; (b) M4 mixer; (c) M1/M0 mixers; and (d) M6/M7 mixers. Mixer FAR is defined as total fuel flow divided by the sum of air flow from main mixer + pilot.

In *Figure 44(a)*, M5F0 configuration is considered the baseline, because it is similar in geometry and technology level to legacy TAPS designs. All other M5 configurations had lower EINOx than M5F0. In other words, F1 or F4fuel injection with the M5 mixer significantly improves EINOx, per design intent. Nevertheless, all the EINOx profiles for the M5 mixer are above the 25% CAEP/6 point.

Figure 44(b) shows that the M4 mixer realizes further EINOx improvement over the M5 mixer for each injection type. The M4 with F4 produces slightly lower EINOx than M4F1, and it is predicted to satisfy the 25% CAEP/6 NOx requirement.

Figure 44(c) indicates that the M1 mixer also improves EINOx over the M5 mixer for each injection type; however, differences relative to the M4 vary between injector designs. Unlike the M4 mixer, the M1 with F4 injection did not show any significant benefit over the M1F0. The M1F1 did show significant EINOx improvement over the

baseline F0 fuel injection. There were only slight differences between the F1 and F2 nozzles' performance, and both configurations are predicted to satisfy the 25% CAEP/6 requirement.

The M6 mixers / nozzles in *Figure 44(d)* produced the lowest EINOx of all configurations, and they all are predicted to satisfy 25% CAEP/6 NOx.

Figure 45 is a summary of the EINOx measurements for each configuration at higher pilot fuel split, 1000F inlet air temperature, 250psia inlet pressure and 3 to 5% dP/P3. Sample probe traverse issues prevented data for the M5F1 configuration in *Figure 45(a)*. Similarly, a secondary fuel supply issue prevented data for the M1/F4 and M7F5 designs in *Figure 45(c)* and *Figure 45(d)*, respectively. The EINOx trends between configurations are the same as for the target pilot test points in *Figure 44*; the main difference being that the higher pilot EINOx values are consistently higher, as expected. All configurations with higher pilot are predicted to exceed 25% CAEP/6, although the M6 mixers are very close and likely within the uncertainty of the flame tube-to-engine correlations. The ability to shift to a higher pilot split while meeting NOx targets may create more design and / or operational margin.

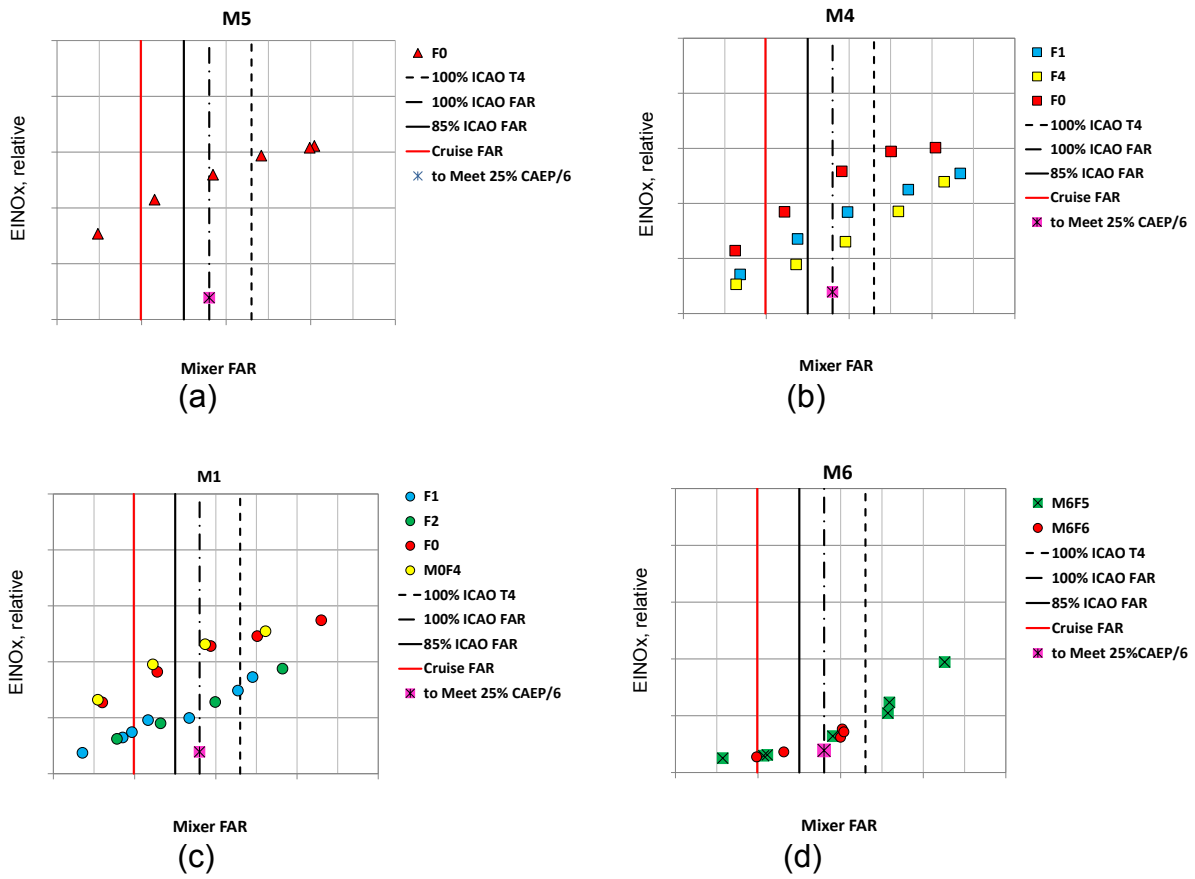

Figure 45 – Summary of EINOx versus Mixer FAR (Higher Pilot Fuel Split)

For all tested mixer / nozzle configurations at higher pilot fuel split, 250psia inlet pressure, 1000F inlet temperature, and 3-5% dome pressure drop: (a) M5 mixer configurations; (b) M4 mixer configurations; (c) M1 mixer configurations; and (d) M6 mixer configurations. Mixer FAR is defined as total fuel flow divided by the sum of air flow from main mixer + pilot.

A summary of the EINOx data at 100% ICAO fuel/air ratio is given in *Figure 46*. The EINOx values were interpolated from the data in *Figure 44* and *Figure 45* to get values at the 100% ICAO FAR. The same interpolation procedure was used for efficiency and combustion dynamic pressure values shown in later figures. In *Figure 46* and following figures, a horizontal line is given which indicates the maximum EINOx value, measured at flametube conditions, which we can expect to result in the target 25% CAEP/6 LTO NOx values at the sector rig / full engine conditions. This correlation is a conservative value, as described below. The mixer / nozzle configurations are ordered from lowest to highest EINOx. The M6 mixers produced the least EINOx, followed by M1 and M4 mixers with F1/F2 or F4 injection, and finally ending with the highest EINOx from the baseline M5F0 configuration.

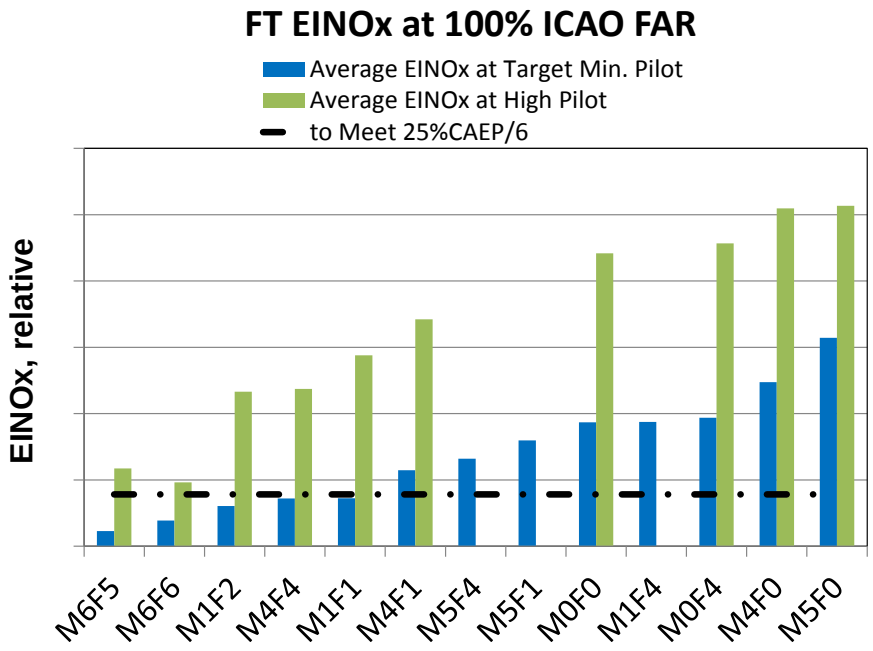

Figure 46 – Summary of EINOx Measurements at 100% ICAO Fuel / Air Ratio

EINOx measurements at 100% ICAO fuel/air ratio and max rig conditions (1000F / 250psia). Two different pilot fuel splits were tested; the design intent pilot fuel split is represented by the blue columns. The black dashed line represents an estimated maximum EINOx value allowed at these conditions to meet 25% CAEP/6 technology goals.

An estimate of LTO NOx performance has been calculated for the tested concepts and is included in *Figure 47*. Extrapolating emissions performance from the low temperature, low pressure conditions of a cylindrical flametube test up to takeoff conditions in a sector, Full Annular Rig (FAR), or engine test geometry is challenging. Based on data from multiple legacy engine programs using lean premixing fuel nozzles, correlations have been generated to translate our N+2 flametube emissions data out to the expected sector emissions performance. As each engine program introduces new levels of technology and mixer design, the correlation functions can vary. In addition, no emissions data could be taken in the present Flametube tests that are appropriate to use for the 7% and 30% ICAO cycle points. Therefore, EINOx correlations from a previous engine program were used to estimate the 7% and 30% ICAO EINOx values for the N+2 cycle conditions. Other correlations, developed from programs containing both Flametube and sector, FAR, or engine data, were used to estimate 85% and 100% ICAO EINOx values based on the current Flametube emissions data. Where a range of correlation coefficients was possible, conservative values were chosen that would tend to increase the extrapolated LTO NOx value and avoid over-predicting the CAEP/6 NOx margin.

The estimated LTO NOx values are also shown in *Figure 47*, as a percentage of CAEP/6 regulated limits, along with the NOx data at the 100% ICAO fuel-air ratio. Based on the NASA N+2 Technology Goal of emissions reduction to 25% of the CAEP/6 NOx standard, the data indicate that 5, and potentially up to 8 or more, of the

tested concepts show potential for meeting the program objectives during the future sector test. As mentioned above, a conservative value was used for the correction factor from flametube to sector / FAR / engine geometry. In fact, there has been a range of correction factors measured over multiple engine programs. The uncertainty bars in *Figure 47* represent the smallest actual correction factor previously measured; more than one engine program has measured even larger correction factors. Therefore, there is the possibility that even more than the first five concepts could in fact successfully meet the EINOx goal.

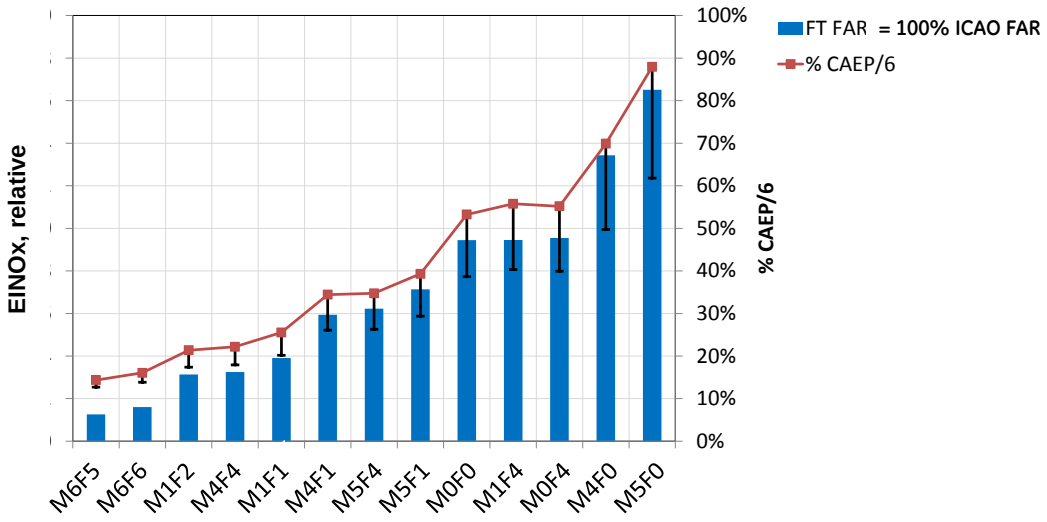

Figure 47 – Estimated LTO NOx Values

Flametube NOx emissions for a mixer fuel / air ratio (FAR) representative of 100% ICAO thrust conditions. The estimated LTO NOx, plotted as % CAEP/6, is based on flametube data at 85% and 100% ICAO mixer FAR along with correlations from other engine programs.

4.5.4.4 Additional Performance Criteria: Efficiency and Combustion Dynamics

The team also considered performance criteria other than EINOx during the down-selection process. Measured combustion efficiency, EICO and EIHC – although misrepresented in the cylindrical geometry and excessive cooling flows of the flametube rig – are nonetheless used for relative comparison of concepts. Combustion dynamics was another important factor considered in the down select.

In *Figure 48*, combustion dynamic pressure values are included to show the trade-off with EINOx. The EINOx values are interpolated from the data in *Figure 44* to get values at the 100% ICAO FAR. The same interpolation procedure is used for efficiency and combustion dynamic pressure values. The EINOx differences between configurations are sufficient for a clear ranking, with the M6 configurations demonstrating the lowest EINOx and the M5F0 showing the highest EINOx. Dynamic pressures are shown for the target pilot split. The F4 injection configurations (F4) tended to have higher dynamic pressure levels, and there is a general inverse correlation between EINOx and dynamics for the other configurations. The M6 is an exception, because it has the

lowest EINOx and also low combustion dynamics; however, combustion efficiency also tended to be lower compared to other configurations. The flame tube dynamics measurements indicate configurations which may continue to have dynamics issues in the eventual sector configuration. Specifically, the F4 design produced the highest dynamic levels at both pilot fuel split levels over multiple mixer combinations. Such other performance factors result in a trade-off such that the overall best configuration may not have the absolute lowest EINOx.

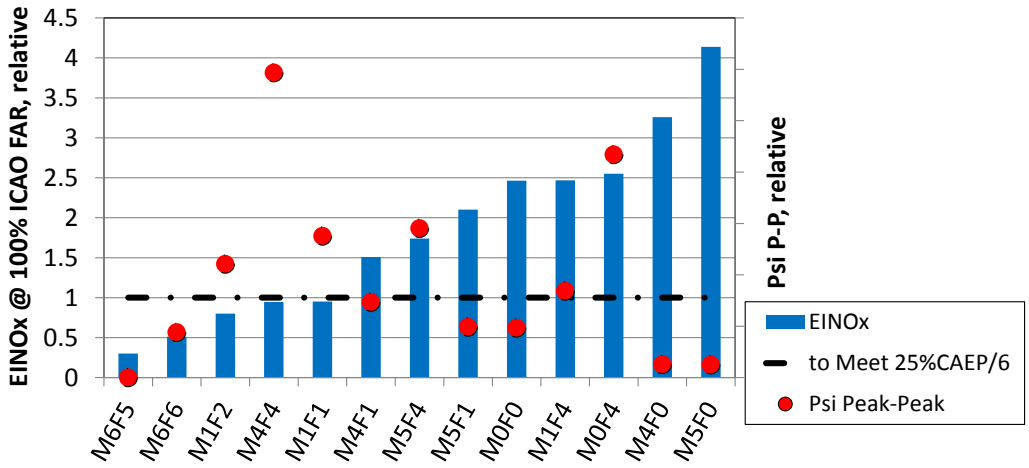

Figure 48 –Ranking of the Concepts, including Combustion Dynamic Pressure Values

EINOx ranking of the flametube configurations, with peak dynamic pressures for comparison. Peak-to-peak psi (PSIPP) indicates the maximum peak of the time averaged combustion dynamic pressure spectra, which occurred within the same frequency range for all configurations.

4.5.5 Conclusions

The flametube testing is a cost-efficient, highly valuable tool for rapidly screening many fuel nozzle / mixer configurations. Fuel nozzle and mixer mechanical design work will form the foundation for the full-up nozzle design in the eventual sector test. 14 configurations were screened at a variety of operating conditions, and the results were compared on the basis of sampled emissions and dynamic pressure measurements.

Based on the flametube NOx, dynamics, and efficiency data, the concepts that have been down-selected for the upcoming TCA tests in Task 3.3 are M6F6, M1F2, M4F4, and M4F1. The selected configurations represent a mix of fuel nozzle and mixer styles, and all show strong potential for meeting LTO NOx targets. Because the F4 designs consistently indicated significantly higher combustion dynamics than all other concepts, this fuel nozzle design will receive the lowest priority.

4.6 Task 3.3 – Tunable Combustor Rig Dynamics Testing (NASA Funded)

4.6.1 Summary

Three N+2 fuel nozzle / mixer configurations were tested in the Tunable Combustor Acoustics (TCA) rig at GE Aviation, representing a range of fuel nozzle and mixer concepts down-selected from the Task 3.2 flame tube tests. The combustion dynamics maps contribute to the ranking of concepts going into the Task 3.8 HTP tests, and indicate the sensitivity of each concept to dynamic tones. From this testing, and in agreement with previous development programs, the aggressive M1 mixer is shown to have the highest dynamics (smallest operability range with dynamic pressures below pre-defined limits) compared to the M4 mixer and the M6 configuration.

4.6.2 Introduction

The TCA rig at GE Aviation is a unique vehicle for exploring the sensitivity of a specific mixer / fuel nozzle design to combustion dynamics. The upstream plenum and test section (combustor) is the exact same hardware as was used in the Task 3.2 flame tube testing. The down-selected fuel nozzle and mixer designs tested here are also the same hardware that was used in Task 3.2.

In any combustor geometry, acoustic frequencies inside the chamber interact with the flame – causing fluctuations in both fuel and air flow and, ultimately, flame shape and heat release locations. Certain acoustic frequencies are able to resonantly interact with the flame structure, causing a positive feedback loop which drives the pressure oscillations higher towards a limit cycle condition. These frequencies are typically in the range of 150 to 2000Hz. If pressure amplitudes become too large, the combustor hardware can suffer high cycle fatigue and mechanically fail, shortening the life of the combustor.

The purpose of the TCA testing is to examine the sensitivity of a given design to the whole range of acoustic frequencies, across a broad range of combustor conditions – temperatures, pressures, fuel-air ratios, dome dP/P, and fuel splits. Although this particular rig is limited to 1000 F / 250psia conditions, the relative dynamic pressure amplitudes generated by different designs can be a leading indicator of how well the design will perform in the full combustor geometry at many engine conditions. In the frequency range of interest, the TCA rig can provide good relative comparison of designs and aid in the down-select for future testing.

Three fuel nozzle / mixer configurations were selected from the tested flame tube configurations for further evaluation in the TCA test facility: M4F1, M1F2, and M6F6. The configurations chosen represent a mixture of fuel nozzle and mixer designs for which the flame tube data of Task 3.2 indicated capability to meet LTO NOx goals, sustained moderate to low combustion dynamics signatures, and had reasonable (relative) combustion efficiency values at low combustor fuel-air ratios (FAR's).

4.6.3 Methods, Assumptions, and Procedures

Data is collected by operating the rig over a range of combustor conditions (T3, P3, dP/P, fuel splits, fuel/air ratio) in order to map out the combustion dynamic amplitudes.

4.6.4 Results and Discussion

During the test, the pressure drop across the fuel nozzle tip is measured and used to verify the flow number of the nozzle. When compared to pre-test flow checks, this comparison is generally expected to be within +/-10% to be considered acceptable. The data for all three fuel circuits indicate that all fuel nozzles were working within the targeted range (*Figure 49 – Figure 51*).

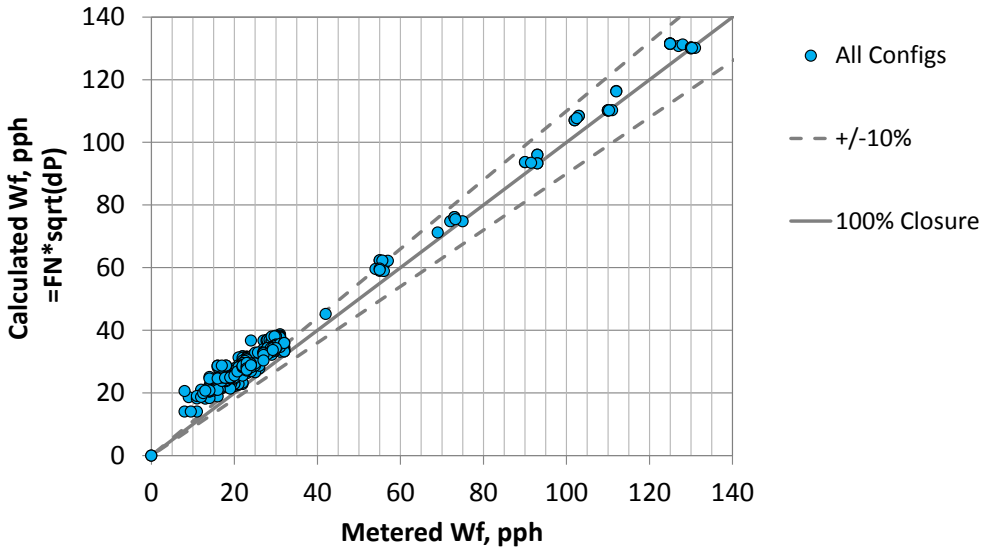

Figure 49 – Pilot Primary Fuel Closures

Verifying that the fuel nozzle was flowing per the pre-test flow tests.

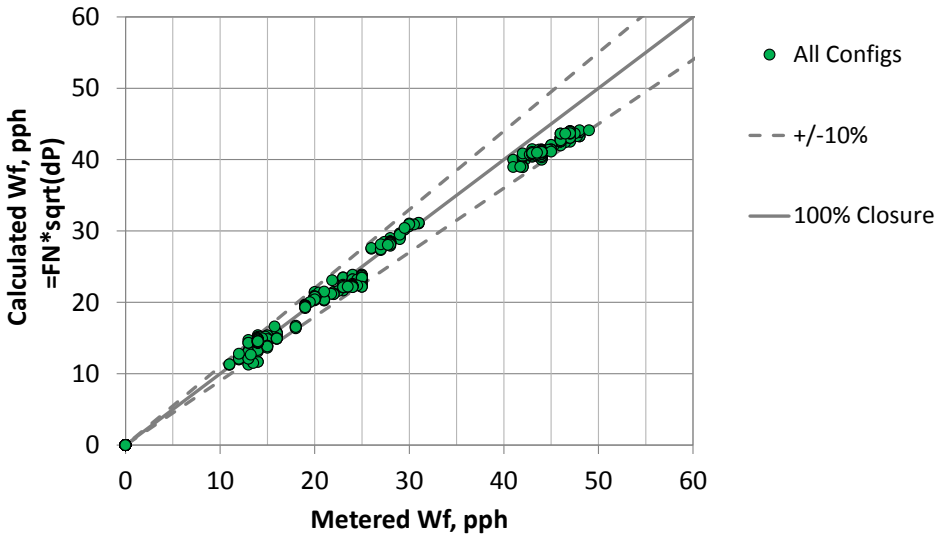

Figure 50 – Pilot Secondary Fuel Closures

Verifying that the fuel nozzle was flowing per the pre-test flow tests.

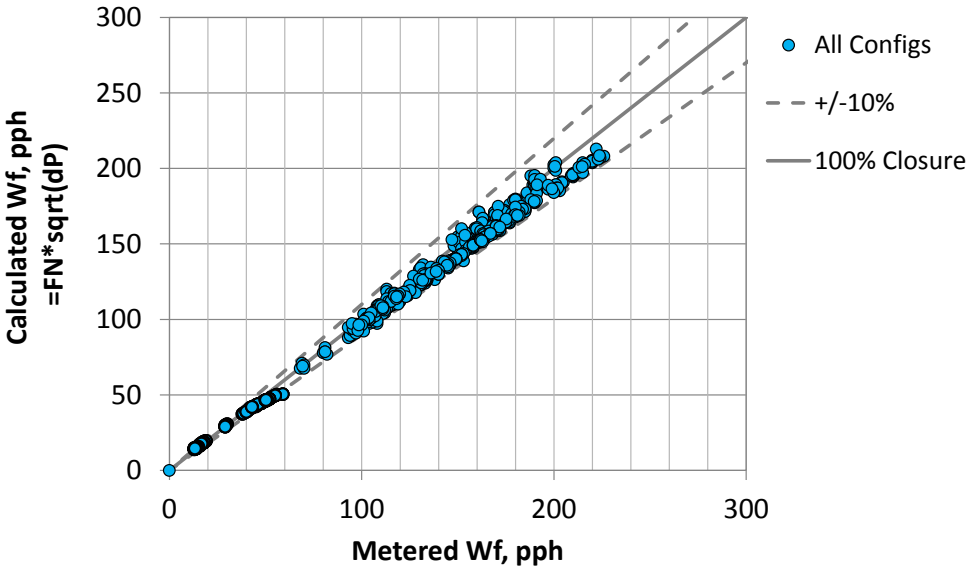

Figure 51 – Main Fuel Closures

Verifying that the fuel nozzle was flowing per the pre-test flow tests.

Three different air flow conditions were run: 1000F / 200psia, 775F / 200psia, and 440F / 60 psia. Acoustics results from these tests are given in *Table 7*. At the lowest T3/P3, the combustor is being operated in pilot-only mode, so the dynamics are measured as a function of the pilot Equivalence Ratio (ER).

In *Table 7*, the fuel/air ratio margin is shown for all three designs operating at 1000F/200psia. The margin here is calculated as the FAR36 value where the pre-set acoustic limits are hit, minus the FAR36 value for the 100% ICAO cycle point. All

numbers represent the margin for fully-staged operation. It is clear that M4F1 has the most margin, and that M1F2 has negative margin. While the test conditions are quite far from the actual 100% ICAO cycle conditions, experience has taught us that the relative comparison of combustion dynamic sensitivities measured in this rig can be a good indicator of resistance to combustion acoustics in the actual combustor.

Table 7 – Dynamics results at 1000F / 200psia

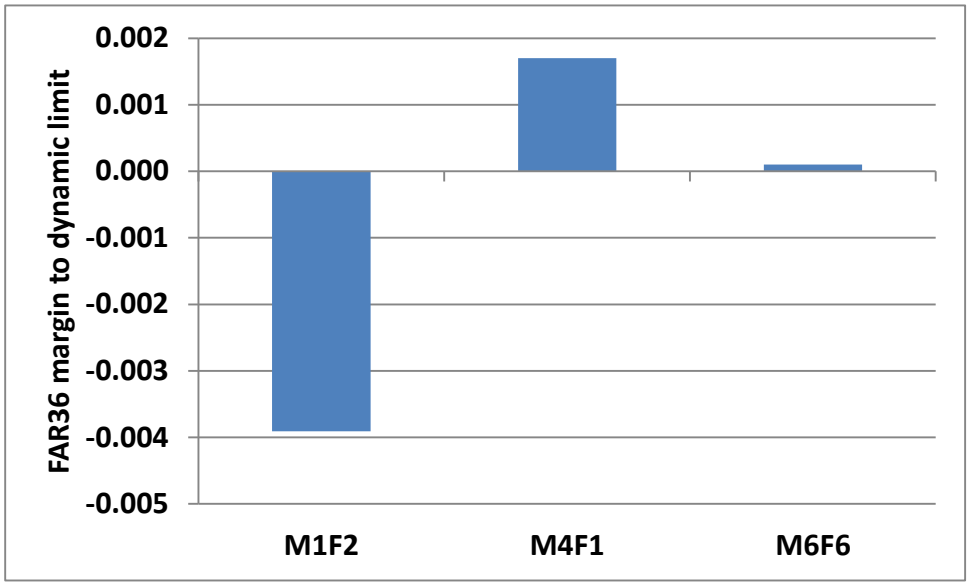

Fuel/air ratio margin between 100% ICAO takeoff FAR and FAR at the dynamics P4' upper limit.

These data provide relative comparisons of the operability limits of the three tested configurations, and delineate the differences and features of these designs. At 1000F, the M4F1 and M6F6 configurations show operability (acoustics < limit) throughout the desired FAR36 and main / pilot split range of the nozzles. The M1F1 design encounters the boundary at lower FAR36 and Main Equivalence Ratio (ERM), making it the less attractive design from an acoustics point of view.

At 775F, the acoustic boundaries for all three fuel nozzles occur at similar Main equivalence ratios.

4.6.5 Conclusions

The TCA data points to the preferred mixer designs from a relative acoustics performance standpoint, as well as elucidating the impact of fuel split. Based on this data, the M4 mixer was prioritized in the line-up for Task 3.8 HTP testing due to its low acoustics and low (good)-to-marginal NOx performance.

4.7 Task 3.4A – TAPS Full Annular Rig (FAR) Dynamics Mapping (GE Funded)

4.7.1 Summary

A Full Annular Rig (FAR) test was used to map out the combustion dynamics characteristics of one specific TAPS combustor. Data was collected over a range of T3 / P3 / FAR36 / fuel split conditions, and a database was generated to guide the eventual turbofan engine operation.

4.8 Task 3.5A – TAPS Engine Dynamics Mapping (GE Funded)

4.8.1 Summary

A turbofan engine test was used to map out the combustion dynamics characteristics of a TAPS combustor. Data was collected during transients and steady-state operation, over a range of engine acceleration rates and using various fuel scheduling modes. A database was generated.

4.9 Task 3.6A – TAPS Core Engine Dynamics Mapping (GE Funded)

4.9.1 Summary

Combustion dynamics were evaluated in a Core engine test, including both steady-state and transient operation. Steady-state data was obtained by running the engine at a range of core speeds covering the entire op-line. Combustor mapping involved recording dynamic pressures at various P3 / T3 test conditions variable. Transient data was similarly recorded during bursts from ground idle at a range of combustor inlet temperatures, fuel splits, and fuel schedules.

4.10 Task 3.7A – Auto-Ignition Testing (GE Funded)

4.10.1 Summary

Auto-ignition testing of a TAPS fuel nozzle / mixer configuration has been conducted in a single cup high-temperature and -pressure rig. The objective of this testing was to examine the impact of various design and fuel parameters on the auto-ignition behavior. The database contributed to the successful design and evaluation of the N+2 fuel nozzle / mixer.

4.11 Task 3.8 – HTP Auto-Ignition Margin Validation Testing (NASA Funded)

4.11.1 Summary

The High Temperature and Pressure (HTP) single cup flame tube rig was utilized to evaluate auto-ignition boundaries and emissions performance at near-engine cycle conditions. The fuel nozzle concepts from Task 3.2 have undergone an extensive redesign, thermal and mechanical analysis, and manufacturing / instrumentation process. Three designs were tested: F1 and F2, both with the M4 mixer) and the M6F6 mixer configuration.

The F1 design has acceptable auto-ignition margin for sector rig operation at N+2 cycle conditions. All three concepts show promise to meet the N+2 LTO NOx Technology Goal of 75% emissions reduction from the ICAO CAEP/6 standard. As expected based on flame tube test data from Task 3.2, EINOx performance of the M6F6 was significantly better than other tested configurations; however, operability margin at N+2 T/O conditions (margin to auto-ignition) is not as high as the F1M4 design. Emissions data and auto-ignition operability margins are compared for all three tested mixers. The F1M4 has been down-selected for the sector rig as the best overall performer of the tested configurations.

4.11.2 Introduction

Autoignition is a characteristic behavior of any fuel, and must be considered for high-OPR engines operation. GE's High Temperature and Pressure (HTP) flame tube rig is a uniquely capable test facility for screening and validating fuel nozzle / mixer designs for high-OPR combustors. The work in Task 3.8 utilized the HTP rig facility to evaluate multiple fuel nozzle / mixer concepts for both high power emissions performance as well as to validate adequate margin to auto-ignition limits for the aggressive N+2 cycle. Aside from an actual engine test, the HTP facility provides the only opportunity to validate durability and other key performance criteria at engine conditions beyond the take-off cycle point.

For testing in the HTP rig, the flame tube fuel nozzle designs from Task 3.2 and 3.3 had to be reworked into full engine-style nozzles capable of operation at temperatures in excess of the maximum engine cycle conditions. New mixer designs (including the high mixer flow split that enables low NOx) and fuel nozzle features generate a significant differentiation from previously tested technology, and required a significant design effort to ensure proper function and life for these tests. This also serves as the preliminary design for the hardware that will eventually be tested in the 5-cup Sector Rig at NASA. Full heat transfer, thermal / mechanical stress, and vibrational analyses were conducted to determine acceptable material temperatures and stresses for these limited-time tests. While the outer envelope and mounting points of the fuel nozzle were purposefully designed to match previously tested designs (to maximize use of common test hardware), the internal design of the fuel nozzle is significantly different than legacy hardware.

The test rig (combustor dome) was only slightly modified to match the size and design targets for the N+2 hardware. Because the fuel nozzle concepts developed in this program are very similar in envelope to production hardware, different concepts could be tested fairly efficiently, requiring only a few hours of change-over time.

4.11.3 Methods, Assumptions, and Procedures

4.11.3.1 HTP Rig Combustor Design and Manufacturing

The HTP combustor design was largely utilized from testing on a previous program. Due to some geometry changes, a new dome and deflector were designed and manufactured for the N+2 testing. The team also took this opportunity to redesign certain mounting and locating features to continue to improve the robustness and data quality of the rig.

4.11.4 Results and Discussion

4.11.4.1 CFD Pre-Test Predictions

Early in the program, the team completed High Temperature and Pressure (HTP) rig CFD pre-test prediction calculations for the pre-selected three M1 and one M6 configurations. The calculations were carried out at 100% and 85% ICAO points. NOx emissions were post-processed based on the CFD results. *Figure 52* shows the predicted EINOx values for the four configurations. The M1 with F1 and F2 fuel nozzles are predicted to produce lower NOx than the M1 with F4 fuel nozzle.

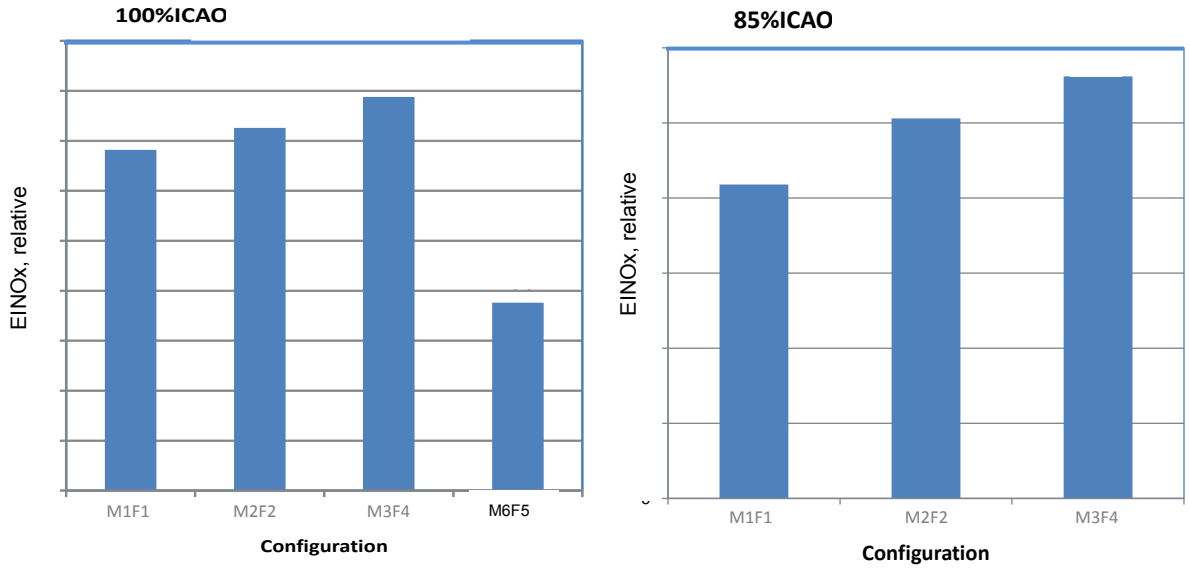

Figure 52 – Predicted EINOx Values for 4 Configurations

Predicted EINOx for three different M1 and M6 configurations at 100% (left) and 85% (right) ICAO points.

Comparing to predictions for the flame tube rig conditions in Task 3.2, it is clear that all of the calculated conditions yield the same relative ranking of NOx performance among the three different M1 (F1, F2, F4) configurations. However, the M6F5 design is predicted to have significantly lower NOx at engine (HTP) conditions, whereas its NOx at flame tube conditions was calculated to be amongst the highest of all nozzle configurations to be tested. Because of the design of the M6 concept versus the F-series configurations, the correlations between low-pressure flame tube rig results and high-pressure engine cycle conditions may be quite different. Within this program the combination of CFD calculations, low- and high-pressure single module data, and mixer diagnostic data across a range of concepts, along with the final sector combustor results at low- and high-pressure, will ideally provide a useful data set for determination of better performance correlations and model validations to aid future engine development programs – including Phase II of the NASA N+2 program.

4.11.4.2 Emissions Data

Emissions data on JetA fuel was collected using a single point, traversing probe located downstream of the fuel nozzle tip at a location that yields an effective combustor volume similar to a single cup in the sector rig. Most data was collected using a 5-point traverse in order to get data at more conditions in the available test time.

Example emissions profile data is shown in *Figure 53* for the M4F1 configuration at a condition representing the closest data point to the 100% ICAO take-off conditions. EINOx and EICO are calculated using local NOx and CO concentrations and the local derived Fuel / Air Ratio (FAR) based on measured O2 concentrations. For this high FAR point, CO has a relatively flat profile with a slight peak at the outer diameter. Both NOx and FAR_O2 are symmetric and center-peaked, as expected.

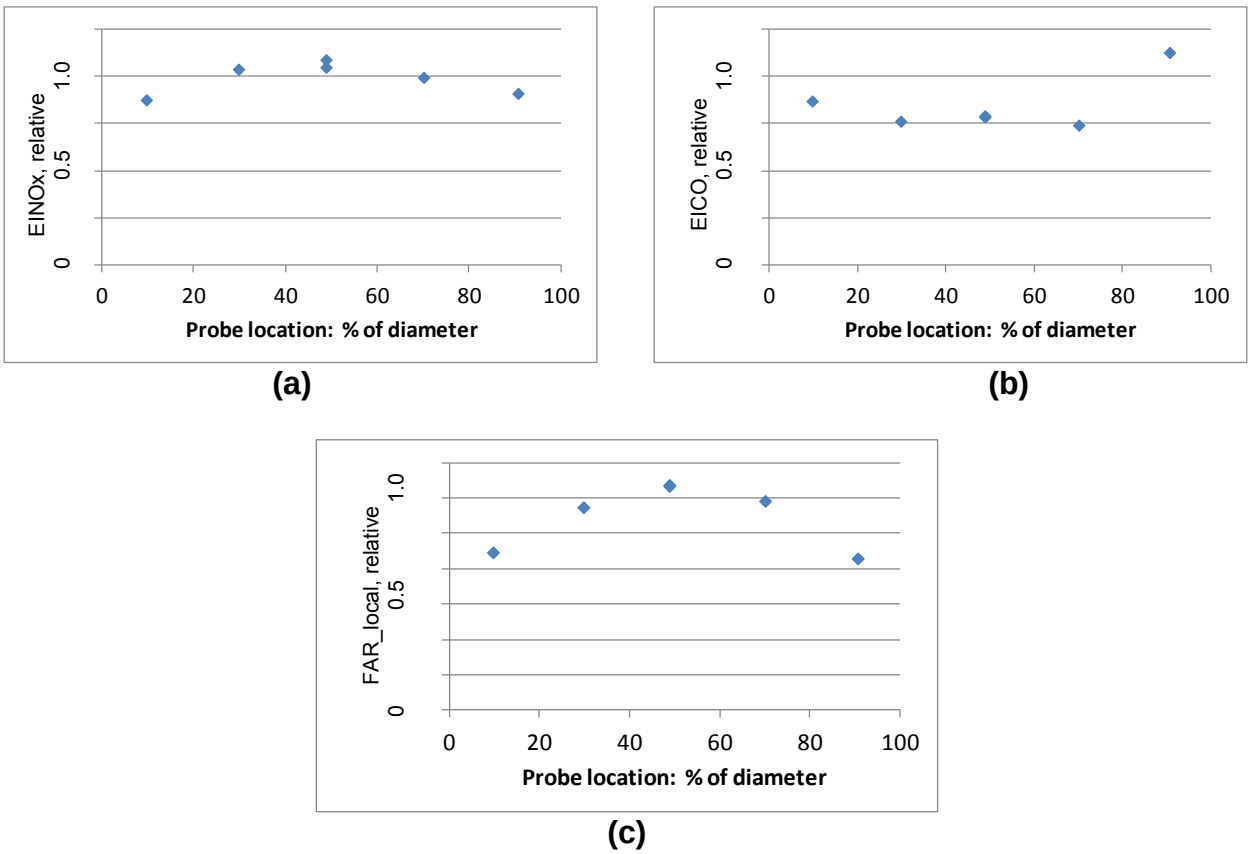

Figure 53 – Example Emissions Profile Data (at Near-100% ICAO Conditions)

Emissions profiles for M4F1 configuration at near-100% ICAO conditions. (a) EINOx (b) EICO (c) Local Fuel / Air Ratio (FAR) calculated using measured O2 concentrations.

NOx emissions (area-averaged) for the F1 configuration are given in *Figure 54*. Critical data for this program are the FAR sweeps at conditions near 100% ICAO and 85% ICAO, as these points contribute to LTO NOx calculations. Conditions matching Task 3.2 Flametube experiments (1000F / 250psia) were also run in order to compare the two sets of data. Intermediate pressure points were taken as a means to bridge the gap between low and high pressure data.

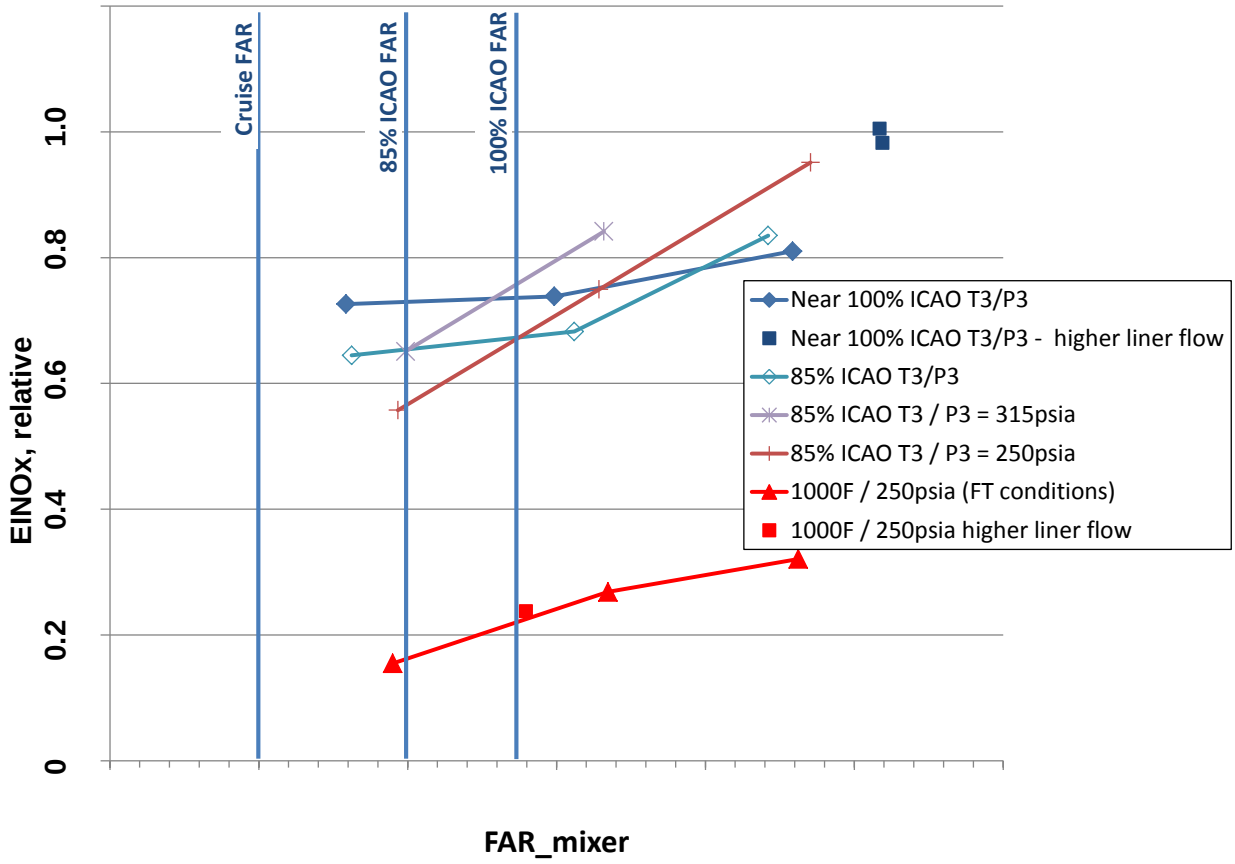

Figure 54 – NOx Emissions for the M4F1 Configuration

Data over the P3 range of 250 to 750psia indicates fairly low pressure dependence for NOx – within the scatter of the data. On the other hand, dropping T3 from 1200F to 1000F (at 250psia) appears to have a strong impact on NOx. Increasing liner cooling flow does not measurably affect the NOx emissions at low T3/P3. At high T3 / P3 the impact is uncertain, as there is no direct comparison at the same value of FAR_mixer. However, NOx trends would tend to put the high-liner-flow points on or only slightly above an extrapolated NOx curve, and certainly within the scatter of the collective NOx data for all high T3 conditions.

A direct comparison with Flametube data is provided in *Figure 55*. EINOx data is very similar, but EICO tends to be higher in the HTP rig. This could be due, in part, to the higher liner flow split in the HTP rig versus the Flametube rig.

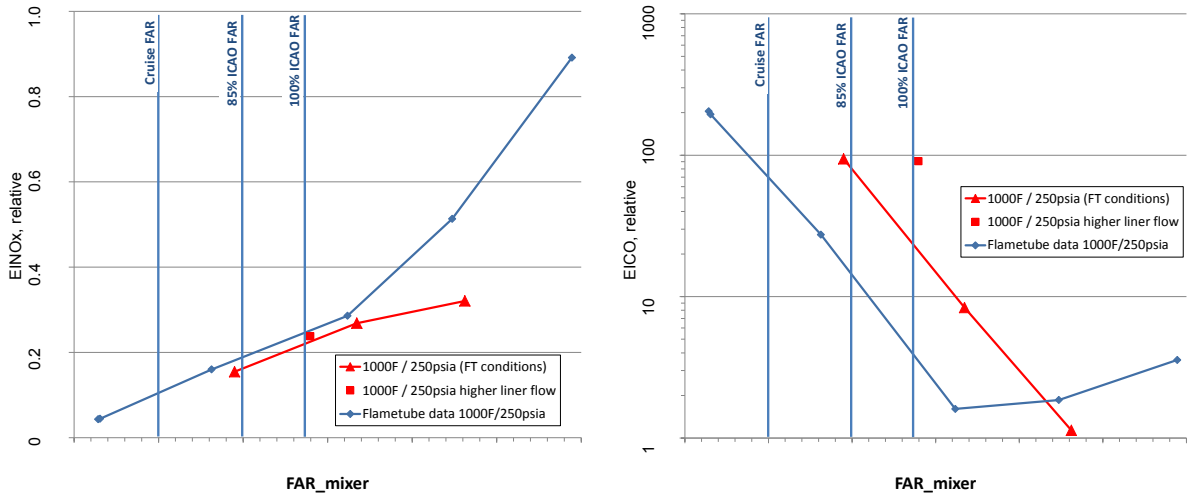

(a) **(b)**

Figure 55 – Direct Comparison with Flametube Data

Comparison of M4F1 HTP data (red) with M4F1 Flametube data (blue). (a) EINOx (b) EICO.

NOx and CO data for all three tested configurations at 85% and near-100% ICAO conditions are given in *Figure 56* and *Figure 57*, respectively. Similar to Flametube measurements in Task 3.2, the M6F6 configuration exhibits the best NOx performance but worse CO (and therefore efficiency) compared to the M4F1 design.

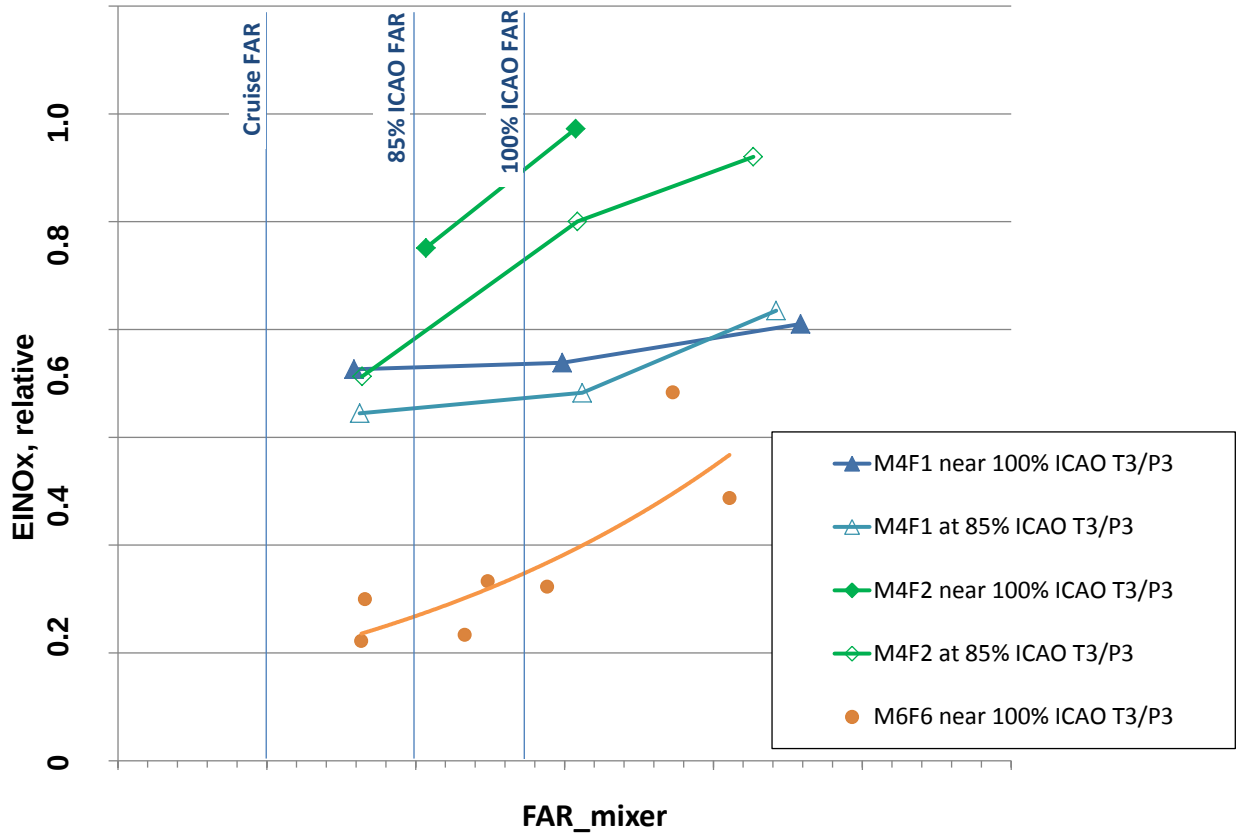

Figure 56 – EINOx Data for All Tested Configurations

EINOx data for all tested configurations at 85% and near-100% ICAO conditions.

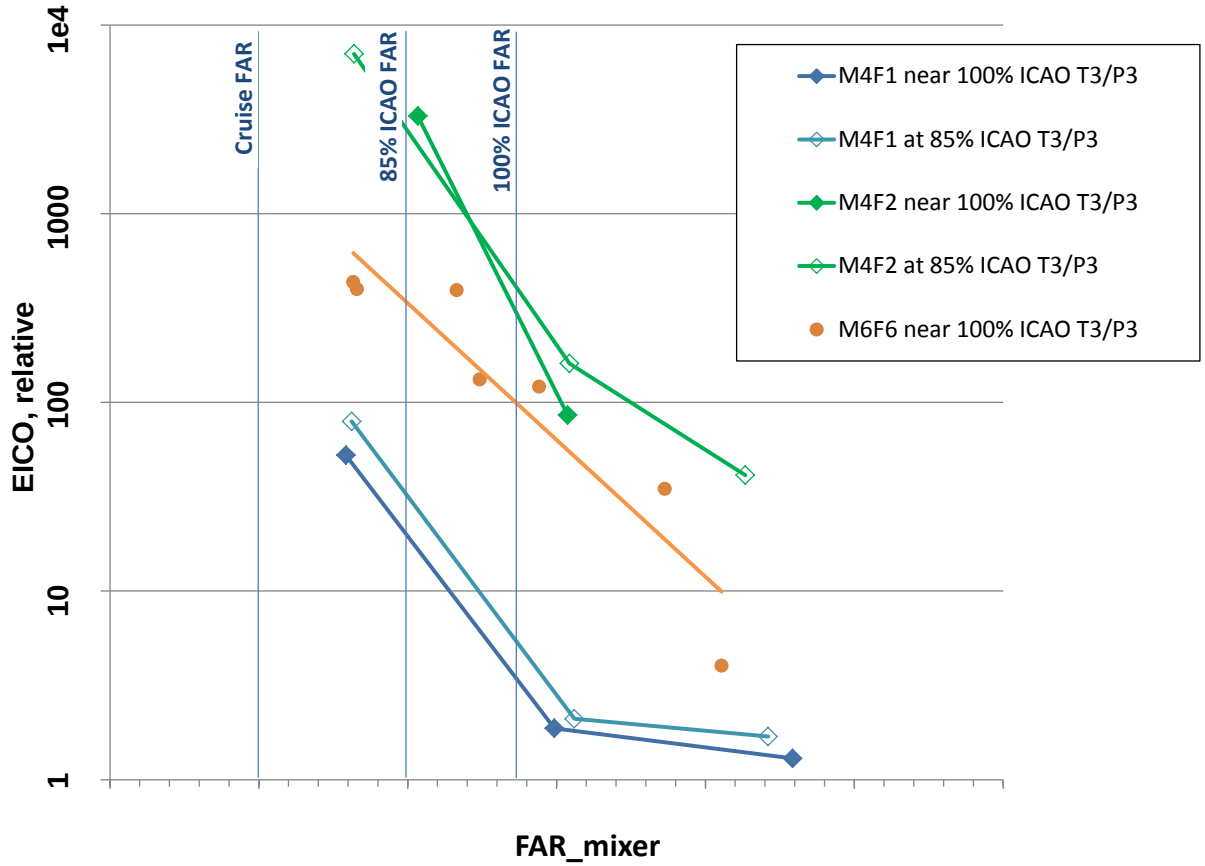

Figure 57 – EICO Data for All Tested Configurations

EICO data for all tested configurations at 85% and near-100% ICAO conditions.

The HTP rig was designed specifically for auto-ignition margin validation at high T3 and P3 conditions. The liner cooling was designed for durability; cooling air is separately measured and controlled. For the N+2 emissions measurements, the liner cooling flow was decreased to the minimum liner dP/P (while still allowing margin for backflow). Even still, the cooling air flow split (~20-30% Wa36) is significantly higher than we will have in the sector rig. The data figures above indicate that NOx may not be sensitive to this excess cooling air, whereas near-wall CO quenching is clearly sensitive to it.

LTO NOx for all three tested configurations can again be estimated from the 100% and 85% ICAO HTP emissions data. Like the LTO NOx predictions performed using the Task 3.2 Flametube data, NOx expectations for 7% and 30% ICAO points are estimated based on correlations for pilot-only operation from another similar TAPS fuel nozzle design. This must be done, as pilot-only NOx measurements in the flametube test geometry are not reliable. For the 100% ICAO point, data measured in the HTP rig is conservatively scaled from the experimental P3 up to the actual N+2 P3. This scaling constitutes a conservative (high) NOx estimate. *Table 8* summarizes the LTO NOx calculation and expected reduction below CAEP/6, assuming no downward correction from flametube to sector geometries. Clearly the M6F6 has margin to the LTO NOx

technology goal of 25% CAEP/6 levels, and the F1M4 is essentially on target. Historically, a significant geometry correction (downwards) in EINOx from the flametube to sector geometry has been experienced; if this is assumed for 85% and 100% ICAO points, the data in *Table 8* would indicate that all three configurations are likely to meet the LTO NOx technology goal.

Table 8 – LTO NOx Calculations, Assuming Zero Correction

Config	% CAEP/6
M4F1	26.6%
M4F2	31.6%
M6F6	16.8%

4.11.4.3 Auto-Ignition Margin Data

Autoignition data was collected for all three configurations.

The data has been reduced, and a relative risk is calculated for the different designs at 100% ICAO N+2 conditions on JetA fuel (*Figure 58*). Of the three N+2 designs, only the M4F1 meets criteria for operational margins. The margins and risk level will be re-assessed for the specific alternative fuels of interest to NASA for use in the ASCR tests.

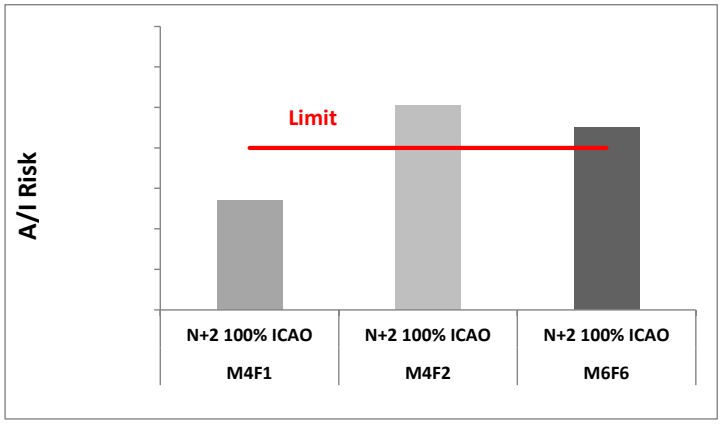

Figure 58 – Relative Risk Calculation for Different Designs at 100% ICAO N+2 Conditions

Relative durability risk for different mixer configurations at N+2 100% ICAO cycle conditions and JetA fuel. The line represents an acceptable limit, and the M4F1 is the only tested N+2 design that stays below this risk criteria.

4.11.5 Conclusions

Data from the HTP test campaign, as well as previous Flametube and Tunable Combustor Acoustics (TCA) rig data, were presented to NASA during the PDR in November 2011. Among the three designs tested in all three rigs, the M4F1 design results in the best balance between NOx emissions performance, combustion efficiency, auto-ignition margin, and combustion dynamics. This design recommendation was accepted by NASA, and procurement of the Sector Rig mixer hardware commenced.

4.12 Task 4.1A – Dynamics Suppression in Liquid-Fueled Combustors using Fuel Modulation (GE Funded)

4.12.1 Summary

In the present work, an atmospheric pressure combustor using a modern aviation gas turbine fuel nozzle was used to demonstrate active combustion control. The combustor exhibited a low-frequency dynamics mode under fuel-rich conditions. A fast-response fuel injection valve was adapted as an in-line modulation valve upstream of the nozzle. Large fuel modulation amplitudes were achieved with the combination of the valve and the engine nozzle at frequencies exceeding 200 Hz. Open-loop flame response to fuel modulation was first examined when the instability mode was absent; for a range of inlet air temperatures, fuel flow rates, and combustor pressure drops. Simple open-loop control at discrete off-resonance frequencies was found ineffective in suppressing the instability mode. An advanced, fast algorithm was developed to enable closed-loop control. In this scheme, the entire fuel supply to the combustor was modulated with the control valve and injected through the fuel nozzle. The control algorithm adaptively commanded the fuel injector to produce a steady fuel flow or to modulate the fuel based on the level of pressure oscillations in the combustion chamber. With the optimized control algorithm, an 88% reduction in the amplitude of the low-frequency dynamics mode was achieved.

4.12.2 Introduction

A major challenge that combustion engineers face is that new engine designs driven by the demands for better efficiencies and lower emissions are more prone to combustion instabilities. These instabilities are typically associated with large amplitude pressure oscillations, which can result in serious performance degradation and/or premature system failures. Given the complex nature of engine systems or combustion sub-systems, it can be a time-consuming and costly iterative process to find the specific passive fixes to combustion dynamics. Active combustion control (ACC) provides a more universal and flexible alternative to suppress combustion dynamics. The basic concepts of active combustion control can be found in review papers [16,17,18,19].

There have been extensive research and development efforts on ACC for many decades since the combustion instability issue was encountered in a liquid rocket engine in 1952 [51]. Most of successful lab demonstrations of ACC were in combustors fired with gaseous fuels, for example, see references [20,21,22,23,24,25,26,27]. Among these studies, the most notable one is a successful application of ACC on full-scale practical gas turbines (Siemens Vx4.3A family) as reported by Hermann et al.[26,27].

There are relatively much fewer studies performed on ACC with liquid fuels [28,29,30,31,32,33,34,35,36,37,38,39,40,41,42,43] comparing to these on gaseous fuels, because liquid fuels require atomization and vaporization, each of which has their own timescales that further complicate controls for combustion instabilities [37]. As pointed out by Yu et al. [31] that “because of complexity associated with heterogeneous nature of liquid-fueled

combustion, it is difficult to use liquid fuel in combustion control". The majority of these liquid-fueled studies were lab demonstrations, which had the luxuries of installing a secondary fuel injector dedicated to ACC or selecting special fuel nozzles for control.

DeLaat and Chang [37] and Cohen et al. [38] demonstrated effective dynamics suppression with ACC in realistic aero-engine environments, where the combustion instability modes were associated with lean combustion. However, for liquid-fueled combustion, combustion instability can be also excited or promoted with increasing amount of fuel supply, for example, as reported by Lee et al. [43] and McManus et al. [29,30] in lab demonstrations. A strong mode of low frequency instability (between 100 and 200 Hz) was encountered when a modern commercial engine nozzle was operated under conditions where pilot flames are very rich ($\Phi > 4$).

An early full-scale ACC effort under similar fuel rich conditions was performed by Moran et al. [39] on a Rolls-Royce RB199 engine. Combustion instability was effectively suppressed by actively reducing the fuel supply to the afterburner, where thrust gain is only marginal as fuel flow rate increases. However, the approach is unlikely to be adopted to suppress combustion dynamics associated with rich pilot flames. The goal of this work is to develop an ACC strategy that is practical for aero-engines and can effectively suppress combustion instability under fuel rich conditions.

4.12.3 Experimental Set-Up

4.12.3.1 Control Actuator

Given the scale of practical aero-engines, modulating fuel flow appears to be the most feasible approach to realize ACC. However, it should not incur hardware modifications to combustors for ACC to be practical for real engine scenarios, which makes the use of additional fuel injectors and/or specially designed control nozzles not very attractive. A viable option is to install a fast-response valve immediate upstream to the engine nozzle for fuel actuations.

As repeatedly stated, the key to a successful ACC effort is to identify a suitable actuator. A few fast devices have been used by previous researchers as liquid-fuel actuators to suppress combustion dynamics in the frequency range of 100 – 200 Hz as reviewed in reference [18]. Solenoid valves, for example the rapid direct drive valves (DDV) made by MOOG, have been extensively used [20,26,27]. Unfortunately, the maximum frequency of these valves does not exceed 150 Hz, which is not sufficient to control instability on the same order of frequency. Although a study shows that MOOG valves can be modified to have better frequency responses (up to 450 Hz), the fuel line between the solenoid valve and nozzle had to be fine-tuned to have a natural frequency that facilitated fuel forcing [41]. Another possibility is a magneto-restrictive type of valves, as demonstrated in recent studies [22,37,40]. These valves are prototypes and experience hysteresis and temperature-induced valve displacement [40].

Automotive fuel injectors are a viable option and have been used as inline fuel valves in the past [28,31-36]. Our tests suggested that an "off-the-shelf" automotive fuel injector can be operated up to a few hundred Hz if sufficient cooling is provided. Therefore automotive fuel injectors have the potential to control combustion instability near 140 – 160 Hz. In addition, these valves have long life times on automotive engines. As indicated in previous studies, the use of two-position fuel injectors (on-off) introduces non-linearity in fuel modulation. One goal of the current study is to understand how a fuel delivery system responses to the valve events (open and close).

The performance of a fuel injector as an inline valve was first tested in a mock-up setup to gain physical understanding of fuel modulations. The system consists of a modified automotive fuel injector, a single-point nozzle, a piece of 1" polyurethane tube, and fuel lines connecting them, as shown in *Figure 59*. The modification to the fuel injector was to enlarge the orifices to accommodate larger fuel flow rates. The fuel injector will be referred simply as the "valve" in the rest of this paper. The single-point nozzle was to eliminate complications due to complex geometries seen in real commercial engine nozzles. In addition, the piece of polyurethane tube was to simulate the combined elasticity of nozzle, fuel line and liquid fuel.

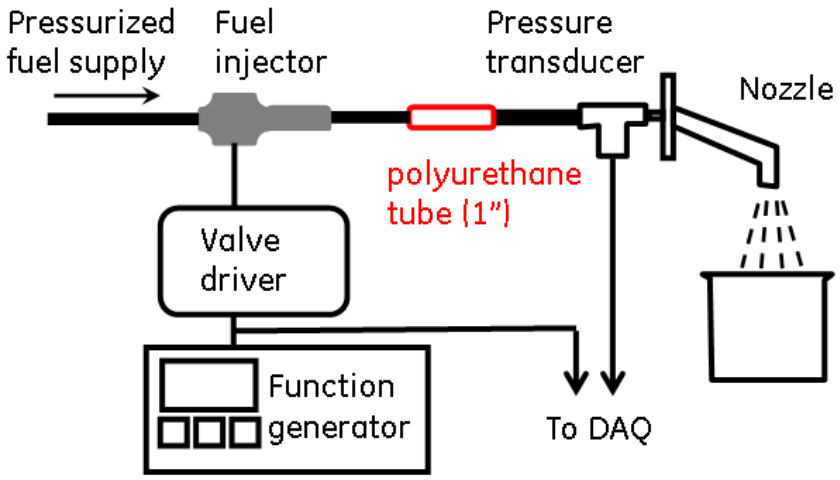

Figure 59 – Set-Up for Understanding Fuel System Response to Valve Actuators

To characterize the system responses to valve actuations at high modulation frequencies, it is essential to first understand the system behavior with a single pulse. Shown in *Figure 60* is an experimental pressure profile recorded by the dynamic pressure transducer shown in *Figure 59*. The initial pressure rise corresponds to the valve-open event and can be approximated by a linear rise. The valve is then closed; the pressurized fuel downstream of the valve then discharges through the nozzle. A pressure decay in the system is observed, which can be approximated by an exponential decay. The characteristic times for both pressure rise and decay are solely determined by the physical properties of the system and are independent of modulation frequencies.

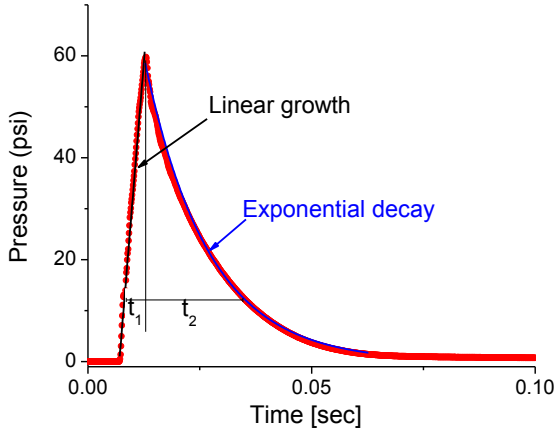

Figure 60 – Pressure Profile in Fuel Line with Single Pulsation from Valve

When the valve is operated at high frequencies, the time interval between two valve pulsations is not sufficient for pressure to fully decay back to zero, which leads to a reduced modulation amplitude. Suppose the peak-to-trough amplitude is P at modulation frequency f, then the following equations hold:

1. $P^+ = P^- = P$
2. $t_1 + t_2 = 1/f$

where t_1 and P^+ are the pressure rise time and the corresponding pressure rise, respectively; t_2 and P^- are the pressure decay time and the corresponding pressure decay. Eq. 1 indicates that at the end of a cycle, pressure should decay back to the level at the beginning of the cycle; Eq. 2 correlates the times for pressure rise/decay to the modulation frequency. Combining with the characteristic times derived from the single pulsation test (see *Figure 60*), the modulation amplitude (peak-to-trough) as a function of f can be derived, as shown in *Figure 61*.

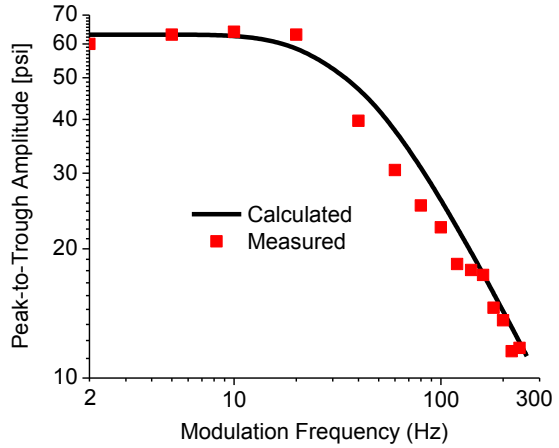

Figure 61 – Modulation Amplitude as a Function of Frequency

Modulation amplitude as a function of frequency for the simple setup shown in Figure 59.

The good agreement between the model predication and experimental data in the simple fuel system (*Figure 59*) shows that the model can capture the physics of fuel modulation reasonably well. The calculation also indicates that the modulation amplitude should decrease monotonically with increasing frequency, if no natural frequency is encountered. Following the same approach, a characterization of the real fuel modulation system was performed as shown in *Figure 62*, where the single point nozzle in the simple setup (*Figure 59*) was replaced by a modern commercial engine nozzle and the polyurethane tube was removed.

It is apparent from *Figure 62* that at the low frequency region of interest to this study (100 – 200 Hz), the system consisting of the fuel injector and the real engine nozzle is able to deliver strong fuel forcing, which is also confirmed by high-speed imaging and subsequent tests with combustion. However, it is noticed that the measured modulation amplitude with the commercial engine nozzle falls lower than the prediction curve at high modulation frequencies. This is because of the assumption made in calculating modulation amplitude that the fuel line pressure upstream to the valve is held constant. However, the assumption may not be accurate when the system has the full-size nozzle, as fuel line pressure decreases substantially as fuel is discharged at significant rates.

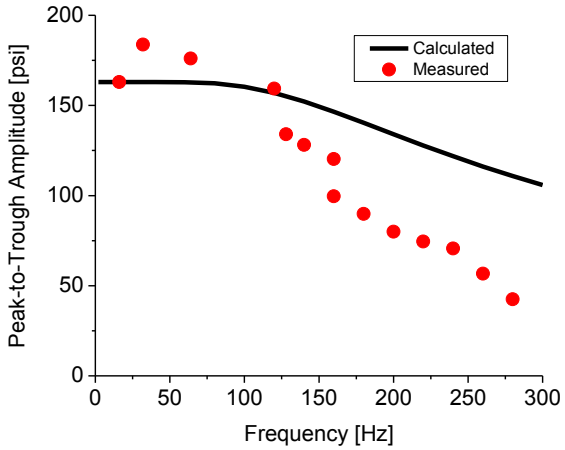

Figure 62 – Modulation Amplitude as a Function of Frequency

Modulation amplitude as a function of frequency with a modern commercial engine nozzle.

4.12.3.2 Combustion Rig

The study was performed on an atmospheric, liquid-fueled (Jet-A), single-nozzle test rig at GE GRC. The combustor rig replicates the complexities of a real engine combustor by using an actual engine fuel nozzle and swirler, as shown in *Figure 63*. The compressed air can be heated up to 700 F by an electrical heater before entering the combustor. The rig also features a quartz liner for optical access, through which a photomultiplier tube (PMT) shielded with a UG5 filter can monitor OH* chemiluminescence from the entire combustor. In addition, a dynamic pressure transducer was installed immediately downstream of the dome plate to record pressure fluctuations in the combustor (P_4').

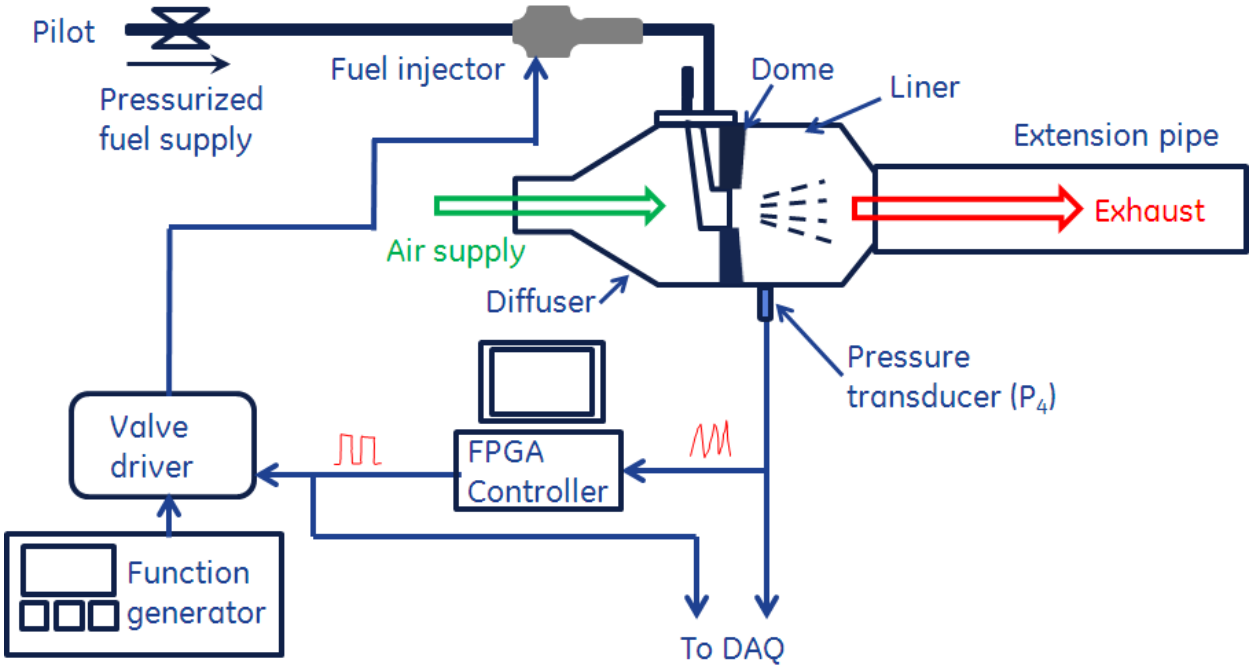

Figure 63 – Combustor Rig Schematic

Schematics of the combustor rig used in this study along with setups for open-loop and closed-loop controls.

In its standard configuration, the combustor rig has a short liner (4.5” in length), which corresponds to a very high natural frequency. In this configuration the combustor did not exhibit thermo-acoustic instability. This stable configuration was used to examinethe control authority of ACC using open-loop forcing. The rig can be also fitted with a 30” extension pipe downstream of the exit cone. With the extension pipe, the system has low natural frequencies (100-200 Hz). We were able to excite this longitude mode using a modern commercial aero-engine nozzle under rich flame conditions to produce combustion instability.

In the present configuration, the entire fuel supply to the combustor was modulated with the valve and injected into the combustion chamber. The mean fuel flow rate was controlled by a control valve upstream of the fuel injector, as can be seen in *Figure 63*.

4.12.4 Results and Discussion

4.12.4.1 Characterization of Control Authority

As indicated in the previous section, the standard test rig is equipped with a short quartz liner (without the extension pipe as illustrated in *Figure 63*) to avoid self-excited instability modes in the low frequency range of interest to this study. The standard rig provides an ideal test environment to characterize flame response to valve actuations. The valve was operated in an open-loop manner at discrete frequencies to measure

pressure fluctuations in the combustor (P_4') and fluctuations in OH* chemiluminescence to quantify the control authority through fuel forcing.

Ideally, the control authority can be represented by the flame transfer function (FTF), which is defined as following:

$$\mathrm{FTF} = \frac{q'/\bar{q}}{\dot{m}'/\bar{\dot{m}}}$$

where $\bar{q}$ and $\bar{\dot{m}}$ are mean heat release rates and mean fuel flow rates; q' and $\dot{m}'$ are fluctuations in heat release rates and fuel flow rates, respectively.

The mean flow rates $\bar{\dot{m}}$ can be directly measured using a flow meter with a long characteristic time. However, the fast fluctuations in fuel flow rates were inferred from instantaneous pressure measurements. In the low frequency range, it is reasonable to assume the flow field for Jet-A fuel is quasi-steady, as the liquid fuel has very low compressibility. Therefore, fuel flow rate fluctuations can be estimated through the nozzle flow number (FN) correlations as given in the reference [44].

However, it is not easy to experimentally measure $\bar{q}$ or q' directly; these two parameters have to be inferred from OH* chemiluminescence measurements. Although the correlation between OH* chemiluminescence and heat release rates are highly nonlinear for fuel rich flames [45] as is the case for this work, the purpose of this step is to qualitatively understand how flame responds to fuel forcing. Therefore, heat rate mean and fluctuations were directly approximated by corresponding values from OH* chemiluminescence measurements without conversion.

The FTF measurements were performed over a wide range of test conditions by varying fuel flow rates, air flow rates, and preheat temperatures of the incoming air stream (T_3). The comparison experiments only involved the primary fuel circuit of the nozzle. Please note that although the control valve is a two-position fuel injector, the modulation amplitude can be varied by applying different duty cycles to the valve. A duty cycle is defined as the portion of time when the valve remains open within each cycle. Since the fuel flow rate is maintained by the control valve upstream of the fuel injector, smaller duty cycles lead to larger modulation amplitudes. This study used duty cycles ranging from 10% to 90%. When the control valve is operated at 90% duty cycle at frequencies above 200 Hz, an essentially steady (unmodulated) fuel supply can be achieved.

The most remarkable results are found by varying T_3. Comparison experiments were performed at T_3 = 500 F and 400 F over a range of fuel forcing frequencies between 100 and 200 Hz, while keeping other parameters fixed. The mean fuel flow rates of these comparison experiments were at 23 pounds per hour (pph); and the air flow rates were kept steady to cause a fixed pressure drop across the dome ($\Delta P/P$ = 4%). The results suggest that the flame response to fuel forcing is very strong at T_3 = 500 F, as evidenced by both P_4 and OH* chemiluminescence measurements. However, at T_3 = 400 F, negligible or very weak fluctuations in both P_4 and OH* chemiluminescence were

measured, as shown in *Figure 64*. The striking comparison indicates that the vaporization of fuel droplets is a factor that controls how flame responds to fuel forcing.

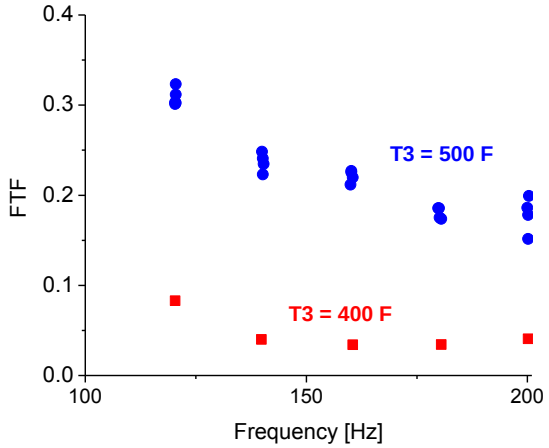

Figure 64 – Comparison of Flame Responses to Fuel Forcing

Comparison of flame response to fuel forcing at T_3 = 400 F and 500 F. Mean fuel flow rates were 23 pph for all tests. Air flow rates were kept steady to cause a fixed pressure drop across the dome ($\Delta P/P$ = 4%).

Other comparison experiments were also conducted to investigate the effects of fuel flow rates and air flow rates. It was found that increasing mean fuel flow rates leads to slightly increased control authority within the tested mean fuel flow rate window from 19 to 25 pph for the primary circuit. This may be explained by the fact that higher mean fuel flow rates are a result of a higher mean pressure difference across the nozzle, resulting in better atomization of the fuel from this pressure-atomized circuit. Smaller droplet sizes can be correlated to larger fluctuations in heat release rates, as will become evident in the discussion section later in this report.

At the same time, comparative experiments conducted at $\Delta P/P$ = 3.5% and 4% reveal no significant impact of air flow rates. This may be explained by the same reason as described for the effects of fuel flow rates. Briefly, since the primary flow is pressure atomized, the air flow rates do not affect the fuel atomization.

4.12.4.2 Low-Frequency Instability

To evaluate the effectiveness of control, baseline cases of the low-frequency combustion dynamic mode under investigation are needed. As described earlier in the paper, a 30” extension pipe needs to be attached to the combustor’s exit cone to introduce a low natural frequency in the range of 100-200 Hz. Once the pilot flame reaches some threshold fuel flow rates, the low-frequency combustion instability can be excited. This mode of combustion instability is very strong; pressure oscillations up to 2 psi (peak-to-trough) were measured in these atmospheric tests.

High-speed images of the flame over a cycle of the combustion instability are shown in *Figure 65*. The first image frame (0^o) was taken when the pressure oscillation in the

combustor (P_4') crossed its mean value on the rising edge. The time interval between any two adjacent frames accounts for a phase delay of 30° at the instability frequency. The nozzle is on the left edge of each frame; and the right edge matches the location of the exit cone. Since the high-speed camera is only sensitive to visible wavelengths, the brightness in the pictures corresponds to soot incandescence.

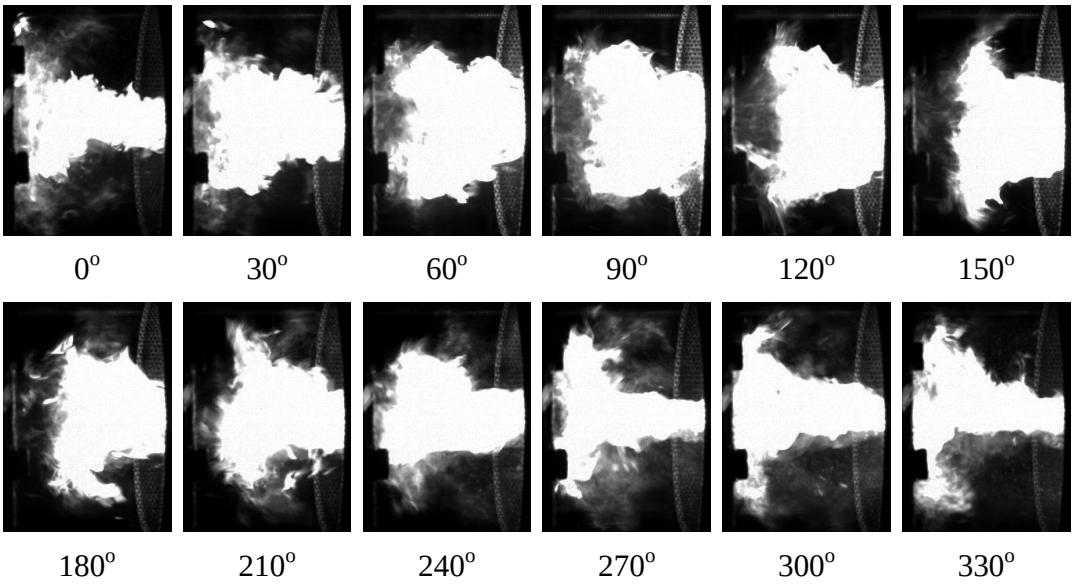

Figure 65 – High Speed Images of Oscillating Sooty Flame

High-speed images of oscillating sooty flame when the low-frequency combustion instability was encountered. Flow direction is from left to right for all frames.

It is apparent from these images that the sooty flame is oscillating violently in space accompanied by pressure fluctuations in the combustor. A hypothesis of the cause of this mode of combustion instability will be discussed in detail later in this report.

4.12.4.3 Open-Loop Control Results

Open-loop control has been successfully demonstrated in suppressing combustion dynamics, e.g., see [20]. The concept of open-loop control is to drive an oscillation in heat release rate at an off-resonance frequency. If the coupling mechanism between heat release fluctuation and pressure oscillations is weak, open-loop control can disrupt the feedback loop and suppress the mode of combustion dynamics. One drawback of open-loop control is that the control actuation itself drives pressure oscillation at the control frequency.

To evaluate the effectiveness of open-loop control in suppressing the target low-frequency instability, comparison experiments were performed by maintaning T_3 (500 F), mean flow rate of primary fuel (28 pph), and air pressure drop ($\Delta P/P$ = 4%). Shown in *Figure 66* are spectra of pressure fluctuations in combustor (P_4') and fluctuations in OH* chemiluminescence (emission).

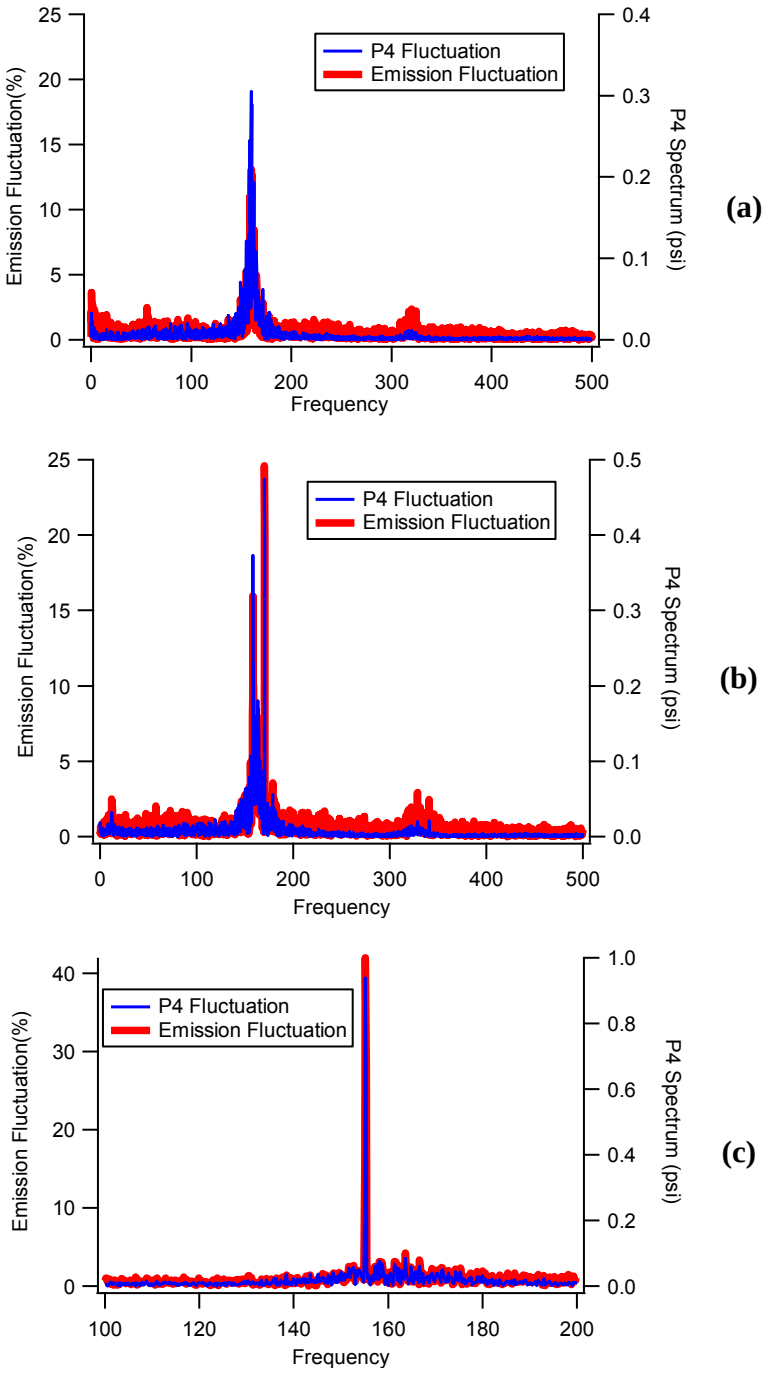

Figure 66 – Comparison Experiments

Comparison experiments to evaluate the effectiveness of open-loop control: (a) Self-excited instability; (b) the self-excited instability (left) co-exists with the excitations from fuel forcing (right); (c) the self-excited instability merges with the excitations from fuel forcing to form one strong peak.

*Figure 66(*a) corresponds to the baseline case, where the self-excited low-frequency instability is clearly seen. The spectrum in *Figure 66*(b) indicates that the amplitude of the self-excited instability remains essentially unchanged despite that the flame was forced by open-loop fuel modulation at an adjacent off-resonance frequency (at a slightly higher frequency). The comparison suggests that the open-loop control was ineffective in suppressing the instability mode.

In *Figure 66*(c), a single strong peak is seen on the spectrum. The only difference in test conditions between *Figure 66*(b) and (c) was that the open-loop control for the *Figure 66*(c) case was closer to the peak frequency of the self-excited instability. In fact, the self-excited instability can shift in frequency domain in both directions up to 4 Hz to merge with the open-loop control frequencies. We also attempted to adjust the phase delay in an open-loop manner, but no difference was observed. These observations are clear indications that the low-frequency instability of interest is resilient.

The new peak seen in *Figure 66*(c) contains contributions from both the self-excited instability and the open-loop fuel forcing. The amplitude of the merged instability is much stronger than the self-excited mode (note the scale difference), which suggests that the constructive interference between the open-loop fuel forcing and the self-excited instability is strong when the open-loop fuel forcing is on the resonance frequency. This implies the potential for effective closed-loop control by creating destructive interference between the fuel forcing and self-excited instability, which can be achieved by managing the phase delay between the two modes.

In addition, recalling that higher T_3's lead to stronger flame response to fuel forcing as presented in *Figure 64*, the open-loop control was also performed at T_3 = 600 F. Results show that the low-frequency instability can be partially suppressed by the open-loop control. However, the control actuation itself excites pressure oscillations, which limits the effectiveness and application of the open-loop control.

4.12.4.4 Closed-Loop Control Algorithm

Many control algorithms have been previously developed, for example: the pulse width modulation (PWM) algorithm [29,30]; the observer algorithm [22,40]; and model-based algorithms [46, 47, 48, 49]. The design of a control algorithm for the present study is mainly governed by the physical properties of the fuel actuator. First and foremost, the fuel injector is a two-position valve; its performance is highly non-linear, which makes the precise control of modulation amplitude inherently difficult. Another major technical challenge is that the fuel injector is a normally closed valve, which is pre-determined by its design functionality. Large current has to be passed through a coil inside the valve to maintain the open position. To protect the valve's coil from over-heating, the valve can be kept open only for a short period of time (5 ms); after which the controller shuts the valve.

Despite these difficulties, our particular fuel injector was selected as the fuel actuator to take advantage of its fast frequency response. Another consideration is that the valve is

commercially available and is based on proven technology. Therefore, a special control algorithm was designed to enable the implementation of fuel injection-type valves for ACC. The core of the control algorithm is a simple phase-shift algorithm.

In the standard phase-shift algorithm, fuel forcing is triggered by pressure oscillations. One pre-requirement in implementing the standard phase-shift algorithm is that the mean fuel supply that sustains combustion is not interrupted by the control valve. This is the case when a mean offset position can be applied to a control valve to maintain a mean fuel flow rate, or when combustion is sustained by a main fuel circuit and the control fuel forcing is introduced through a secondary circuit or auxiliary fuel injector. However, neither of the two cases applies in the present study with the fuel injector as the fuel actuator.

The standard phase-shift algorithm has to rely on input pressure oscillations to trigger the valve to let fuel pass through. In addition, the amplitude of the target combustion instability mode decreases as the fuel flow rate is reduced. As a result, if the controller misses a pressure trigger, the fuel supply is reduced, which in turn causes more pressure triggers to be missed. The downward spiral eventually cuts the fuel supply completely and causes flame out. In fact, this process happens so fast that an immediate flame out was encountered once a standard phase-shift algorithm based controller was turned on.

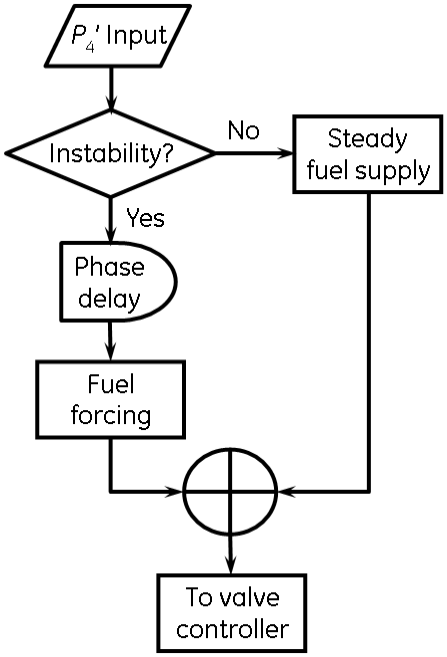

Figure 67 – High-Level Illustration of Control Algorithm

A major modification to the standard phase-shift algorithm is needed to overcome the drawback that the fuel injector is a normally closed valve. Briefly, when the amplitude of the combustion dynamics is high, the algorithm passes P_4' oscillation information (frequency, phase) to the valve controller after adding a phase delay. However, if for a

moment the dynamics level is too low to trigger the controller, the algorithm regains the full control authority by commanding the fuel actuator to sustain the steady fuel supply. For the fuel injector used in the present study, a steady fuel supply can be achieved by modulating the valve at a large duty cycle and at a higher modulation frequency. A high-level illustration of the control algorithm is shown in *Figure 67*. The control algorithm was realized by an FPGA controller for ultra-fast response. The logic gates in the controller can be opened in 20 ns.

4.12.4.5 Closed-Loop Control Results

With the control algorithm imbedded in the FPGA controller, closed-loop control was tested using the experimental setup shown in *Figure 63*. The function generator shown in the figure was for the open-loop control and was not used in the closed-loop control tests. Shown in *Figure 68* is a set of sample time histories of P_4'.

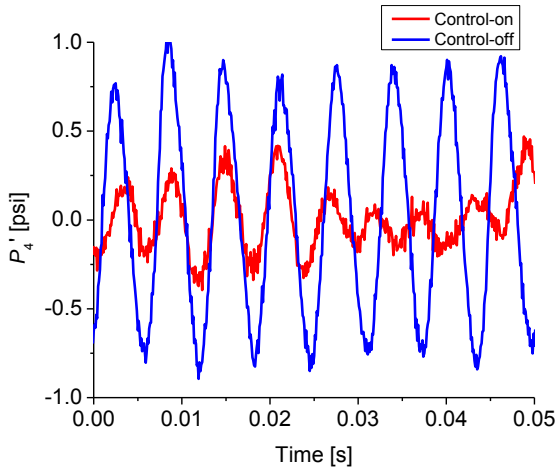

Figure 68 – A comparison of time-histories of P4 fluctuations with and without control

Without control (blue curve) and the best controlled case with the closed-loop control algorithm (red curve).

With the optimal phase delay, the instability amplitude can be suppressed by 88%. Shown in *Figure 69* is a comparison of the baseline case and the best controlled case with the closed-loop control algorithm. The uncontrolled case has a strong mode of combustion instability with an integrated amplitude of 1.56 psi. In contrast, the best controlled case with the closed-loop control algorithm described in *Figure 67* has an integrated amplitude of only 0.19 psi. The tests were performed at T_3 = 500 F, $\Delta P/P$ = 4%, and a mean fuel flow rate of 31 pph.

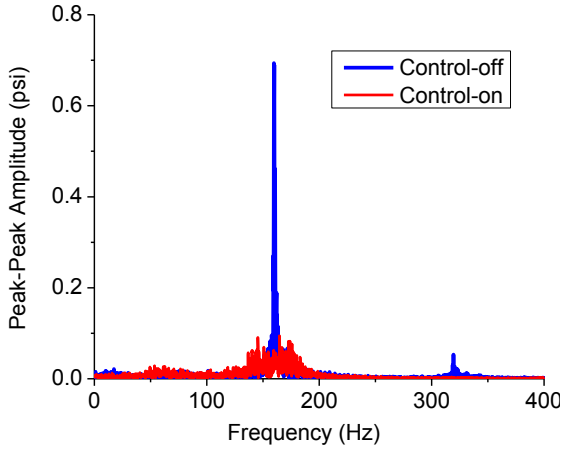

Figure 69 – Comparison to Demonstrate Effectiveness of Closed-Loop Control

A comparison to demonstrate the effectiveness of the closed-loop control. Blue: un-controlled case; red: the best controlled case with the closed-loop control algorithm.

The performances of the closed-loop control at other duty cycles and phase delays are summarized in *Figure 70*. Duty cycle does not have a strong effect on the effectiveness of the closed-loop control. However, the control effectiveness is almost solely determined by the control phase delay.

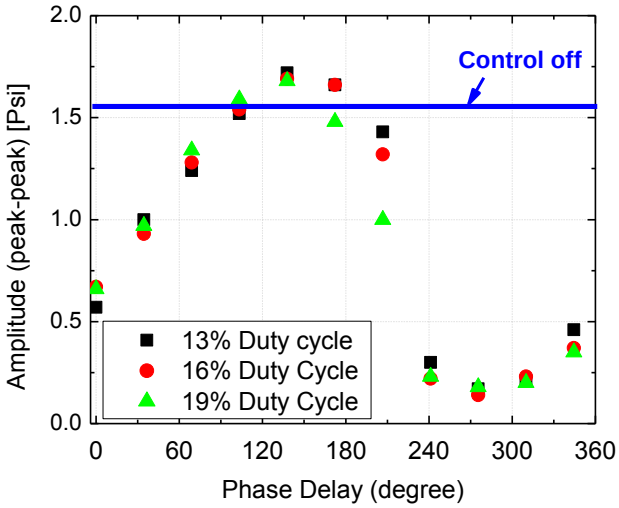

Figure 70 – Summary of Closed-Loop Control Performance

Control effectiveness as functions of phase delay and duty cycles to drive fuel forcing. Test conditions are those of Figure 70.

Effective closed-loop control was also demonstrated for *T*3= 300 and 400 F, although with slightly diminished effectiveness (still, the instability can be suppressed by more than 75% with the optimal delay times at 400 F).The results were surprising, because *Figure 64* suggests that flame does not respond to fuel forcing at *T*3= 400 F. There are a few reasons that may explain this finding. First, the pilot fuel flow rates of *Figure 63* tests (23 pph) were lower than those used here (31 pph). Larger flow rates lead to

better atomization for a simplex nozzle. Second, the extension pipe was used in the tests with closed-loop control, which effectively extends the combustor so that a larger portion of fuel droplets can be consumed in the confined combustor. Finally, a fluctuation in local heat releases rate that is sufficient to suppress the instability mode may be masked when observing the global parameters (fluctuations in *P*4 or OH* chemiluminescence). Nevertheless, this observation indicates that the control algorithm is effective and robust.

4.12.5 Conclusions

A strong mode of low-frequency combustion dynamics under fuel-rich conditions was observed in an atmospheric rig using a commercial aero-engine nozzle. To apply active combustion control to suppress this mode of instability, a fast-response fuel injector was used to produce strong fuel forcing with Jet-A in the frequency range of 100-200 Hz. Simple open-loop control at discrete off-resonance frequencies was found ineffective in suppressing the instability mode. An advanced, fast algorithm was developed to enable closed-loop control. In this scheme, the entire fuel supply to the combustor was modulated with the control valve and injected through the fuel nozzle. With the optimized control algorithm, an 88% reduction in the amplitude of the low-frequency dynamics mode was achieved.

4.13 Task 4.2A – Advanced Ignition Development (GE Funded)

4.13.1 Summary

GE conducted ignition tests for a laser optical igniter and a standard electrode igniter in a 5-cup sector in the spring of 2011. The work in Task 4.2A demonstrated significant progress toward the implementation of the laser optical igniter. The Task 4.2A testing with improvements to the adapter design resulted in over 200 laser light-off events. The laser igniter performance was mapped at various circumferential and axial igniter mounting locations, with two different lens focal lengths and a translating optical stage providing a range of radial positions for the laser spark. Additional mapping is recommended to further improve the light-off fuel flow for laser ignition.

4.14 Task 4.3A – Advanced Liner Material Maturation (GE Funded)

4.14.1 Summary

Work performed under this contract addressed basic material behavior of the GE-developed Ceramic Matrix Composite (CMC) material system. The principal focus was to understand durability of the material system and lay the groundwork for development of life prediction methodologies.

4.15 Task 5.1 – Preliminary Design of Combustor, Fuel Injector, and Mixers (NASA Funded)

4.15.1 Introduction

The N+2 combustor, fuel injector, and mixer preliminary design work built upon the early architecture and concept studies performed during Tasks 1 and 2. At the combustor Conceptual Design Review (CDR), a 2-D flowpath layout was approved for the diffuser-combustor system.

From this point, the team set off to design the first ever 5-cup combustor sector rig incorporating CMC liner material. Managing the thermal and mechanical stresses that are generated at the metal-CMC interfaces became one of the major challenges of Task 5.1. CFD models were used to generate the thermal boundary conditions for the subsequent 3D heat transfer and mechanical analyses.

Along with the CMC combustor, the fuel nozzles are the other critical piece of the sector rig technology and had their own unique design requirements for operation in the ASCR test facility. The successful concept designs used in the Task 3.8 HTP testing needed some refinement to further reduce thermal stresses in the nozzle, improve manufacturability and interface in the sector versus the HTP rig, and apply “lessons learned” during the manufacturing, assembly, and test of the HTP hardware.

The mixer designs are identical (except for minor mounting features) to those tested on all of the previous single cup rigs (Tasks 3.2, 3.3, and 3.8). Their CFD analysis, design, and testing is covered in those and previous conceptual design tasks.

The major activities surrounding the design and analysis of the sector rig and fuel nozzles are described below.

4.15.2 Methods, Assumptions, and Procedures

Wherever applicable, standard GE tools and best practices were used in the design and analysis of the combustor and its subcomponents.

4.15.3 Results and Discussion

4.15.3.1 Combustor Sector PDR Part 1a

A preliminary design review with NASA personnel, called PDR Part 1a, was conducted FW21 2011 and focused on the design, analysis, supporting structure, and assembly of the CMC liners for the 5-cup sector rig.

Extensive CFD and 3-D heat transfer analysis has been performed for all of the hot gas combustor components. After multiple design iterations, the predicted sector rig flow path temperatures are all within GE experience for the components. The inner liner

temperatures are predicted to be slightly hotter than the outer liner; however, both are within successful GE test experience.

The maximum tensile field stress is located on the inner liner, and is an axial stress. The tensile field stresses and hoop stresses are within successful GE test experience. Analysis efforts have optimized the cooling strategy.

The outer liner is predicted to have slightly lower temperature and lower field stress than the inner liner, based on the initial CFD using the M1F1 mixer / fuel nozzle configuration at 100% ICAO conditions. The highest axial stresses on the outer liner are local edge stresses; these locations were studied during analysis refinement. In addition to thermal stress evaluation the outer liner was also analyzed for buckling capability. The outer liner has margin to buckling under the maximum sector pressure load conditions.

4.15.3.2 Combustor Sector PDR Part 1b

A second round preliminary design review of the sector was held at NASA Glenn August 10, 2011. Based on that review, sector components were released for machining. The PDR covered the NASA and GE rig interfaces, the sector mechanical overview and assembly, CMC liner progress, emissions rake design details, and hardware schedule.

An overview of the sector design was presented using views of the solid model to communicate the assembly sequence.

The emission rake design was conducted according to GE experience and best practice. The four-element rakes were designed to correctly position the elements in the hot combustor exit annulus. This means that the rakes are shifted slightly lower in the exit at cold conditions. With the rake water cooling system design, the predicted maximum rake temperatures are within successful experience. The 3D rake model was used to verify extraction capability through the combustor mount plate access port below the inner liner. The cooling water feed and gas sample lines for the emissions rakes pass through the slot in the combustor mounting plate. The rake clearance to the NASA facility has been checked using the provided UG ASCR models.

4.15.3.3 Combustor Sector CFD and Heat Transfer Analysis

Initial thermal / mechanical analysis of the sector was performed using thermal boundary conditions from a CFD analysis with the M1F1 mixer/fuel nozzle design. A second iteration with a different fuel nozzle/mixer configuration allowed the team to determine if there were significant differences in the thermal loading on the combustor liners. We also used this opportunity to investigate the effect of liner multi-hole spacing on liner wall gas temperatures.

A CFD and 3-D heat transfer was performed for hot gas combustor components. The purpose of this analysis was to provide boundary conditions for the mechanical team to conduct another round of detailed thermal-mechanical analysis to make sure the liner

temperatures and stress levels are within design limits. This configuration now also includes the fuel nozzle stem in the computational domain and a modified deflector. The CFD calculation was performed at the 100%ICAO operating condition. The dump lip cooling pattern at the back end of the combustor, which was not in the previous analysis, was also included in this calculation. Results from this study have been transferred to the mechanical team for the thermal-mechanical analyses.

All sector flow path temperatures were within GE experience except the dump lips. Cooling was added to the outer and inner dump lips and another iteration of analysis was performed to verify acceptable dump lip surface temperatures.

Stress analysis based on CFD and 3-D heat transfer was performed for hot gas combustor components with the M6F6 configuration. It is observed that the maximum surface temperatures on the liners for this M6F6 configuration are slightly lower than the M1F1 configuration. This is due to lower flame temperature produced by the M6F6 configuration as a result of better fuel / air mixing performance.

The cooling added to the outer and inner dump lips was effective and hot side metal temperatures are now within allowable limits for the material. Stress analysis has confirmed acceptable dump lip and CMC stress levels.

4.15.3.4 Sector Fuel Nozzle Design

The fuel nozzle designs were slightly modified from those built for the HTP testing in Task 3.8. Wherever possible, components were made common across multiple designs. The adapter housing at the top of the fuel nozzle was re-oriented (and made common between designs) to provide simpler fuel manifold design and connections, and to facilitate nozzle installation and removal. Several locations inside the fuel nozzle were slightly redesigned to reduce thermal stress levels, as well as decreasing wetted wall temperatures in a couple of locations. Finally, the internal fuel tube design was updated for improved manufacturability.

Full conjugate heat transfer analysis and mechanical stress analysis were performed for the redesigned areas of the fuel nozzles. In summary, the thermal and mechanical analysis indicates that the fuel nozzle design for the sector rig meets the requirements for the sector test and shows improvement compared to the HT&P design.

4.15.4 Conclusions

The 5-cup CMC sector design was completed, with acceptable thermal stress and life predictions for all components. Several unique challenges of the design were driven by the sector geometry versus a full annular configuration. Other challenges included the management of thermal and mechanical stresses in the fuel nozzles, and protecting fuel manifold lines from excessive heating in the T3 environment. The ultra-high mixer flow splits, required to meet the aggressive NOx reduction goals, left minimal air for liner cooling and pushed the limits of the material capability. These challenges have all been met with acceptable results for expected temperatures, stresses, and life for this test rig.

Following the PDR Part 1b review, the CMC combustor sector passed through the preliminary design phase and into manufacturing.

4.16 Task 5.2 – Multi-Injector Combustor Sector Hardware Fabrication, Assembly, and Instrumentation (NASA Funded)

4.16.1 Summary

A 5-cup combustor sector with CMC liners, the first ever sector rig using these advanced materials, has been fabricated, assembled, and instrumented. Significant instrumentation has been applied to the combustor rig in order to both maximize the learning from the sector tests as well as protect the hardware at the extreme conditions of the N+2 cycle. The inner and outer combustor liners are instrumented for temperature and pressure, with detailed temperature mapping on the center cup.

The fuel nozzles were individually fitted in their mounting locations for proper alignment and immersion in the mixer. Minor adjustments were made with fabricated shims in order to hold each nozzle at the nominal design location. The spare nozzle was trial fit in each of the five cups, and shims are provided for each location as needed.

4.16.2 Introduction

The fabrication, assembly, and instrumentation of the 5-cup CMC combustor occurred over a 13-month period, beginning in early August 2011 and culminating with delivery to NASA in late August 2012. Many challenges were overcome in the fabrication of the sector, driven primarily by the new experience with the CMC liner attachment methods and prototypical nature of the fuel nozzle fabrication and alignment. The final sector assembly with extensive instrumentation will provide first-of-its-kind data to support the N+2 Phase 1 objectives, and is intended to be utilized well into a Phase 2 program.

4.16.3 Results and Discussion

The sections below walk through the component fabrication, assembly, and instrumentation phases of the sector build.

4.16.3.1 Major Component Manufacturing

All deflectors plus one spare were thermal barrier coated prior to assembly onto the dome. Two deflectors were instrumented with hot side thermocouples. The dome plate was first finish machined and cooling holes were installed. The deflectors were then brazed to the dome and the dome assembly was flow checked. Initially the dome measured below the target effective area; cooling holes were enlarged and hole inlets rounded to increase flow to near-nominal levels. The sidewalls were also reworked to increase the cooling effective area to meet or exceed design intent, and flow re-checks completed.

The fuel manifold was assembled with a jig to simulate the fuel nozzle connection locations. Using the jig, the fuel tube bends were adjusted and the tubes were tacked and brazed into the fuel supply block that distributes fuel for each of the three circuits. The assembly has extra fuel tube length to allow adjustment during the sector

assembly. The two halves of the fuel manifold heat shield box were fabricated and welded, and they are shown ready for sector final assembly.

The CMC liners were manufactured at GE Ceramic Composites Products (Newark, Delaware), the coating was applied at GE Global Research Center (GE-GRC), and the laser drilling and flow checks were performed at GE Evendale. The CMC inner liner multi-hole cooling has been drilled and the airflow is within drawing limits. The CMC outer liner, was finish machined and EBC coated. The liner was drilled for cooling and instrumentation, and the air flow check is within drawing limits.

4.16.3.2 Preliminary Assembly, Fit-Up, and Fuel Nozzle Assembly

A preliminary build was conducted to check fit-up of the combustor components and mount plate. Alignment of the CMC liners to the dome, sidewalls, and metal exit “dump lip” components was good. Some minor rework of metal components and sheet metal work was performed to improve overall fit-up. Following rework, the combustor assembly went through a stress relief cycle and was disassembled in preparation for final assembly and instrumentation.

The dome and sidewalls were instrumented at the component level. The dome includes six embedded deflector thermocouples that measure hot-side metal temperatures (under the TBC). These thermocouples were spliced up to a larger sized sheath for durability. There are also four static pressure probes on the upstream dome face. The sidewalls each have four skin TC’s, and the left sidewall (aft looking forward) near cup 1 also includes a dynamic pressure port.

All six fuel nozzles (five plus one spare) were fully assembled and fuel spray / flow checked. A braze repair on one nozzle was successfully performed and absence of leakage was verified at high pressure.

4.16.3.3 Early Final Assembly and Instrumentation Process

The inner and outer liner instrumentation is applied and cemented in place with the liners assembled to the dome and sidewalls. Each liner has 15 surface thermocouples on the cold side, with 11 concentrated on the center cup and one each at the hot spot of the other four cups. The outer liner has five light-off Type-B thermocouples. Each liner has two cold side static pressure taps and two hot side wall static pressure taps. Finally, the outer liner has three ports for dynamic pressure measurements. A fourth dynamic pressure measurement is on the sidewall next to cup 1.

The fuel nozzles were all fuel flow-checked, with some minor differences between the flow numbers of the pilot and main circuits of the various nozzles. The nozzles are arranged on the dome such that the three center nozzles (and, especially, the nozzles upstream of the emissions rakes) are consistent and closest to the average of all five installed nozzles.

The igniter was installed, with the tip aligned flush with the liner surface.

The fuel manifold tubes are insulated and mounted inside of a heat shield box that will be purged with cooling air. This positive cooling air flow will help to prevent T3 air from entering and overheating the fuel tubes. The forward half of the box can be easily removed to access the fuel nozzle connections and fuel manifold.

Four emissions rakes, with four sample elements per rake, are installed. Two spare rakes have also been provided to NASA with the rig. The sample tubing passes through to the upstream side of the mounting plate where it is bent into position to connect to the steam-traced ASCR emissions lines. The cooling water feed for each rake is also provided from the upstream side.

4.16.3.4 Final Sector Rig Assembly, Instrumentation, and Delivery

The five primary fuel nozzles, mixers, and fuel nozzle brackets were carefully aligned and assembled to the dome. As each nozzle has small variances in its dimensions, shims were fabricated to fit between the fuel nozzle and its mounting bracket, correctly positioning the nozzle tip in the mixer. The fuel nozzles, brackets, and shims are assembled in matched sets, including the spare nozzle.

The final combustor assembly is depicted in *Figure 71 and Figure 72*. The fuel lines inside of the manifold heat shield box are individually wrapped in insulation with a protective stainless steel overwrapping. The fuel feed lines outside of the manifold box are individually insulated and bundled inside of a single protective wrapping. Four emissions rakes are installed and plumbed (*Figure 71*). Each rake has four elements, spaced radially to sample at the center of equal areas of the combustor exit flow. The rakes sample from the center three cups, and are arranged such that all 16 probe elements, when individually sampled, represent an emissions map for a single cup. When ganged together, the rakes should provide comprehensive bulk-average emissions measurements. A view of the inside of the combustor, looking toward the dome at Cups 3, 4, and 5, is shown in *Figure 72*

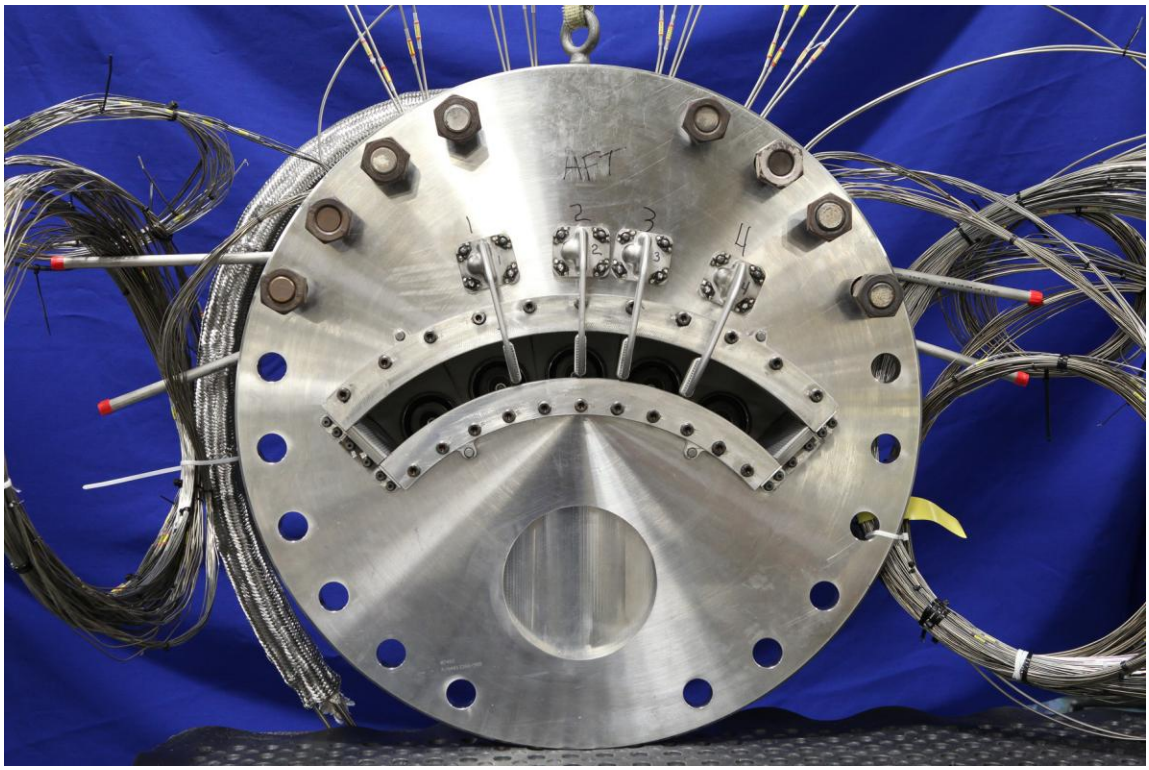

Figure 71 – Final Combustor Assembly (Showing Emissions Rake Installation)

Figure 72 – Cups 3-5 Nozzle and Mixer Installation in Dome

The completed sector rig was delivered to NASA Glenn Research Center in August 2012.

4.16.4 Conclusions

The N+2 5-cup sector with CMC liners was fabricated, assembled, and instrumented over a period of ~10 months. Extensive instrumentation was applied to maximize learnings during combustion testing, help ensure data quality, and provide safety to the hardware. The sector was completed per design intent, ready for testing in the ASCR facility at T3 and P3 conditions never before achieved in a GE combustor sector test.

4.17 Task 7.3.1 –Testing of 5-Cup Combustor Sector (NASA Funded)

4.17.1 Summary

The N+2 5-cup CMC sector was utilized for combustion testing with Jet-A fuel in the NASA ASCR facility on six separate test days from October 25 to December 5, 2012. Emissions data, as well as temperature, pressure, and dynamic pressure data, was collected for a range of test operating conditions. The 7% and 30% ICAO points as well as the nominal cruise cycle point were tested at the exact target conditions. Facility limitations prevented the rig from achieving the full 85% and 100% ICAO conditions. Maximum combustor inlet conditions reached were approximately 400psia / 1200F and 684psia / 1040F. Emissions data collected at the 7% and 30% points, along with an extrapolation based on the highest pressure data up to the 85% and 100% ICAO points, was used to estimate the total LTO NOx. Based on the limited high T3 / P3 data, the sector has achieved 19% CAEP/6 LTO NOx, surpassing the program goal of 25% CAEP/6 NOx. Cruise emissions were measured to be ~5 EINOx with greater than 99.9% efficiency.

4.17.2 Introduction

The 5-cup CMC sector rig tests had several objectives. The primary objective was to demonstrate N+2 Technology Level LTO emissions performance by taking data at the key 7%, 30%, 85% and 100% ICAO cycle points. Evaluation of cruise performance (emissions and efficiency) was also part of the N+2 technology goals. Additional testing on an alternative fuel blend (50% up to 100% alternative fuel, including biofuels) is planned to evaluate the impact of fuel type on emissions and operability and demonstrate similarly good performance. Throughout the testing, significant data beyond the emissions sampling was also collected - including temperatures on the CMC liners, fuel nozzles, deflectors, and sidewalls of the combustor; dynamic pressure data at 4 different locations, and static pressures throughout the combustor. Over a period of roughly 6 weeks, 6 tests were performed including maximizing the flow/T3/P3 capability of the facility on the final day. While the highest desired temperature/pressure conditions were not achieved, the data collected provides sufficient evidence to calculate the LTO emissions levels. Further testing will be highly valuable in verifying the pressure/temperature dependence of the emissions performance and collecting additional data.

4.17.3 Results and Discussion

Fuel, air, and fuel-air ratio closures are a typical indicator of data quality. For all emissions test points of interest, rig air closures = (calculated air flow based on Aeff's and dP's) / (metered air flow) were within +1% / - 6% based on component-level air flow checks prior to rig assembly. Fuel closures = (calculated fuel flow based on FN and dP) / (metered fuel flow) were within +/-2% for the Pilot Primary circuit. For the Pilot Secondary and Main circuits, the closure was farther off but highly repeatable. Fuel-air ratio closures = (FAR based on emissions) / (FAR based on metered flows) was typically well within +/- 4%.

A summary of the major emissions data taken to date is provided in *Figure 73* through *Figure 75* below.

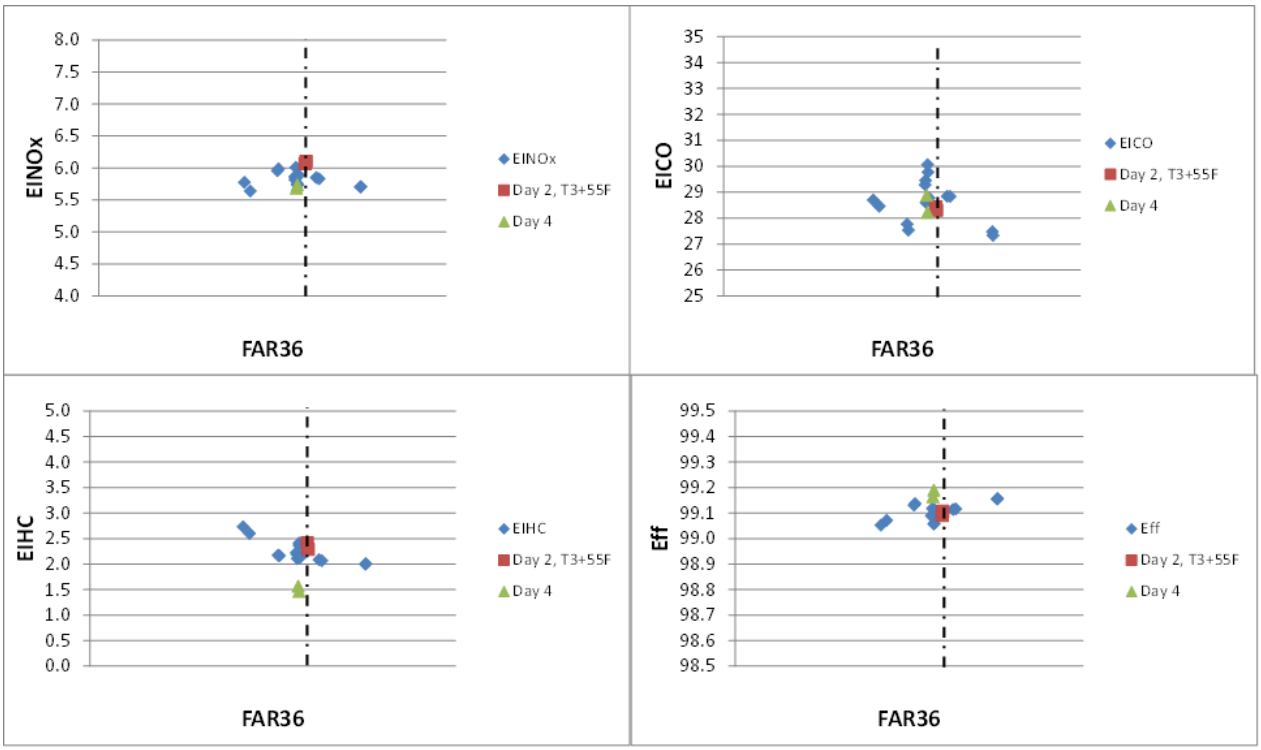

Figure 73 – Sector Rig Emissions Data (7% ICAO Point)

Sector rig emissions data (EINOx, EICO, EIHC, and combustion efficiency) at the 7% ICAO point, plotted vs. the fuel / air ratio based on sampled emissions. Repeated points taken on two additional test days are shown for repeatability. The vertical line indicates the target 7% ICAO cycle fuel / air ratio.

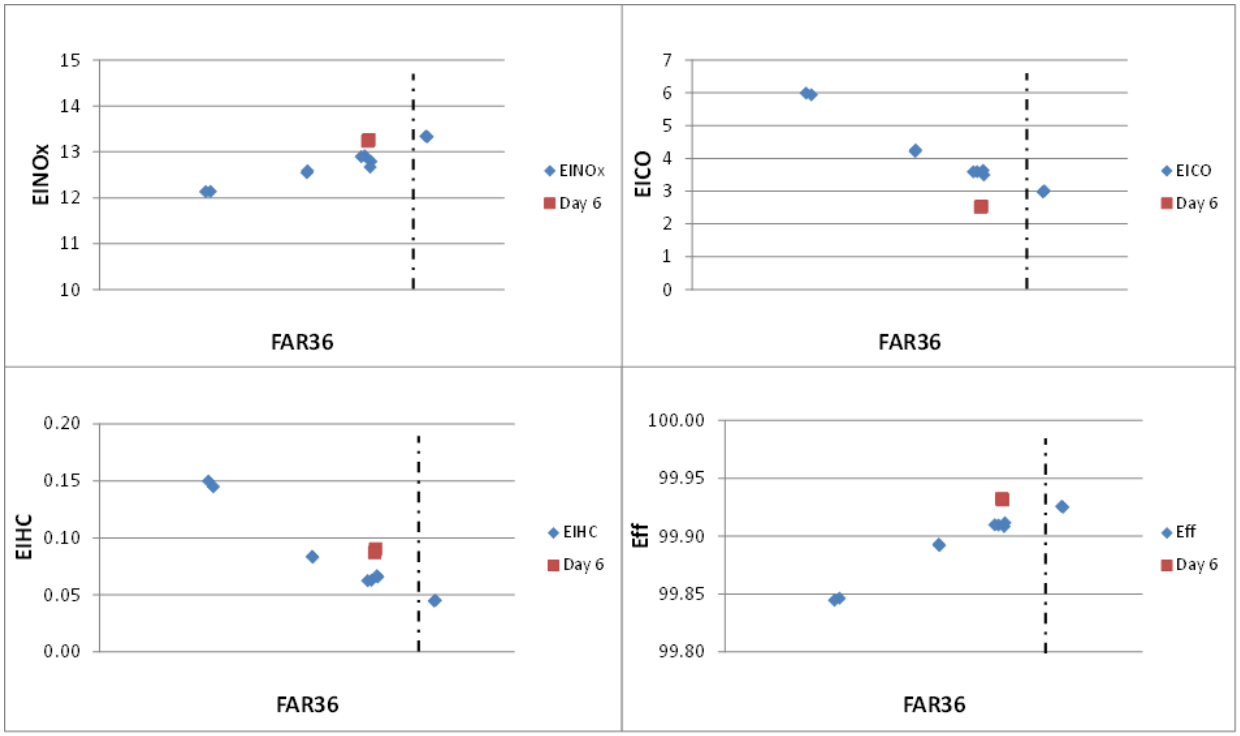

Figure 74 – Sector Rig Emissions data (30% ICAO Point)

Sector rig emissions data (EINOx, EICO, EIHC, and combustion efficiency) at the 30% ICAO point. The vertical line represents the target fuel / air ratio.

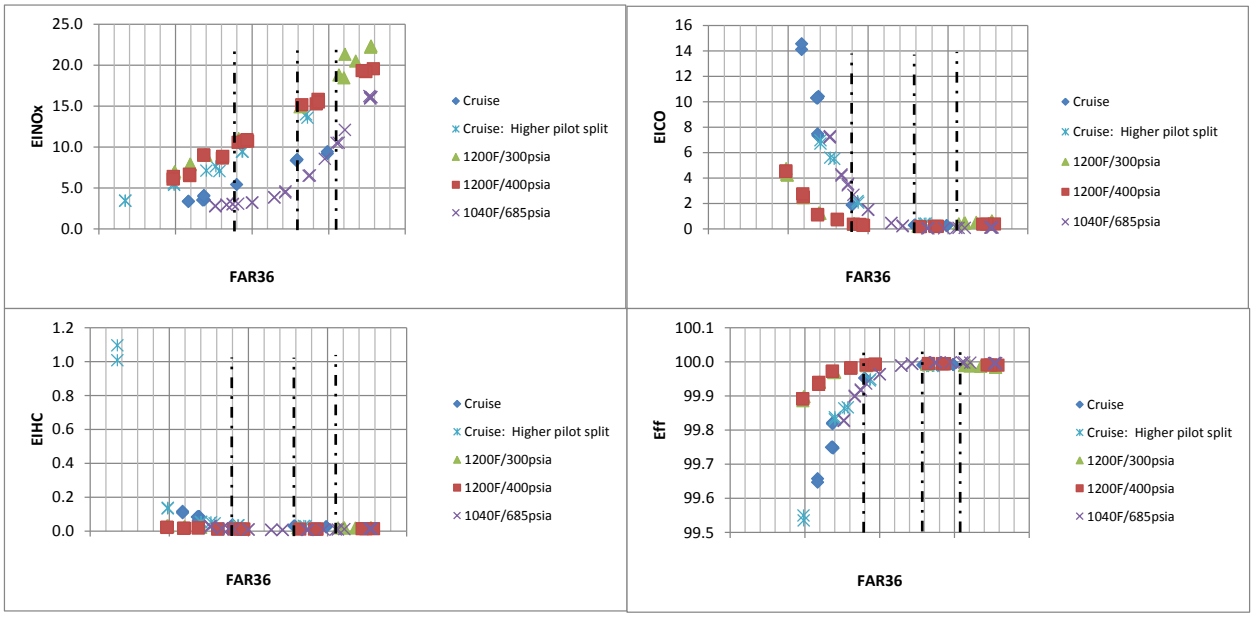

Figure 75 – Sector Rig Emissions Data (All Main-Staged Fuel-Air Ratio Sweeps)

Sector rig emissions data (EINOx, EICO, EIHC, and combustion efficiency) for all main-staged fuel-air ratio sweeps. All points are at the target pilot / main staging, except where noted. The vertical lines represent the target fuel / air ratio at cruise, 85%, and 100% ICAO cycle points.

Data fits were made to correlate and then extrapolate the data. The emissions data is plotted against the mixer flame temperature in *Figure 76*. EINOx values are pulled from a fit to this data at the 85% and 100% ICAO point flame temperatures for the LTO NOx assessment.

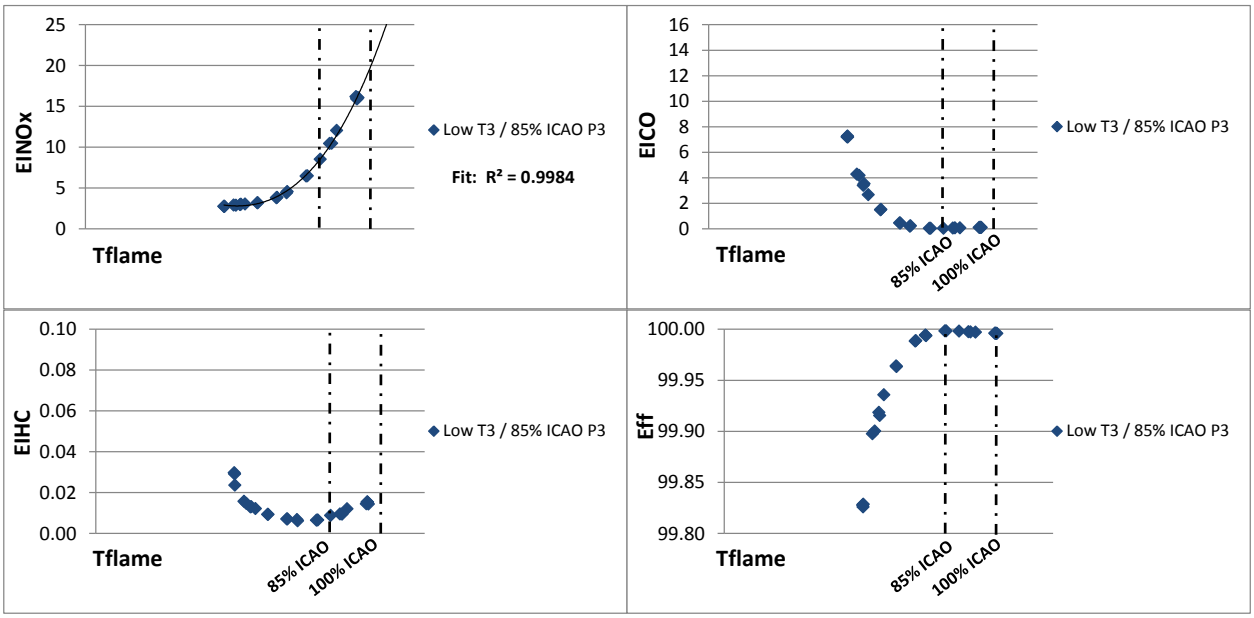

Figure 76 – High Pressure Data at ~685psia

High pressure data at ~685psia, plotted vs. the mixer flame temperature. The method for assessing LTO NOx relies primarily on this high pressure data, picking EINOx values at the appropriate Tflame for the 85% ICAO point and an extrapolated 100% ICAO point.

Table 9 summarizes the LTO NOx data for the ICAO points. The facility was unable to deliver T3 temperatures high enough to run the 85% and 100% ICAO points at the exact T3 / P3 / flow / FAR conditions. The 85% ICAO point is taken directly from the data in *Figure 76* at the appropriate mixer flame temperature. For the 100% ICAO point, the data in *Figure 76* was curve fit and extrapolated to the appropriate flame temperature. The standard humidity correction, based on the measured dew point in the combustor inlet air, was applied to the data in *Figure 73* through *Figure 76* to arrive at the final EINOx values in.*Table 9.*

Table 9 – LTO Emissions Results for the GE N+2 5-Cup Sector

% ICAO	EINOx	EICO	EIHC
100	17.62	0.20	0.01
85	7.89	0.05	0.01
30	11.75	3.13	0.05
7	5.18	28.44	2.13
% CAEP/6:	**18.9%**	**20.4%**	**8.8%**

Cruise NOx emission, taken from the data in *Figure 75*, is ~5 EINOx. This is more than a 50% reduction compared to the current fielded state-of-the-art, and >75% reduction from the 2005 reference B777-200 aircraft, while maintaining better than 99.9% efficiency.

4.17.4 Conclusions

The sector has performed as designed, achieving LTO NOx below the 25% CAEP/6 target while demonstrating ~5 EINOx with >99.9% efficiency at cruise conditions. Thermal data for the liners and other components is still under evaluation.

5 Detailed Plan to Refine Phase 1 Low Emissions Combustor Concept

The technical approach to increase the Technology Readiness Level (TRL) from 4 to 5 includes tasks related to fuel nozzle design and single-cup validation testing, followed by parallel high pressure sector (HPS) demonstration testing at NASA's ASCR facility and full annular rig (FAR) demonstration testing at GE facilities. The overall effort would also include enabling technology development in the area of advanced pilot designs, as well as combustion dynamics predictive model development to support the design of lean burn combustion systems.

5.1 Fuel Nozzle Design

The details of the main fuel injection are primary design features that impact emissions, auto-ignition margins, and dynamics. In Phase 1, the design evolved through conceptual design, flametube screening, and single cup validation testing. This process included some changes to the design that came later in the program. To advance the technology, the design features established in Phase 1 should be analytically re-evaluated based on potential for additional gains in emissions reduction, auto-ignition margin, and dynamics mitigation in a manufacturable fuel nozzle design that can be carried forward to additional high pressure sector tests and full annular demonstration trials. The design space for analytical studies should include multiple fuel nozzle/mixer configurations in order to better understand the design space. The detailed mechanical design of the fuel nozzle will also need to be revisited to achieve both life requirements as well as improved manufacturability. Stress and thermal analyses should be conducted if the final fuel nozzle design is significantly different from the successful Phase 1 fuel nozzles designed for the high pressure sector rig. The mechanical design effort would build off of "lessons learned" from Phase 1 nozzle design and manufacturing.

5.2 Single-Cup Validation Testing

Single-cup validation testing for the newly designed/fabricated N+2 fuel nozzle/mixer configurations should constitute the first test campaign of additional technology development efforts. The goal of this testing phase would be to assess the operational characteristics of the Phase 1 fuel nozzle/mixer configuration (prime design) and alternate designs that focus on the features of the main fuel nozzle. Single-cup testing can be carried out to evaluate fuel nozzle/mixer designs using the GE GRC high temperature and pressure (HTP) flametube rig, GE Aviation's Tunable Combustor Acoustics (TCA) rig for high pressure combustion dynamics assessment, and NASA's CE-5 flame tube rig for flow field measurements of injector mixing and combustion characteristics.

Lean combustion systems are susceptible to dynamics. GE has a dedicated facility to understand and abate this risk, the TCA rig, to determine potential dynamics sensitivities over a range of conditions that encompass low- to high-frequencies analogous to those that could be encountered in a full-annular geometry.

The single-cup testing plan can also include use of NASA's CE-5 facility to obtain diagnostic flow field measurements during high pressure operation, as part of the effort to understand the role of air-assist in fuel/air mixing performance.

5.3 Demonstration Testing to Achieve TRL5

In Phase 1, TRL4 was achieved through successful technology demonstration at NASA's ASCR facility with a GE-designed high pressure sector featuring an advanced N+2 fuel nozzle/mixer configuration and GE-developed CMC liners as the enabling technology. Further development effort would extend the TRL to 5 through parallel high pressure sector and full annular rig testing.

5.3.1 High Pressure Sector Demonstration Testing

The 5-cup high pressure sector developed in Phase 1 would be the workhorse for the sector tests planned as part of a continued technology refinement effort. Continued testing of the high pressure sector is desired, including tests with alternative fuels as well as additional T3 and P3 derivatives to understand the high pressure emissions behavior. Upon completion of testing with the Phase 1 configuration, the high pressure sector would be sent back to GE for any necessary refurbishment. The refurbishment would involve instrumentation repair as necessary, as well as the fit-up and installation of newly validated fuel nozzle/mixer configurations. The liners for the HPS should be assessed after testing with alternative fuels is complete. If needed, an additional set of sector CMC liners may have to be manufactured.

The high pressure sector with the final fuel nozzle/mixer configuration and instrumentation would be delivered for emissions testing at NASA's ASCR facility at full cycle conditions. In support of the test design, new CFD pre-test predictions of the combustor flowfield and emissions should be conducted for the final fuel nozzle/mixer in the high pressure sector combustor geometry. Emissions results of the NASA tests with the final-design fuel nozzle/mixer configuration, along with similar results for the FAR testing, would elevate the NASA N+2 technology to TRL5. Measureable metrics would include emissions, combustion dynamics, and thermal data.

5.3.2 FAR Demonstration Testing

GE's plans for NASA N+2 FAR technology demonstration leverages use of an existing FAR rig. The FAR test preparation for TRL5 demonstration effort involves material engineering design and analysis, and engineering work involving aero and mechanical design and analysis necessary for manufacturing the combustor module, coupled with product definition of the hardware. The design and hardware would be shared and utilized for the NASA N+2 FAR demonstration testing.

Additionally, CFD pre-test predictions of the combustor flowfield and emissions for the final-design fuel nozzle/mixer in the FAR combustor and the HPS combustor geometry would provide insight into possible flowfield differences and their impact on emissions performance.

In addition to the advanced fuel nozzles and mixers, key FAR combustor hardware will also include the combustor dome assembly, liners, and other rig components which are existing GE property. The FAR would be instrumented for the NASA N+2 demonstration tests.

GE would conduct NASA N+2 demonstration testing with the FAR rig configured with the final fuel nozzle/mixer hardware to demonstrate stability, operability, durability and performance acceptable for commercial airline operations. Testing could include both baseline jet fuel and an alternative fuel at temperatures and pressures up to facility limits. Measureable metrics would include emissions, profile and pattern factor, lean blow-out (LBO), ignition, dynamics mapping, and thermal data. Emission results of the FAR tests with the final-design fuel nozzle/mixer configuration along with similar results for the HPS at higher inlet temperature/pressure conditions would together elevate the NASA N+2 combustor technology to TRL5.

6 Conclusions

1. The NNC10CA10C program developed an advanced engine cycle and state-of-the-art combustor technology to meet N+2 fuel burn, noise, and emission goals. The combustor technology was developed to a Technology Readiness Level of 4 (high sector test at representative engine conditions.)

2. The combustor development program progressed through a successful conceptual fuel nozzle/mixer design effort, flametube test rig screening of those designs, and the ultimate selection of a single concept for testing in the 5-cup combustor sector at the NASA ASCR facility. The final design successfully demonstrated >75% reduction in LTO NOx from CAEP/6 standards and 76% reduction in cruise NOx from the 2005 reference aircraft. This was achieved while maintaining >99.9% cruise efficiency, acceptable combustion dynamic pressures, and low CO and UHC emissions.

3. The sector test demonstrated CMC liner technology, including design methodology, fabrication, instrumentation, and evaluation at high pressure and temperature conditions. CMC mechanical property and life data were separately acquired to advance the design process for CMC liners.

4. Additional technology work was conducted in the areas of combustion dynamics mapping, advanced fuel-air mixing diagnostics, laser ignition, and active combustion control. These areas all contribute knowledge to lean burn combustor performance, and are potential enabling technologies as combustion systems are pushed to higher pressure/temperature and more highly premixed conditions.

5. Further development and maturation of the combustor concept will require continued sector testing, including more comprehensive derivatives in conditions and alternative fuels testing. The sector hardware is in excellent condition, suitable for further testing.

6. Maturation of the combustor technology and advancement to Technology Readiness Level = 5 will require design, fabrication, and test of a full annular combustor. The fuel nozzle tested in the high pressure sector was designed and analyzed as an engine-style configuration, simulating a production fuel nozzle envelope, and is similar to the geometry that will be required for a full annular combustor test.

Additional Authors / Technologists

The following contributors are GE Aviation engineers, unless otherwise noted. Many contributors beyond this list deserve recognition for enabling the program to finish in a successful manner. The program would not have been successful except for the expertise and efforts of several test operators; instrumentation, assembly, and test technicians; machinists; and support personnel.

Phil Viars performed Task 1 cycle analysis, and led the following team to complete the task: Kevin Rowe – airframe / mission analysis, Tom Viars – engine cycle analysis, and Greg Szczepkowski – engine acoustic analysis. David Burrus performed initial combustor conceptual design and layout.

For Task 2.1A and 2.1, Shi-Yang Hsieh led the evaluation of a large number of fuel / mixing concepts via CFD and empirical means. Shai Birmaher contributed significant effort in the design of the M6F6 configuration. Randall Boehm designed the pilot and other fuel nozzle features.

For Task 3.1, Russell Fitzgerald at GE Global Research Center conducted the mixer diagnostic experiments and documented the work.

Task 3.2 flame tube testing and Task 3.3 TCA testing were led and reported by Shai Birmaher and John Herbon. Shui-Chi Li assisted with the TCA tests. Dan Brown designed the flametube combustor hardware.

Task 3.4A FAR dynamics, 3.5A engine dynamics, and 3.7A auto-ignition testing were performed and documented by Nayan Patel.

Task 3.6A Core engine dynamics was documented by Raghavan Pandalai.

Task 3.8 HTP testing was conducted at GE Global Research under the leadership of Joel Haynes. Fuel nozzle detailed design, analysis, and procurement were accomplished by Marie McMasters, Will Jansen, Brian Schaldach, Doug McClure, and Sean Henderson. John Herbon reported the results.

Task 4.1A Active Combustion Control was conducted and documented by Zekai Hong at GE Global Research. Hejie Li, Keith McManus, and Joel Haynes of GE Global Research contributed.

Task 4.2A Advanced Ignition Development design and testing was led by Sara Rocci-Denis of GE Global Research and supported by Shai Birmaher. Simon Schoewel of Global Research and Mark Kelsey contributed significantly to the development and hardware procurement, respectively.

Task 4.3A Ceramic Matrix Composite Characterization was led and documented by Doug Carper.

Task 5.1 Sector Design and 5.2 Sector Fabrication were led by Dan Brown. The fuel nozzle design and manufacturing were led by Will Jansen and Brian Schaldach, with analysis support by Sean Henderson and Doug McClure. CMC liner development was led by Don Corsmeier and Matt Deepe. Hardware support was provided by Charlie Baum of ETC Technical Services.

Task 7.3.1 ASCR Testing was led and documented by John Herbon.

John Aicholtz served as the GE program manager (Task 7.1) and contributed to the final report.

Michael Foust and Clay Cooper deserve recognition for their vision and strong leadership.

Finally John Herbon should be recognized for his expertise, perseverance, and commitment to excellence.

8 References and Bibliography

[1] Foust, M.J., Thomsen, D., Stickles, R., Cooper, C., and Dodds, W., 2012. "Development of the GE Aviation Low Emissions TAPS Combustor for Next Generation Aircraft Engines." In the 50th AIAA Aerospace Sciences Meeting, Nashville, TN, Paper AIAA-2012-0936.

[2] Tong, M.T., Jones, S.M., Haller, W. J., and Handschuh, R.F., "Engine Conceptual Design Studies for a Hybrid Wing Body Aircraft."

[3] Thomas, R.H., Burley, L.B., and Olson, E.D., "Hybrid Wing Body Aircraft System Noise Assessment with Propulsion Airframe Aeroacoustic Experiments," AIAA Paper No. 2010-3913.

[4] Kawai, R., Brown, D., Roman, D., Odle, Richard, "Acoustic Prediction Methodology and Test Validation for an Efficient Low-Noise Hybrid Wing Body Subsonic Transport," NASA Final Report PWDM08-0006A, October 30, 2008.

[5] Collier, Fayette, "Overview of NASA's Environmentally Responsible Aviation (ERA) Project, A NASA Aeronautics project focused on midterm environmental goals," 48th AIAA Aerospace Sciences Meeting – January 4, 2010.

[6] Nickol, C.L., and McCullers, L., "Hybrid Wing Body Configuration System Studies," AIAA Paper No. 2009-931.

[7] Nickol, C.L., "N+2 waterfall update 2 5 10rev4," pdf, May 2010.

[8] Wu, P. K., K. A. Kirkendall, and R. P. Fuller, Breakup Processes of Liquid Jets in Subsonic Crossflows, Journal of Propulsion and Power, Vol. 13 (1) 1997.

[9] Spalding, D.B., Some Fundamentals of Combustion, Academic Press, New York; Butterworths Scientific Publications, London, 1955.

[10] Lozano, A., Laser-excited Luminescent Tracers for Planar Concentration Measurements in Gaseous Jets, Ph.D. dissertation, Department of Mechanical Engineering, Stanford University, 1992.

[11] Thurber, M. C. and R. K. Hanson, Simultaneous Imaging of Temperature and Mole Fraction using Acetone Planar Laser-Induced Fluorescence, Experiments in Fluids, Vol. 30, 2001.

[12] Dimotakis, P. E., and P. L. Miller, Some Consequences of the Boundedness of Scalar Fluctuations, Phys. Fluids A, Vol. 11 (2), 1990.

[13] Fu, Y., J. Cai, and S. M. Jeng, Characteristics of the Swirling Flow Generated by a Counter-rotating Swirler, AIAA Paper 2007-5690.

[14] Mohammad, B. S. and S. Jeng, Gas Turbine Combustor Sector Flow Structure, Journal of Propulsion and Power, Vol. 27 (3), 2011.

[15] Cremers, C. J. and R. C. Birkebak, Application of the Abel Integral Equation to Spectrographic Data, Applied Optics, Vol. 5 (6), 1966.

[16] McManus, K.R., Poinsot, T., and Candel, S.M., 1993. "A review of active control of combustion instabilities". Prog. Energy Combust. Sci., 19, pp. 1-29.

[17] Candel, S., 2002. "Combustion dynamics and control: progress and challenges". Proc. Combust. Inst., 29, pp. 1-28.

[18] Dowling, A.P., Morgans, A.S., "Feedback control of combustion oscillations". Annu. Rev. Fluid Mech., 37, pp. 151-182.

[19] Dowling, A.P., "Active control of instabilities in gas turbines". In the RTO AVT Symposium on Active Control Technology for Enhanced Performance Operational Capabilities of Military Aircraft, Land vehicles and Sea Vehicles, Braunschweig, Germany, RTO MP-051, Paper K2.

[20] Richards, G.A., Thornton, J.D., Robey, E.H., Arellano, L., 2007. "Open-loop active control of combustion dynamics on a gas turbine engine". J. Eng. Gas Turbines Power, 129, pp. 38-48.

[21] Barbosa, S., de La Cruz Garcia, M., Ducruix, S., Labegorre, B., Lacas, F., 2007. "Control of combustion instabilities by local injection of hydrogen". Proc. Combust. Inst., 31, pp. 3207-3214.

[22] Neumeier, Y., Zinn, B.T., 1996. "Experimental demonstration of active control of combustion instabilities using real time modes observation and secondary fuel injection". Proc. Combust. Inst., 26, pp. 2811-2818.

[23] Lee, J.G., Kim, K., Santavicca, D.A., 2000. "Effect on injection location on the effectiveness of an active control system using secondary fuel injection". Proc. Combust. Inst., 28, pp. 739-746.

[24] Lee, J.G., Hong, B.-S., Kim, K., Yang, V., Santavicca, D.A., 1998. “Optimization of active control systems for suppressing combustion instability”. In Gas Turbine Engine Combustion, Emissions and Alternative Fuels, Lisbon, Portugal, RTO MP-14, Paper 41.

[25] Kim, K., Jones, C.M., Lee, J.G., Santavicca, D.A., 2005. “Active control of combustion instabilities in lean premixed combustors”. In the 6th Symposium on Smart Control of Turbulence, Tokyo, Japan.

[26] Hermann, J., Orthmann, A., Hoffmann, S. Berenbrink, P., 2000. “Combination of active instability control and passive measures to prevent combustion instabilities in a 260 MW heavy duty gas turbine”. In the RTO AVT Symposium on Active Control Technology for Enhanced Performance Operational Capabilities of Military Aircraft, Land vehicles and Sea Vehicles, Braunschweig, Germany, RTO MP-051, Paper 3.

[27] Hermann, J. Orthmann, A., 2001. “Combustion Dynamics: Application of active instability control to heavy duty gas turbines”. In the RTO AVT Course on Active Control of Engine Dynamics, Brussels, Belgium, RTO-EN-020, Paper 6.

[28] McManus, K.R., Magill, J.C., 1997. “Control of thermo-acoustic instabilities using pulse width modulation”. Proceedings of the 1997 IEEE International Conference on Control Applications, Hartford, CT, pp. 824–829.

[29] McManus, K.R., Magill, J.C., Miller, M.F., 1998. “Control of combustion oscillations in liquid-fueled gas turbines”. Proceedings of the 1998 IEEE International Conference on Control Applications, Trieste, Italy, pp. 1170-1174.

[30] McManus, K.R., Magill, J.C., Miller, M.F., 1998. “Combustion instability suppression in liquid-fueled combustors”. In the 36th Aerospace Sciences Meeting and Exhibit, Reno, NV, Paper AIAA 98-0642.

[31] Yu, K., Wilson, K.J., Parr, T.P., Schadow, K.C., 2000. “An experimental study on actively controlled dump combustors”. In the RTO AVT Symposium on Active Control Technology for Enhanced Performance Operational Capabilities of Military Aircraft, Land vehicles and Sea Vehicles, Braunschweig, Germany, RTO MP-051, Paper 36.

[32] Yu, K., 2001. “Active control of engine dynamics: fundamentals and fluid dynamics – experiments”. In the RTO AVT Course on Active Control of Engine Dynamics, Brussels, Belgium, RTO-EN-020, Paper 3.

[33] Yu, K., Wilson, K.J., Schadow, K.C., 1998. “Scale-up experiments on liquid-fueled active combustion control”. In 34th AIAA/ASME/SAE/ASEE Joint Propulsion Conference and Exhibit, Cleveland, OH, Paper AIAA-1998-3211.

[34] Yu, K., Wilson, K.J., Schadow, K.C., 1999. “Liquid-fueled combustion control: scale-up experiments and effects of fuel droplet size”. In the 37th AIAA Aerospace Sciences Meeting and Exhibit, Reno, NV, Paper AIAA 1999-0328.

[35] Yu, Y.H., Wilson, K.J., Schadow, K.C., 1998. “Liquid-fueled active instability suppression”. Proc. Combust. Inst. 27, pp. 2039-2046.

[36] Hibshman, J.R., Cohen, J.M., Banaszuk, A., Anderson, T.J., Alholm, H.A., 1999. “Active control of combustion instability in a liquid-fueled sector combustor”. In the International Gas Turbines & Aeroengine Congress & Exhibit, Paper GT-1999-215.

[37] DeLaat, J.C., Chang C.T., 2003. “Active Control of High Frequency Combustion Instability in Aircraft Gas-Turbine Engine”. In 16th International Symposium on Airbreathing Engines, Cleveland, OH, Paper ISABE-2003-1054.

[38] Cohen, J.M., Rey, N.M., Jacobson, C.A., Anderson, T.J., Rosfjord, T.J., 1998. “Active control of combustion instability in a liquid-fueled, low NOx combustor”. J. Eng. Gas Turbines Power, 121(2), pp. 281-284. Also In the RTO AVT Symposium on Gas Turbine Engine Combustion, Emissions and Alternative Fuels, Lisbon, Portugal, RTO MP-14, Paper 38.

[39] Moran, A.J., Steele, D., Dowling, A.P., 2000. “Active control of combustion and its applications”. In the RTO AVT Symposium on Active Control Technology for Enhanced Performance Operational Capabilities of Military Aircraft, Land vehicles and Sea Vehicles, Braunschweig, Germany, RTO MP-051, Paper 2.

[40] Coker, A., Neumeier, Y., Lieuwen, T., Zinn, B.T., Menon, S., 2003. “Studies of active instability control effectiveness in a high pressure, liquid fueled combustor”. In the 41st AIAA Aerospace Science Meeting and Exhibit, Reno, NV, Paper AIAA-2003-1009.

[41] Hantschk, C., Hermann, J., Vortmeyer, D., 1996. “Active instability control with direct-drive servo valves in liquid-fueled combustion systems”. Proc. Combust. Inst., 26, pp. 2835-2841.

[42] Golovanevsky, B., Levy, Y., 2002. “Suppression of combustion instability using an aerodynamically excited atomizer”. In the 11th International Symposium on Applications of Laser Techniques to Fluid Mechanics, Lisbon, Portugal, Paper 14-5.
[43] Lee, J.-Y., Lubarsky, E., Zinn, B.T., 2004. “‘Slow’ active control of combustion instabilities by modification of liquid fuel spray properties”. Proc. Combust. Inst., 30, pp. 1757-1764.
[44] Lefebvre, A.H., 1998. “Gas turbine combustion”. Taylor & Francis, Philadelphia, PA. pp. 235.
[45] Lee, J.G., and Santavicca, D.A., 2003. “Experimental Diagnostics for the study of combustion instabilities in lean premixed combustors”. J. Prop. Power, 19(5), pp. 735-750.
[46] Le, D.K., DeLaat, J.C., Chang, C.T., 2003. “Control of thermo-acoustic instabilities: the multi-scale extended Kalman approach”. In the 39th Joint Propulsion Conference and Exhibit, Huntsville, AL, Paper AIAA-2003-4934.
[47] Kopasakis, G., 2003. “High frequency adaptive instability suppression controls in a liquid-fueled combustor”. In the 39th Joint Propulsion Conference and Exhibit, Huntsville, AL, Paper AIAA-2003-4491.
[48] Hathout, J.P., Fleifil, M., Annaswamy, A.M., Ghoniem, A.F., “Heat-release actuation for control of mixture-inhomogeneity-driven combustion instability”. Proc. Combust. Inst., 28, 721-730.
[49] Hathout, J.P., Annaswamy, A.M., Ghoniem, A.F., 2000. “Modeling and control of combustion instability using fuel injection”. In the RTO AVT Symposium on Active Control Technology for Enhanced Performance Operational Capabilities of Military Aircraft, Land vehicles and Sea Vehicles, Braunschweig, Germany, RTO MP-051, Paper 23.
[50] Oldenberg, Richard, Early, James and Lester, Charles. 1998. LA-UR 98-2272: Advanced Ignition and Propulsion Technology Program. s.l. : Los Alamos National Laboratory, 1998.
[51] Tisen, H.S., 1952. “Servo-Stabilization of Combustion in Rocket Motors”. ARS J., 22, pp. 256-263.